

DECOHERENCE IN OPEN QUANTUM SYSTEMS: A REALISTIC APPROACH

A THESIS

SUBMITTED TO THE DEPARTMENT OF PHYSICS
AND THE INSTITUTE OF ENGINEERING AND SCIENCE
OF BILKENT UNIVERSITY
IN PARTIAL FULFILLMENT OF THE REQUIREMENTS
FOR THE DEGREE OF
DOCTOR OF PHILOSOPHY

By

Kerim Savran

January 2006

I certify that I have read this thesis and that in my opinion it is fully adequate, in scope and in quality, as a dissertation for the degree of doctor of philosophy.

Assoc. Prof. Tuğrul Hakioglu (Supervisor)

I certify that I have read this thesis and that in my opinion it is fully adequate, in scope and in quality, as a dissertation for the degree of doctor of philosophy.

Prof. Dr. Alexander Shumovsky

I certify that I have read this thesis and that in my opinion it is fully adequate, in scope and in quality, as a dissertation for the degree of doctor of philosophy.

Assoc. Prof. Ulrike Salzner

I certify that I have read this thesis and that in my opinion it is fully adequate, in scope and in quality, as a dissertation for the degree of doctor of philosophy.

Prof. Dr. Mehmet Tomak

I certify that I have read this thesis and that in my opinion it is fully adequate, in scope and in quality, as a dissertation for the degree of doctor of philosophy.

Assist. Prof. Oğuz Gülseren

Approved for the Institute of Engineering and Science:

Prof. Mehmet Baray,
Director of Institute of Engineering and Science

Abstract

DECOHERENCE IN OPEN QUANTUM SYSTEMS: A REALISTIC APPROACH

Kerim Savran

PhD in Physics

Supervisor: Assoc. Prof. Tuğrul Hakioglu

January 2006

Decoherence mechanisms of open quantum systems in interaction with an environmental bath is investigated using the master equation formalism. Widely used two-level approximation is questioned.

It has been shown that decoherence has different behavior in short and long time regimes. In short times, decoherence mechanisms, relaxation, dephasing and leakage show a Gaussian-like behavior, whereas in the long time regime, they have exponential-like behavior as predicted by the Markov approximation. The non-negligible effects of the non-resonant transitions in the short time regime is observed to be more destructive in terms of decoherence, than the long time resonant transitions. Multilevel effects are also investigated in order to question the validity of the two-level approximation. It has been observed that the higher levels above the qubit subspace have significant effects in decoherence rates. Therefore, the assumptions of the two-level approximation are proved to be irrelevant with the validity of the two-level approximation. The reliability analysis of the Born-Oppenheimer approximation, which is the only approximation used, is also been explained.

Finally, the outcome of the driving fields, which are tools for the manipulation of quantum systems, for a multilevel open quantum system has been demonstrated. It has been shown that Rabi oscillations cannot be observed in a multi-leveled system as smoothly as in a two-leveled system.

Keywords: Decoherence, Master Equation Formalism, Non-resonant Transitions, Multilevel Systems, Two-level Approximation, Born-Oppenheimer Approximation, Rabi Oscillations.

Özet

AÇIK KUVANTUM SİSTEMLERDE UYUMSUZLUK: GERÇEKÇİ BİR YAKLAŞIM

Kerim Savran

Fizik Doktora

Tez Yöneticisi: Assoc. Prof. Tuğrul Hakioglu

Ocak 2006

Çevresel bir rezervuar ile etkileşimde olan açık kuvantum sistemlerindeki uyumsuzluk mekanizmaları ana denklem formalizmi kullanılarak incelendi. Yaygın olarak kullanılan iki-seviye yaklaşıklığı sorgulandı.

Uyumsuzluğun kısa ve uzun zaman bölgelerinde farklı davranışlar gösterdiği gösterildi. Kısa zamanlarda uyumsuzluk mekanizmaları, durulma, eşvre kaybı ve sızıntı, Gaussal-benzeri bir davranış gösterirken, uzun zamanlarda Markov yaklaşıklığının öngördüğü şekilde üstel davranış gösteriyorlar. Kısa zamanlardaki ihmal edilemeyecek rezonant olmayan geçişlerin, uyumsuzluk konusunda uzun zamanlardaki rezonant geçişlerden daha yıkıcı olduğu gözlemlendi. İki seviye yaklaşıklığının geçerliliğini sorgulamak için çok-seviye etkileri de incelendi. Kubit alt-uzayının üstündeki enerji seviyelerinin uyumsuzluk zamanları üzerinde önemli etkileri olduğu gözlemlendi. Dolayısıyla, iki-seviye yaklaşıklığı için öngörülen varsayımların, yaklaşıklığın geçerliliği ile ilgili olmadığı gösterildi. Kullanılan tek yaklaşıklık olan Born-Oppenheimer yaklaşıklığının da güvenilirlik analizi yapıldı.

Son olarak, kuvantum sistemlerin manipülasyonunda kullanılan sürücü alanların çok seviyeli açık kuvantum sistemlerindeki sonuçları gösterildi. Çok

seviyeli sistemlerde Rabi salımlarının iki seviyeli sistemlerdeki kadar kolay elde edilemeyeceđi gözlendi.

Anahtar

sözcükler: Kuantum Uyumsuzluk, Ana Denklem Formalizmi, Rezonant Olmayan Geçişler, Çok Seviyeli Sistemler, İki Seviye Yaklaşıklığı, Born-Oppenheimer Yaklaşıklığı, Rabi Salımları.

Acknowledgement

I would like to express my deepest gratitude to Assoc. Prof. Tuğrul Hakioglu for his supervision during research, guidance and understanding throughout this thesis.

I like to thank to all my friends in physics department, as they kept my morale up all the time. I also like to express my thanks to Haldun Sevinçli for the discussions on the last chapter.

I am also grateful for the improvements on my text made by Assoc. Prof. Ulrike Salzner and Çağrı Öztürk.

Last but not the least, I would like to thank my family for their never ending support.

Contents

Abstract	iv
Özet	vi
Acknowledgement	viii
Contents	ix
List of Figures	xii
List of Tables	xix
1 Introduction	1
2 Methods and models	4
2.1 Master equation formalism	5
2.1.1 Schrödinger picture	5
2.1.2 Heisenberg picture	6
2.1.3 Interaction picture	7
2.1.4 Decoherence in master equation approach	8
2.2 Approximations	10
2.2.1 Born-Oppenheimer approximation	10
2.2.2 Two-level system approximation	12
2.2.3 Rotating wave approximation	13
2.2.4 Markov approximation	16

2.2.5	A general application	18
2.3	Models	22
2.3.1	Spin-boson model	22
2.3.2	Central spin model	24
2.3.3	Bloch-Redfield model	25
2.3.4	Lindblad formalism	27
3	Superconducting systems and the Josephson effect	29
3.1	Josephson effect	29
3.1.1	The RCSJ model	30
3.1.2	Josephson effect in the presence of magnetic flux	33
3.2	SQUID devices	35
3.2.1	dc-SQUID	36
3.2.2	rf-SQUID	37
3.2.3	SQUID-EM field model	38
4	Noise and decoherence of the system	45
4.1	Decoherence in SQUID-EM field model	46
4.2	Spectral dependencies	54
4.2.1	Temperature	55
4.2.2	Ohmic dependencies	60
4.2.3	Cut-off frequency	60
4.2.4	Spectral center	62
4.2.5	Spectral width	64
4.2.6	Spectral amplitude	65
5	Effects of Noise Parameters in Decoherence	68
5.1	Decoherence rates at short and long times	70
5.2	Multilevel effects	73
5.2.1	Leakage	75
5.3	Nonresonant effects	76
5.3.1	Short-time behavior	77

5.3.2	Long-time behavior	80
5.4	Limitations of the Born-Oppenheimer approximation	82
6	Driving fields in the realistic system-environment model	87
6.1	Rabi oscillations	88
6.1.1	The effect of higher levels	89
6.1.2	The effect of the environment	91
6.1.3	Expected outcome of realistic Rabi oscillations	92
6.2	NOT gate simulation	95
7	Conclusions	99
A	The analysis of the compensating term	101
B	Proof of the reality and positivity of $\Lambda^{(G)}$	105
C	Numerical code	107

List of Figures

3. 1	The effective circuit used in the RCSJ model.	31
3. 2	The tilted-washboard potential for $I/I_{c0} = 0.1$	32
3. 3	A circular ring with two Josephson junctions. The dotted lines indicate the contour for the integration.	34
3. 4	A rf-SQUID coupled to a rf circuit with mutual inductance coupling M	38
3. 5	A rf-SQUID coupled to an electromagnetic field with mutual inductance coupling M . There is also an external flux Φ_x effecting the SQUID ring.	39
3. 6	The potential and low lying energy eigenvalues, for a specific single degenerate case. Here the parameters are $\beta \simeq 1.616$ and $\gamma \simeq 1.753$. The axes are normalized and dimensionless.	43
3. 7	The potential and low lying energy eigenvalues, for a specific double degenerate case. Here the parameters are $\beta \simeq 0.772$ and $\gamma \simeq 2.187$. The axes are normalized and dimensionless.	44
4. 1	The dipole matrix elements defining the transitions from ground and first excited state for a specific single degenerate case. Here the parameters are $\beta \simeq 1.616$ and $\gamma \simeq 1.753$. Here, the potential wells are symmetric with $\varphi_x = 0.5$	47
4. 2	The dipole matrix elements defining the transitions from ground and first excited state for a specific single degenerate case. Here the parameters are $\beta \simeq 1.616$ and $\gamma \simeq 1.753$. Here, the potential wells are asymmetric with $\varphi_x = 0.6$	48

4. 3	The variation of the spectral function $I(\omega)$ versus ω and ν for $-1 \leq \nu \leq 1$ and parametrized as $\Lambda/T = 10, 50, 100$ from the innermost to the outermost surfaces respectively.	51
4. 4	The variation of the spectral function $I(\omega)$ versus ω for Lorentzian spectrum. In (a), $\epsilon = 0.5$ and $\omega_0 = 4$ are fixed parameters whereas A changes. In (b), $\epsilon = 0.5$ and $A = 3$ are fixed parameters and ω_0 changes. In (c), $\omega_0 = 4$ and $A = 3$ are fixed parameters and ϵ changes.	52
4. 5	The relaxation curves for a degenerate two level system, that is in interaction with a power-law type spectrum with $\Lambda = 10$ and $\nu = -1$ for various temperatures. On the left, we have a broader time range where time is normalized with an energy scale Ω , and on the right we observe closely the short time range.	56
4. 6	The dephasing curves for a degenerate two level system, that is in interaction with a power-law type spectrum with $\Lambda = 10$ and $\nu = -1$ for various temperatures. On the left, we have a broader time range where time is normalized with harmonic frequency, and on the right we observe closely the short time range.	57
4. 7	The relaxation and dephasing curves for a degenerate two level system, that is in interaction with a power-law type spectrum with $\Lambda = 10$ and $\nu = 0$ for various temperatures.	58
4. 8	The relaxation curves for a degenerate two level system, that is in interaction with a Lorentzian type spectrum with $A = 3$, $\epsilon = 3$ and $\omega_0 = 5$ for various temperatures. On the left side is the overall behavior where short time range is magnified on the right hand side.	58
4. 9	The dephasing curves for a degenerate two level system, that is in interaction with a Lorentzian type spectrum with $A = 3$, $\epsilon = 3$ and $\omega_0 = 5$ for various temperatures. On the left side is the overall behavior where short time range is magnified on the right hand side.	59

4. 10	The relaxation curves for a degenerate two level system, that is in interaction with a power-law type spectrum with $\Lambda = 1$, $T = 0$ for various ν values. On the left side is the overall behavior where short time range is magnified on the right hand side.	61
4. 11	The dephasing curves for a degenerate two level system, that is in interaction with a power-law type spectrum with $\Lambda = 1$, $T = -$ for various ν values. On the left side is the overall behavior where short time range is magnified on the right hand side.	61
4. 12	The relaxation curves for a degenerate two level system, that is in interaction with a power-law type spectrum with $\nu = 0$, $T = 0$ for various Λ values. On the left side is the overall behavior where short time range is magnified on the right hand side.	62
4. 13	The dephasing curves for a degenerate two level system, that is in interaction with a power-law type spectrum with $\nu = 0$, $T = 0$ for various Λ values. On the left side is the overall behavior where short time range is magnified on the right hand side.	63
4. 14	The relaxation curves for a degenerate two level system, that is in interaction with a Lorentzian type spectrum with $A = 3$ and $\epsilon = 3$ for various ω_0 values. On the left side is the overall behavior where short time range is magnified on the right hand side.	64
4. 15	The dephasing curves for a degenerate two level system, that is in interaction with a Lorentzian type spectrum with $A = 3$ and $\epsilon = 3$ for various $\omega_0 = 5$ values. On the left side is the overall behavior where short time range is magnified on the right hand side.	65
4. 16	The relaxation curves for a degenerate two level system, that is in interaction with a Lorentzian type spectrum with $A = 3$ and $\omega_0 = 5$ for various ϵ values. On the left side is the overall behavior where short time range is magnified on the right hand side.	65

4. 17	The dephasing curves for a degenerate two level system, that is in interaction with a Lorentzian type spectrum with $A = 3$ and $\omega_0 = 5$ for various ϵ values. On the left side is the overall behavior where short time range is magnified on the right hand side.	66
4. 18	The relaxation curves for a degenerate two level system, that is in interaction with a Lorentzian type spectrum with $\epsilon = 3$ and $\omega_0 = 5$ for various spectral amplitudes. On the left side is the overall behavior where short time range is magnified on the right hand side.	67
4. 19	The dephasing curves for a degenerate two level system, that is in interaction with a Lorentzian type spectrum with $\epsilon = 3$ and $\omega_0 = 5$ for various spectral amplitudes. On the left side is the overall behavior where short time range is magnified on the right hand side.	67
5. 1	The Gaussian decay fit to the RDM element $\rho_{11}(t)$ at short times, under the influence of a Lorentzian spectrum with spectral parameters $A = 3$, $\epsilon = 3$ and $\omega_0 = 5$. The system is taken as a degenerate 2LS.	71
5. 2	The exponential decay fit to the RDM element $\rho_{11}(t)$ at short times, under the influence of a Lorentzian spectrum with spectral parameters $A = 3$, $\epsilon = 3$ and $\omega_0 = 5$. The system is taken as a degenerate 2LS.	73
5. 3	The relaxation and dephasing rates for a degenerate two level system, that is in interaction with a Lorentzian type spectrum with $\epsilon = 0.1$, $\omega_0 = 1$ and $A = 1$. The coupling range is $R = 10$ and the coupling strength is $\kappa = 0.1$. The system is a singly degenerate system.	75

5. 4	The Leakage curves for multileveled systems in interaction with a Lorentzian spectrum with $A = 3$, $\omega_0 = 5$ and $\epsilon = 3$. The system has coupling range $R = 10$ and coupling strength $\kappa = 0.2$. On the left side we see the long time range whereas the short time range is focused on the right hand side.	76
5. 5	The leakage rates for a degenerate two level system, that is in interaction with a Lorentzian type spectrum with $\epsilon = 0.1$, $\omega_0 = 1$ and $A = 1$. The coupling range is $R = 10$ and the coupling strength is $\kappa = 0.1$. The system is a singly degenerate system. . .	77
5. 6	The relaxation and dephasing rates for a multi-level system, that is in interaction with a Lorentzian type spectrum with $\epsilon = 0.1$ and $A = 1$ for various spectral locations. The system is prepared with coupling range $R = 10$ and coupling strength $\kappa = 0.1$. Energy levels are equally spaced with $\Delta E = 1$	78
5. 7	The Gaussian (a)relaxation, (b)dephasing and (c)leakage rates for multi-level systems, that is in interaction with a Lorentzian type spectrum with $\epsilon = 0.1$ and $\omega_0 = 2.4$ for various spectral amplitudes. The system has equal energy level spacings $\Delta E = 1$, coupling range $R = 10$ and coupling strength $\kappa = 0.1$	79
5. 8	The Gaussian (a)relaxation, (b)dephasing and (c)leakage rates for multi-level systems, that is in interaction with a Lorentzian type spectrum with $\epsilon = 0.1$ and $\omega_0 = 2.4$ for various spectral amplitudes. The system has equal energy level spacings $\Delta E = 1$, coupling range $R = 10$ and coupling strength $\kappa = 0.1$. The axes have logarithmic scales this time.	80
5. 9	The Gaussian relaxation (first column), dephasing (second column) and leakage (third column) rates for multi-level systems, that is in interaction with a realistic power-law spectrum of different characteristics, sub-ohmic (first row), ohmic (second row) and super-ohmic (third row) for various cut-off frequencies Λ . Note that the axes have logarithmic scales.	81

5. 10	The exponential (a)relaxation, (b)dephasing and (c)leakage rates for multi-level systems, that is in interaction with a Lorentzian type spectrum with $\epsilon = 0.1$ and $A = 1$ for various spectral locations. The system has equal energy level spacings $\Delta E = 1$, coupling range $R = 10$ and coupling strength $\kappa = 0.1$	82
5. 11	μ_R for 3LS and 5LS as a function of spectrum center ω_0 . The figure is an illustration of the data in the Table 5.1.	86
6. 1	Rabi oscillations in a 2LS. On the left hand side, we have full population inversion as the Rabi field is resonant with ΔE , whereas on the right hand side, as $\omega_R \neq \Delta E$, we cannot observe a full population inversion.	88
6. 2	Rabi oscillations in a 2LS. On the left hand side, we have full population inversion as the Rabi field is resonant with ΔE , whereas on the right hand side, as $\omega_R \neq \Delta E$, we cannot observe a full population inversion.	90
6. 3	Rabi oscillations in a 2LS. On the left hand side, we have full population inversion as the Rabi field is resonant with ΔE , whereas on the right hand side, as $\omega_R \neq \Delta E$, we cannot observe a full population inversion.	91
6. 4	Rabi oscillations in a 2LS in interaction with an environmental bath, as the environmental coupling strength is varied.	93
6. 5	Rabi oscillations in a 4LS in interaction with an environmental bath, for various environmental coupling strengths. On the left hand side, we see the populations of the qubit subspace, whereas on the right hand side, we see the leakage to higher levels.	93
6. 6	The time average over the Rabi pulse of the third-level occupancy is shown as a function of pulse area, for different third level energies, where $E_1 = 1$, $E_2 = 2$. The Rabi frequency is set as resonant with the first two levels. The inset shows the state occupations for the equally spaced system levels, resonant with the Rabi frequency.	95

6. 7	The occupation $\rho_{11}(t)$ versus the number of couples of NOT operations performed, in a 2LS that is in interaction with the environment, for various environmental coupling strengths.	97
6. 8	The occupation $\rho_{11}(t)$ versus the number of couples of NOT operations performed, in a 4LS that is in interaction with the environment, for various environmental coupling strengths.	98

List of Tables

5.1	The μ parameter of the RDL processes for 2LS, 3LS and 5LS against varying ω_0 . The other spectral parameters are $\epsilon = 0.1$ and $A = 1$	85
-----	---	----

Chapter 1

Introduction

Quantum computation is one of the hottest fields of research in the recent years, as theoretically, it promises great computational speed for certain algorithms and extensive security.¹ Numerous scientists are working on quantum algorithms, measurement techniques, state preparations, manipulations and so on. There are several candidate physical systems for the proposed quantum algorithms, and their dynamics are investigated in detail. Yet, still there is no certain answer to the question, whether the long sought quantum computer will be built one day, since there are still many practical problems on the way.

One of the most important problems is decoherence, i.e. the loss of coherence in a quantum system that is in interaction with an environment. It is practically impossible to isolate any quantum mechanical system from the environment, and the interaction with the environment, which is often called "noise", destroys the initially prepared quantum state very quickly. This is a great obstacle for the quantum algorithms, as they need a certain amount of time to be executed. Theoretically, any quantum computation algorithm may be expressed in one and two qubit gate operations. Qubits are indeed the fact behind the power of quantum computation, as they are the quantum equivalent of bits in digital computation. But the distinctive property of the qubits is that, apart from the classical bit values 1 and 0, they can take any value between 0 and 1 as well. In order to benefit from the quantum computation, a typical algorithm should

perform about 10^3 to 10^4 gate operations on the qubits before the decoherence takes place. Yet, such a task is still far from possible with the current techniques and knowledge.

As qubits are the quantum analogous of digital bits, and as the name suggests, they consist of systems with two levels. Though, apart from certain systems, such as organic molecules with certain discrete rotational symmetries, or spin-1/2 systems, the physical systems consist of many levels, and often infinitely many levels. But this fact does not constrain the researchers to use such systems as qubit candidates, as several approximation techniques and models help to analyze the systems of interest as two level systems. Apart from the number of levels in the system, there are still many hardships to face concerning the decoherence analysis.

The system-environment interaction itself is mainly a problem. Though the system is often truncated to finite levels, the environment should be continuous, and should contain infinitely many levels, for the analysis to produce reasonable and realistic results. The interaction of the system with these infinitely many environmental modes is still impossible to trace, still further approximations need to be used. The system-environment couplings cause the system levels to couple to each other, in addition to the entanglement between system and environment. Furthermore the time evolution of the system turns out to be memory dependent, i.e. the behavior of the system at any time depends on the configuration of the system at all earlier times. After presenting these obstacles, it is clear that a full analytical and exact solution of decoherence is impossible. Even after many approximations, only the simplest system-environment models are analytically solvable.

In this thesis, I worked on the decoherence as well, though, I tried to avoid all approximations that I could. Eventually, my analysis was a numerical analysis. I also questioned the validity of the well-known two level approximation, that truncates the physical system down to two levels as certain conditions are held.

In Chapter 2, I will introduce the most frequently used approximations and interaction models that are used in the studies of decoherence, and present

an example solution making use of these approximations. In Chapter 3, I will briefly introduce superconducting systems, Josephson effect and SQUID (Superconducting QUantum Interference Device) systems, as they are the most widely referred systems that are being studied, and the model system adopted for my analysis. In Chapter 4, I will be solving the SQUID-EM field interaction model, using the master equation approach, explained briefly in Chapter 2. Also the dependence of decoherence on the spectral parameters will be observed qualitatively in this chapter. In Chapter 5, I will investigate the effect of system parameters in decoherence, make quantitative analysis, and also question the 2LA in detail, by comparing the outcome of multileveled systems and two leveled systems. In Chapter 6, I will finally be inspecting the outcome of applying driving fields to systems that are also in interaction with the environment. In this chapter, I will also demonstrate for a simple single-qubit gate, and present the effect of environment and multilevels on the execution.

Chapter 2

Methods and models

Decoherence is the result of interaction of a physical system with the environment, which is usually considered as a reservoir, i.e. infinitely large. Solution of the interaction of a finite system with an infinite reservoir is impossible by pure analytical methods. Even as the reservoir is taken finite, it should have a much higher dimension of Hilbert space than the system, and even in this case, tracing every possible process between the environment and the system is practically impossible. In order to overcome this fundamental problem, several methods and approximations are used.

For a SQUID system that is used as a qubit, there may be several decoherence sources such as electromagnetic environment, phonons, quasiparticles, background charges, critical current noise, gate voltage fluctuations, etc. In order to investigate the effects of such decoherence mechanisms there is a widely used technique called the master equation technique. Basically master equation technique consists of writing an equation of motion for the reduced density matrix. In closed quantum systems, i.e. systems that are isolated and not in interaction with any kind of environment, this method is quite simple and effective. As density matrix can describe anything one may wish to know about the system, solving the master equation, that is determining the time behavior of the density matrix enables us to deduce any behavior about the system at any time. However, for open systems, one cannot obtain exact

solutions due to the reasons mentioned above. In order to obtain reasonable answers, one has to use some simpler models and approximations. Among the simple, solvable models, the well-studied spin-Boson model,²⁻⁵ spin-bath model,⁶ Bloch-Redfield⁷⁻⁹ theory are the most frequently used ones. Also as further simplification is required some approximations such as Markov approximation, two-level system approximation,^{2,15} Born-Oppenheimer approximation¹⁶ are also used frequently.

2.1 Master equation formalism

Master equation, i.e. equation of motion of the density matrix may be obtained using basic quantum mechanical facts.¹⁷ This formalism has been used since the early works of Bloch, Redfield and Fano,⁷⁻⁹ and there have been many studies using this formalism.¹⁸⁻²⁰ There are three major pictures that are used in determining the time dependency of quantum mechanical observables, Schrödinger picture, Heisenberg picture and the interaction picture.

2.1.1 Schrödinger picture

First, as we consider the basic Schrödinger picture we know that the state vectors evolve in time with the Hamiltonian as

$$i\frac{d}{dt}|\psi(t)\rangle = H(t)|\psi(t)\rangle \quad (2.1)$$

where $H(t)$ is the Hamiltonian and for simplicity the Planck's constant \hbar is set to 1. As we define a propagator $U(t, t_0)$ that propagates the state $|\psi(t_0)\rangle$ at initial time t_0 to the state $|\psi(t)\rangle$ at final time t , one obtains the relevant equation of motion for the propagator

$$i\frac{d}{dt}U(t, t_0) = H(t)U(t, t_0). \quad (2.2)$$

Integrating the above equation for a time independent Hamiltonian gives us the well-known propagator form

$$U(t, t_0) = \exp[-iH(t - t_0)] \quad (2.3)$$

where for an explicitly time dependent Hamiltonian one obtains

$$U(t, t_0) = T_{\leftarrow} \exp \left[-i \int_{t_0}^t ds H(s) \right] \quad (2. 4)$$

where the symbol T_{\leftarrow} defines a chronological time ordering operator which orders products of time-dependent operators such that their time-arguments increase from right to left as indicated by the arrow.

After defining the time evolutions of states, we can now write down the density matrix and obtain the master equation for Schrödinger picture. As we write down the density matrix as

$$\rho(t_0) = \sum_i \omega_i |\psi_i(t_0)\rangle \langle \psi_i(t_0)| \quad (2. 5)$$

where ω_i are the weights of the states defining the initial wavefunction, and propagate the states by the propagator, we find that at a later time t ,

$$\rho(t) = \sum_i \omega_i U(t, t_0) |\psi_i(t_0)\rangle \langle \psi_i(t_0)| U^\dagger(t, t_0). \quad (2. 6)$$

As we differentiate the above equation, we obtain the master equation

$$\frac{d}{dt} \rho(t) = -i [H(t), \rho(t)] \quad (2. 7)$$

which is also known as *Liouville-von Neumann equation*.

2.1.2 Heisenberg picture

As for the Heisenberg and interaction pictures, the master equations are obtained in a very similar manner. It is known that in the Heisenberg picture, the time dependence is transferred to the operators defining the observables from the wave functions. Any operator in the Heisenberg picture (including the Hamiltonian) is obtained as

$$\mathcal{O}_H(t) = U^\dagger(t, t_0) \mathcal{O}(t) U(t, t_0) \quad (2. 8)$$

where the subscript H denotes the Heisenberg picture and the operator without the subscript is in the Schrödinger picture. Here it is assumed that the operators

in both pictures coincide at the initial time t_0 . Differentiating both sides of Eq. 2. 8 we obtain the equation of motion

$$\frac{d}{dt}\mathcal{O}_H(t) = i[H_H(t), \mathcal{O}_H(t)] + \frac{\partial\mathcal{O}_H(t)}{\partial t} \quad (2. 9)$$

where H_H is the Hamiltonian in the Heisenberg picture. It can be seen that if the operator \mathcal{O} has no explicit time dependence and the system is isolated, i.e. $\partial H/\partial t = 0$, the equation of motion obtained is same as the *Liouville-von Neumann equation* obtained in Schrödinger picture:

$$\frac{d}{dt}\mathcal{O}_H(t) = i[H, \mathcal{O}_H(t)] \quad (2. 10)$$

as we put the density matrix ρ instead of the operator \mathcal{O} .

2.1.3 Interaction picture

The interaction picture is however a little bit different from both Schrödinger picture and Heisenberg picture as it is a more general picture while the other two are limiting cases for the interaction picture. Interaction picture can be considered for a case where two different systems interact with each-other as the name depicts. Let us write the Hamiltonian in two parts as

$$H(t) = H_0 + \hat{H}_I(t) \quad (2. 11)$$

where H_0 is the free part of the Hamiltonian, and H_I is the interaction Hamiltonian. Free Hamiltonian defines the systems in the absence of interaction and usually considered time independent, whereas the interaction Hamiltonian defining the interaction between the systems, is time dependent. Now we define two time evolution operators as

$$U_0(t, t_0) = \exp[-iH_0(t - t_0)] \quad (2. 12)$$

and

$$U_I(t, t_0) = U_0^\dagger(t, t_0)U(t, t_0) \quad (2. 13)$$

where $U(t, t_0)$ is the time evolution operator of the total system, the time evolution of any operator may be written as

$$\mathcal{O}_I(t) = U_0^\dagger(t, t_0)\mathcal{O}(t)U_0(t, t_0) \quad (2.14)$$

and time evolution of any state may be written as

$$|\psi_I(t)\rangle = U_I(t, t_0)|\psi(t_0)\rangle. \quad (2.15)$$

The relevant density matrix and interaction Hamiltonian in the interaction picture can be obtained as follows:

$$\rho_I(t) = U_I(t, t_0)\rho(t_0)U_I^\dagger(t, t_0) \quad (2.16)$$

$$H_I(t) = U_0^\dagger(t, t_0)\hat{H}_I(t)U_0(t, t_0) \quad (2.17)$$

and the corresponding Liouville-von Neumann equation is therefore given as

$$\frac{d}{dt}\rho_I(t) = -i[H_I(t), \rho_I(t)]. \quad (2.18)$$

Due to this equation of motion, density matrix may be obtained as

$$\rho_I(t) = \rho_I(t_0) - i \int_{t_0}^t ds [H_I(s), \rho_I(s)]. \quad (2.19)$$

This form of Liouville-von Neumann equation is frequently used in decoherence calculations where a system-bath interaction occurs. For the master equation formalism this may be used as a starting point where the interaction Hamiltonian in the interaction picture H_I may be defined differently for different systems and different interaction mechanisms.

2.1.4 Decoherence in master equation approach

While using the master equation formalism the decoherence of the system can be observed via the reduced density matrix. The reduced density matrix is the density matrix defining only the system, and obtained by tracing the total density matrix over the environmental degrees of freedom. It thus has the dimensions of the system's Hilbert space.

As we consider a closed system, which is not in interaction with an environment, and work on the density matrix, which also has the dimensionality of the Hilbert space, the time dependence of the density matrix elements may be obtained as

$$\rho_{kj}(t) = c_k(0)c_j^*(0)\exp(-i(E_k - E_j)t) |k\rangle\langle j| \quad (2.20)$$

where $c_k(0)$, $c_j(0)$ are the amplitudes of the respective eigenstates for the initial state, and E_k , E_j are the respective eigenenergies. It is obvious that the diagonal elements are stationary in this Schrödinger picture, and the non-diagonal elements evolve freely with the relevant energy difference as a frequency.

However, for an open system that is in interaction with an environment we have a totally different evolution for the density matrix. First, decoherence produces a spontaneous diagonalization of the density matrix. The non-diagonal elements of the density matrix rapidly reduce to zero as a manifestation of dephasing. As the non-diagonal elements define the phase difference between the states, losing this phase information is named dephasing. Depending on the type of coupling with the environment other differences are expected to occur between the open and closed systems. Rather than staying stationary the diagonal elements of the density matrix change with time depending on the interaction, and this process is called relaxation. As a principle property the trace of the reduced matrix still sums up to 1 at all times. This means that the population of eigenstates change, though as the population of one eigenstate increases, another decreases. For instance, Rabi oscillations in two-level systems demonstrate this population inversion perfectly.

There is also another process of decoherence called leakage. As the quantum computation is concerned, the two levels (conveniently the lowest two levels) are the only important levels in a physical system. Because of this fact most of the models that are commonly used, as will be discussed later in this chapter, include only the lowest two levels of a system. However, the probability of the higher levels to achieve a finite population is not negligible. This population escape is

called leakage, and can be expressed as

$$L(t) = 1 - \sum_{n=1,2} \rho_{nn}(t). \quad (2. 21)$$

For an exactly two-level system, this expression is zero. However, for the truncated systems it is critical to choose the truncation limit so that non-negligible leakage effects are correctly included in the solutions.

2.2 Approximations

As mentioned before, open quantum systems cannot be dealt with, without any approximation. As both the system of interest and the environment that it is interacting with, has infinite degrees of freedom, a direct approach for an exact result fails. In order to overcome this situation, some approximations are frequently used for these type of calculations. The most common of these approximations are the Born-Oppenheimer approximation (BOA),¹⁶ the Two-Level approximation (2LA),^{2,15} and the Markov approximation.^{21,22}

2.2.1 Born-Oppenheimer approximation

Born-Oppenheimer approximation (BOA) in the most general sense, suggests that if the Hamiltonian is separable into two or more terms, the total eigenfunctions are products of the eigenfunctions of the separate parts of the Hamiltonian. This can be simply shown as

$$H = H_1(q_1) + H_2(q_2) \rightarrow \psi(q_1, q_2) = \psi_1(q_1)\psi_2(q_2) \quad (2. 22)$$

where $\psi_1(q_1)$ is an eigenfunction of $H_1(q_1)$, $\psi_2(q_2)$ is an eigenfunction of $H_2(q_2)$, and $\psi(q_1, q_2)$ is an eigenfunction of the total Hamiltonian H .

This approximation was first used on nuclear and atomic physics, considering the Hamiltonians and wavefunctions of electrons and nucleus. Another aspect of this approximation also takes place where the movement of the nucleus due to electronic interaction is so slow that it is negligible compared to the movement of

the electrons. Finally, the nucleus can be considered stationary while electrons orbit around it, and their eigenfunctions can be separately solved to find the eigenfunction of the whole atom.

In our case of open quantum systems, the Hamiltonian can be separated into the system Hamiltonian H_s and the environmental Hamiltonian H_e . Considering the eigenfunctions of both Hamiltonians separately, and, assuming the total eigenfunction to be a product of those two, we obtain a separable master equation solution for the open system such as

$$\rho_T(t) = \rho(t) \otimes \rho_e(t) \quad (2. 23)$$

where $\rho(t)$ defines the density matrix built with system eigenfunctions and $\rho_e(t)$ defines the density matrix built with environmental eigenfunctions. With this approach, the interaction is treated perturbatively. Here, the entanglement of the system and the environment is totally neglected. This approximation may give doubtful results in the long time regime however, it would be impossible to calculate the behavior of the system, considering the entanglement with an infinitely large environmental reservoir.

Going one step further in the Eq. 2. 23 would be to assume the environment stationary. This is like neglecting the movement of the nucleus with respect to the electrons. Although the system of interest may be infinitely large, practically it may be truncated in the energy spectrum. This truncation will be analyzed in a later section. The truncated system will have much less degrees of freedom compared to an infinitely large environmental reservoir. Therefore the processes occurring between the system and the reservoir affect the system, however it may be neglected for the reservoir. Finally, with the Born-Oppenheimer approximation we are left with an expression like

$$\rho_T(t) = \rho(t) \otimes \rho_e(0). \quad (2. 24)$$

This expression assumes the system and environment to be separable and also the environment is left unchanged throughout the time. Thus Born-Oppenheimer approximation greatly simplifies the calculation of the open system dynamics.

The environmental density matrix with this approximation is considered as a thermal equilibrium or a vacuum most of the time.

2.2.2 Two-level system approximation

While analyzing the interactions of a system with an infinite environment it is impossible to make analytical calculations with the master equation formalism if the system under consideration is also considered to have large dimensional Hilbert space. Therefore a truncation is often done making use of the fact that the system energy levels that are of concern are mostly affected from the levels that are in a finite range

The most aggressive truncation procedure is used to obtain a two-level system. Two-level systems have considerable importance concerning the quantum computation and qubit operations. Although not essentially required, the qubit operations and quantum algorithms are executed trivially in two-level systems. There are some exact two-level physical systems such as spin 1/2 systems where most of the real physical systems have higher dimensions of Hilbert space.

This truncation scheme has been defined in numerous places,^{2,3} although not rigorously proven. The procedure is rooted, rather intuitively, to the condition that

$$\Delta, \frac{k_B T}{\hbar} \ll \omega_0 \quad (2.25)$$

where Δ is defined as the tunneling matrix element between the double wells in the potential, and ω_0 is the resonant transition frequency between the lowest two levels. In this case, the environmental oscillators are separated into two cases. The oscillator frequencies that are $\gtrsim \omega_0$ are thought to effect the transition through the barrier between potential wells, therefore renormalizing the tunneling matrix element. On the other hand, the oscillator frequencies that are $\lesssim \omega_0$ detune the potential wells, and thereby destroy the phase coherence between the localized states in the two wells. However, throughout this reasoning possible transitions to higher levels due to higher environmental oscillator frequencies are totally neglected, as possible non-resonant transitions are not considered.

The 2LA is one of the most frequently used approximations in studies of decoherence, though for most of the cases its use is not justified. We believe that this approximation should be handled with care, and the validity conditions should be checked meticulously. The 2LA will be questioned in detail in Chapter 5, where also the condition of low temperatures, i.e. Eq. 2. 25 will be discussed.

2.2.3 Rotating wave approximation

Even if a system is truncated to two levels, its interaction with an environment such as a field does not have a closed-form analytical solution. Therefore, further approximations are essential in order to achieve analytical progress. The rotating wave approximation^{21,22} is one approximation widely used to eliminate the effects of non-resonant processes. In order to present the complications a sample calculation will be presented below.

Consider a two level system which is in interaction with a classical electric field. A typical Hamiltonian for this system-environment is

$$H = \hbar\omega_1|1\rangle\langle 1| + \hbar\omega_2|2\rangle\langle 2| - \mu \cdot \mathbf{E}(t)(|1\rangle\langle 2| + |2\rangle\langle 1|) \quad (2. 26)$$

where the coupling with the electric field is taken to be of the electric dipole form, coupling the different parity states $|1\rangle$ and $|2\rangle$. Here for the sake of simplicity, μ is taken to be real. If we examine the evolution of a generic state

$$|\psi(t)\rangle = a_1(t)|1\rangle + a_2(t)|2\rangle \quad (2. 27)$$

under the Hamiltonian given by Eq. 2. 26, we obtain the coupled amplitude equations as

$$\dot{a}_1(t) = -i\omega_1 a_1(t) + \frac{i}{\hbar} \mu \cdot E(t) a_2(t) \quad (2. 28)$$

$$\dot{a}_2(t) = -i\omega_2 a_2(t) + \frac{i}{\hbar} \mu \cdot E(t) a_1(t). \quad (2. 29)$$

As a further simplification, as we assume the field to be a monochromatic field, we can express $E(t)$ as $E_0 \cos(\omega t + \varphi)$ which simplifies the amplitude equations to

$$\dot{a}_1(t) = -i\omega_1 a_1(t) + iV \cos(\omega t + \varphi) a_2(t) \quad (2. 30)$$

$$\dot{a}_2(t) = -i\omega_2 a_2(t) + iV \cos(\omega t + \varphi) a_1(t) \quad (2. 31)$$

where $V = \mu \cdot E_0/h$. Now, as we pass on to the interaction picture where the free evolution of the amplitudes are removed from Eqs. 2. 30 and 2. 31, and the new amplitudes are defined as $a_1(t) = b_1(t) \exp(-i\omega_1 t)$ and $a_2(t) = b_2(t) \exp(-i\omega_2 t)$, the resulting coupled amplitudes turn out to be

$$\dot{b}_1(t) = iV \cos(\omega t + \varphi) \exp[i(\omega_1 - \omega_2)t] b_2(t) \quad (2. 32)$$

$$\dot{b}_2(t) = iV \cos(\omega t + \varphi) \exp[i(\omega_2 - \omega_1)t] b_1(t). \quad (2. 33)$$

By this transformation, the only time dependence on the amplitudes is reduced to the one caused by the coupling. In the next step, as the cosine terms in Eqs. 2. 32 and 2. 33 are written as sum of complex exponentials, we obtain two exponential time dependent terms in both amplitudes in the form $\exp[i(-\omega + \omega_1 - \omega_2)t]$ and $\exp[i(\omega + \omega_1 - \omega_2)t]$ for the first term, and the complex conjugate of these terms for the second. Here lies the essence of the rotating wave approximation, where the terms $\exp[i(-\omega + \omega_1 - \omega_2)t]$ and their complex conjugates are neglected and we are left with the new amplitude equations in the rotating wave approximation

$$\dot{b}_1(t) = i \frac{V}{2} \exp(i\varphi) \exp(-i\Delta t) b_2(t) \quad (2. 34)$$

$$\dot{b}_2(t) = i \frac{V}{2} \exp(-i\varphi) \exp(i\Delta t) b_1(t) \quad (2. 35)$$

where the term $\Delta = \omega_2 - \omega_1 - \omega$ is the detuning between the transition frequency between the levels and the driving electric field. The main idea behind the rotating wave approximation lies in the choice of the frequency of the field. As the frequency of the driving field is very close to the separation between the energy levels of the system, we can safely neglect the rapidly oscillating nonresonant terms given by $\exp[i(-\omega + \omega_1 - \omega_2)t]$ and its complex conjugate, and only take the resonant terms given by $\exp[i(\omega + \omega_1 - \omega_2)t]$ and its complex conjugate. The simplicity supplied by the rotating wave approximation becomes clearer in the next step where another transformation is made on the amplitude equations 2. 34 and 2. 35 as $b_1(t) = c_1(t) \exp(-i\delta t)$ and $b_2(t) = c_2(t) \exp[i(\Delta - \delta)t]$ where

δ may be chosen arbitrarily. The final amplitude equations, which are stripped from explicit time dependencies turn out to be

$$\dot{c}_1(t) = i\delta c_1(t) + i\frac{V}{2}\exp(i\varphi)c_2(t) \quad (2. 36)$$

$$\dot{c}_2(t) = i(\delta - \Delta)c_2(t) + i\frac{V}{2}\exp(-i\varphi)c_1(t). \quad (2. 37)$$

Typical choices for the arbitrary frequency δ may be zero and $\Delta/2$. Here since the explicit time dependency is taken care of, solving these coupled equations become much simpler.

The power of the rotating wave approximation can be used safely, when the driving field frequency is very close to the energy separation of two levels and also at long times. As the difference between the frequency of the field and the energy separation becomes greater, the nonresonant terms as well as the resonant terms become effective in the dynamics of evolution. Furthermore here, the driving field is accepted as a monochromatic field. As the field starts to include a wide frequency range, the rotating wave approximation becomes questionable. However, for an isolated system that is driven by a resonant field where the Rabi solutions are expected to be observed, the rotating wave approximation is perfectly applicable and transforms the typical Hamiltonian

$$H = \frac{\hbar}{2} [\omega_1|1\rangle\langle 1| + \omega_2|2\rangle\langle 2|] - \hbar V (|1\rangle\langle 2| + |2\rangle\langle 1|) \cos(\omega t + \varphi) \quad (2. 38)$$

into a much simpler form as

$$H = \frac{\hbar}{2} [\omega_1|1\rangle\langle 1| + \omega_2|2\rangle\langle 2|] - \frac{\hbar V}{2} [|2\rangle\langle 1|\exp[-i(\omega t + \varphi)] + |1\rangle\langle 2|\exp[i(\omega t + \varphi)]]]. \quad (2. 39)$$

The monochromatic field approach will not be useful in the consideration of the system-environment interaction, as the environment is usually modeled as a bath having a continuous frequency range, as neglecting the non-resonant effects for such a large frequency range will not give dependable results in the short time regime. So in our calculations, all the non-resonant effects will be considered.

2.2.4 Markov approximation

Markov approximation^{21,22} is another popular approximation which simplifies analytical calculations in the time domain. In analytical calculations, the system behavior has a memory, so that the evolution of the system at any time depends on the behavior at previous times. This dependence makes analytical calculations rather hard, and numerical computations costly. In order to present the nature of the Markov approximations one should consider a system where a single discrete state $|0\rangle$ is weakly coupled to higher continuum of levels via a monochromatic classical field. The Hamiltonian of this system may be written as

$$\begin{aligned}
 H &= \hbar\omega_0|0\rangle\langle 0| + \hbar \int \omega_h|h\rangle\langle h|d\omega_h + \\
 &\hbar \int \eta_h [|0\rangle\langle h|exp(i\varphi_h)exp(i\omega t) + |h\rangle\langle 0|exp(-i\varphi_h)exp(-i\omega t)] d\omega_h
 \end{aligned} \tag{2. 40}$$

with the rotating wave approximation applied, where the subscript h denotes the higher levels of the system. The first line represents the free part of the Hamiltonian and the second line defines the interaction with the monochromatic field. Here the states are defined orthonormal so that $\langle 0|0\rangle = 1$, $\langle h|h'\rangle = \delta(\omega_h - \omega'_h)$ and $\langle 0|h\rangle = 0$. Also $\eta_h exp(i\varphi_h)$ defines the transition matrix element between the single discrete state $|0\rangle$ and the higher state $|h\rangle$.

The generic wavefunction of the system is given as

$$|\psi(t)\rangle = c_0 exp(-i\omega_0 t)|0\rangle + \int c_h exp(-i\omega_h t)|h\rangle d\omega_h \tag{2. 41}$$

and inserting this wavefunction into the Schrödinger equation gives the equations of motions for the state amplitudes as

$$\dot{c}_0 = -i \int \eta_h exp(i\varphi_h) c_h exp(-i\Delta_h t) d\Delta_h \tag{2. 42}$$

$$\dot{c}_h = -i\eta_h exp(-i\varphi_h) c_0 exp(i\Delta_h t) \tag{2. 43}$$

where the term $\Delta_h = \omega_h - \omega_0 - \omega$ defines the detuning between the higher state $|h\rangle$ and discrete state $|0\rangle$ via a one photon resonance. In order to solve these coupled equations of motions it is best to integrate Eq. 2. 43 and insert the

result as $c_h(t)$ in Eq. 2. 42 to obtain an equation for the amplitude of single state $c_0(t)$. The resulting equation is an integro-differential equation

$$\dot{c}_0(t) = - \int_0^t c_0(t')K(t-t')dt' \quad (2. 44)$$

where the kernel $K(t-t')$ is given as

$$K(t-t') = \int \eta_h^2 \exp[-i\Delta_h(t-t')] d\delta_h. \quad (2. 45)$$

It is obvious that the value of the amplitude c_0 at any time depends on the values of c_0 at all previous times. This is usually defined as the amplitudes (i.e. the system) with memory. Here the kernel function is merely a function. Nonetheless, similar integro-differential equations are found with the master equation formalism and density matrices. In that case, however, the kernel is not a function, but generally a complicated operator, usually called as the superoperator. It may include projections, commutations etc. But the dependence on the previous times is inevitable. The Markov approximation comes into scene at this point. The aim of the approximation is merely to reduce the integro-differential equation into a simpler differential equation, by erasing the memory effects on the system.

Consider a special case, where the transition matrix element is flat throughout the higher frequency range, so that $\eta_h^2 = \eta_0^2$. This transforms Eq. 2. 45 into

$$K(t-t') = \eta_0^2 \int_{-\infty}^{\infty} \exp[-i\Delta_h(t-t')] d\Delta_h = 2\pi\eta_0^2\delta(t-t') \quad (2. 46)$$

so that the kernel is only contributing at $t = t'$. This delta function behavior simplifies the Eq. 2. 44 into

$$\dot{c}_0(t) = -\pi\eta_0^2 c_0(t). \quad (2. 47)$$

A less trivial result arises when the continuum of transition matrix elements are not flat but slowly varying. For that case, the kernel will not have a delta function behavior, but it will still be sharply peaked at $t = t'$. As the kernel will

contribute mostly near $t = t'$, its contribution to the amplitude equation may be neglected so that

$$\dot{c}_0(t) = -c_0(t) \int_0^t K(t-t') dt' = -c_0(t) \int_0^t K(\tau) d\tau \quad (2.48)$$

By this equation it is possible to solve the simple differential equation as the kernel is integrated. Since the kernel is independent of amplitudes, the problem is reduced to the integration of the kernel. During these calculations with Markov approximation, it is assumed that; (1) the kernel is sharply peaked at $t = t'$, i.e. the transition matrix elements are slowly varying throughout the levels, (2) the integral is independent of the upper limit $\tau = t$, so that the integral may further be simplified as taking the upper limit as infinity.

Markov approximation significantly simplifies the analytical solutions for the integro-differential equations, whether they arise from the amplitude equations of motions or the master equation. However, there is a serious assumption: the kernel is assumed to be sharply peaked. In this case, this means that the transition matrix elements are slowly varying, i.e. the transition from the discrete level to all higher levels is nearly equally probable. In the master equation approach, this may lead to different assumptions, which will be depicted later.

2.2.5 A general application

In order to demonstrate the master equation approach and the approximations mentioned, it will be helpful to solve a simple problem.²¹ Consider a system with equally spaced energy levels that is in interaction with a continuum of a harmonic oscillator bath. The system operators, denoted as s^\dagger and s create and annihilate a quantum of energy $\hbar\Omega$ in the system, as raising and lowering operators. The environmental raising and lowering operators are denoted as b_ω^\dagger and b_ω . In the interaction picture, H_0^s , the free Hamiltonian of the system, introduces a time dependence on the system operators so that s^\dagger is multiplied by $\exp(i\Omega t)$ and s is multiplied by $\exp(-i\Omega t)$. In the rotating wave approximation, system and environment operators pair as $s^\dagger b_\omega$ and $b_\omega^\dagger s$, and introducing a unitary

transformation $U = \exp[i\Omega t \int b_\omega^\dagger b_\omega d\omega]$ renders these coupled operators time independent. Finally, the interaction Hamiltonian where the free part of the system is removed is given as

$$H_I = \hbar \int \omega b_\omega^\dagger b_\omega d\omega + \hbar \int \eta_\omega [s^\dagger b_\omega \exp(-i\varphi_\omega) + s b_\omega^\dagger \exp(i\varphi_\omega)] d\omega \quad (2. 49)$$

where $\eta_\omega \exp(-i\varphi_\omega)$ is the system-bath coupling. Making a second transformation to get rid of the free evolving environment part, introduces the time dependencies on the environment operators b_ω and b_ω^\dagger and the final Hamiltonian is reduced to

$$V_I(t) = \hbar \int \eta_\omega [s^\dagger b_\omega \exp[-i\varphi_\omega] \exp[-i\omega t] + s b_\omega^\dagger \exp[i\varphi_\omega] \exp[i\omega t]] d\omega. \quad (2. 50)$$

Defining a Langevin operator for the environmental operators in the form of

$$F(t) = -i \int \eta_\omega \exp[-i\varphi_\omega] \exp[-i\omega t] b_\omega(0) d\omega \quad (2. 51)$$

and using the fact that the Heisenberg operator $b_\omega(0)$ is indeed the interaction operator b_ω here, the interaction Hamiltonian is further reduced to

$$V_I(t) = i\hbar [s^\dagger F(t) - F^\dagger(t)s]. \quad (2. 52)$$

Remembering the Eq. 2. 18 we obtain the master equation for the total density matrix

$$\dot{\rho}_T(t) = \frac{i}{\hbar} [V_I(t), \rho_T(t)]. \quad (2. 53)$$

In order to observe the system behavior only -not to mention that observing an infinitely large environment realistically would be impossible- we need to take the trace of the total density matrix, over the environmental degrees of freedom. However in order to take this trace we also need to apply the Born-Oppenheimer approximation given as in Eq. 2. 24. Using the fact that $Tr[\rho \mathcal{O}] = Tr[\mathcal{O} \rho] = \langle \mathcal{O} \rangle$ we obtain factors as $\langle F(t) \rangle$ and $\langle F^\dagger(t) \rangle$ from Eq. 2. 53, which results in zero. Therefore, we need to go to a higher order, at least to second one. It is also trivial to see that all odd orders of the expansion of Eq. 2. 53 give zero contribution, whereas the even orders give finite results.

Using the simple relation

$$\rho_T(t) = \rho_T(0) - \frac{i}{\hbar} \int_0^t [V_I(t'), \rho(t')] dt' \quad (2. 54)$$

and inserting this into Eq. 2. 53, we obtain the second order equation

$$\dot{\rho}(t) = -\frac{i}{\hbar} Tr_e [V_I(t), \rho_T(0)] - \frac{1}{\hbar^2} \int_0^t Tr_e [V_I(t), [V_I(t'), \rho_T(t')]] dt'. \quad (2. 55)$$

The first term here is also zero as explained above. The second term expands as

$$\dot{\rho}(t) = \frac{-1}{\hbar^2} \int_0^t Tr_e [(s^\dagger F(t) - F^\dagger(t)s), [(s^\dagger F(t') - F^\dagger(t')s), \rho_e(0) \otimes \rho(t')]] dt'. \quad (2. 56)$$

Using the cyclic property of trace $Tr_e[\mathcal{A}\mathcal{B}\mathcal{C}] = Tr_e[\mathcal{C}\mathcal{A}\mathcal{B}] = Tr_e[\mathcal{B}\mathcal{C}\mathcal{A}]$, we obtain the master equation consisting of 16 terms grouped below:

$$\begin{aligned} \dot{\rho}(t) = & \int_0^t \{ [s\rho(t')s^\dagger - s^\dagger s\rho(t')] \langle F(t)F^\dagger(t') \rangle \\ & + [s\rho(t')s^\dagger - \rho(t')s^\dagger s] \langle F(t')F^\dagger(t) \rangle \\ & + [s^\dagger \rho(t')s - ss^\dagger \rho(t')] \langle F^\dagger(t)F(t') \rangle \\ & + [s^\dagger \rho(t')s - \rho(t')ss^\dagger] \langle F^\dagger(t')F(t) \rangle \\ & - [s^\dagger \rho(t')s^\dagger - s^{\dagger 2} \rho(t')] \langle F(t)F(t') \rangle \\ & - [s^\dagger \rho(t')s^\dagger - \rho(t')s^{\dagger 2}] \langle F(t')F(t) \rangle \\ & - [s\rho(t')s - s^2 \rho(t')] \langle F^\dagger(t)F^\dagger(t') \rangle \\ & - [s\rho(t')s - \rho(t')s^2] \langle F^\dagger(t')F^\dagger(t) \rangle \} dt'. \end{aligned} \quad (2. 57)$$

Here, the last four lines may be dropped out since they include the expectation values for two annihilation or two creation operators, which are zero for most environment models. The other environmental expectation terms come as a multiplication, and they are defined as

$$\langle F^\dagger(t')F(t) \rangle = \int \eta_\omega^2 \bar{n}_\omega \exp[-i\omega(t-t')] d\omega \quad (2. 58)$$

and

$$\langle F(t)F^\dagger(t') \rangle = \int \eta_\omega^2 [\bar{n}_\omega + 1] \exp[-i\omega(t-t')] d\omega. \quad (2. 59)$$

As we insert these definitions into Eqn. 2. 58, we obtain

$$\begin{aligned} \dot{\rho}(t) = & \int_0^t dt' \int \eta_\omega^2 d\omega \{ [s\rho(t')s^\dagger - s^\dagger s\rho(t')] [\bar{n}_\omega + 1] \exp[-i\omega(t-t')] \\ & + [s\rho(t')s^\dagger - \rho(t')s^\dagger s] [\bar{n}_\omega + 1] \exp[i\omega(t-t')] \\ & + [s^\dagger \rho(t')s - ss^\dagger \rho(t')] n_\omega \exp[i\omega(t-t')] \\ & + [s^\dagger \rho(t')s - \rho(t')s^\dagger s] n_\omega \exp[-i\omega(t-t')] \}. \end{aligned} \quad (2. 60)$$

The next step in the analytical calculations is introducing the Markov approximation. As described in the previous section the integro-differential equation above may be reduced to a differential equation with the help of the Markov approximation. In the master equation approach we have a kernel of the form of a superoperator, but we still have a familiar spectral dependency. Assuming that the continuous transition matrix element η_ω is slowly varying, we can think that the main contribution from the density matrix in the equation is not from the history, but from the instance the observation is made. Excluding the density matrix from the integral we obtain

$$\begin{aligned} \dot{\rho}(t) = & - i\delta\omega [s^\dagger s, \rho(t)] - i\delta\omega' [[s^\dagger, s], \rho(t)] \\ & + \Gamma [\bar{n}(0) + 1] [2s\rho(t)s^\dagger - s^\dagger s\rho(t) - \rho(t)s^\dagger s] \\ & + \Gamma \bar{n}(0) [2s^\dagger \rho(t)s - ss^\dagger \rho(t) - \rho(t)ss^\dagger] \end{aligned} \quad (2. 61)$$

where $\Gamma = \pi\eta^2(0)$ and the integral terms are defined as

$$\delta\omega = -\mathbb{P} \int \frac{\eta_\Delta^2}{\Delta} d\Delta \quad (2. 62)$$

and

$$\delta\omega' = -\mathbb{P} \int \frac{\bar{n}(\Delta)\eta_\Delta^2}{\Delta} d\delta. \quad (2. 63)$$

These integral equations result in the frequency shifts on the system, and they should be small compared to the latter two terms in order to produce meaningful results. The master equation obtained is much simpler to solve than a system with multilevels which entangles with the environment immediately, and has a rather sharp transition matrix distribution over the spectrum that would have an incredibly hard to solve master equation, if not completely impossible.

2.3 Models

In the previous section the most general approximations are discussed briefly. Perhaps the most frequently used one is the two-level approximation. There are also different models that describe system and environment interactions. In this section the most common models used in this problem will be discussed, including the famous spin-boson model, central spin model, and the Bloch-Redfield model.

2.3.1 Spin-boson model

Perhaps, the most intensely studied model in the decoherence field is the spin-boson model. Basically it consists of a spin system (a two level system) in interaction with an environmental bosonic bath (several, if truncated, or infinitely many harmonic oscillators).^{2,23-28} First, as we are accepting a two-level system, let us write a simple Hamiltonian describing the system in a two-dimensional Hilbert space isolated from the environment as

$$H = -\frac{1}{2}\hbar\Delta\sigma_x + \frac{1}{2}\varepsilon\sigma_z \quad (2.64)$$

where σ_x and σ_z define the Pauli matrices, Δ defines the coupling between the two states and ε defines the eigenenergy of the system. This Hamiltonian may define a spin $\frac{1}{2}$ system in interaction with a magnetic field. Also a two level system is commonly thought of as a system having a double-well potential, and the truncated two levels are the combinations of the localized ground states in the wells ψ_R and ψ_L , which is also the case for SQUID systems, that will be discussed in the next chapter. In this case of double-well potential the coupling between the two states is considered to be the tunneling amplitude between the two wells. The system having the above Hamiltonian can be diagonalized and a set of new eigenenergies may be defined to govern the time evolution, though it is not preferable in this case, since experimentally real observables are needed to examine the system. In case of a weak tunneling, where $\hbar\Delta/\varepsilon$ is very small, the eigenenergies of the Hamiltonian would be very close to $\mp\varepsilon$. However, if the ratio is high, then there will not be a set of localized states in both wells, but rather

a superposition of them. In the special case of $\varepsilon = 0$, the eigenstates turn out to be even-odd parity states as

$$\psi_E = \frac{1}{\sqrt{2}}(\psi_L + \psi_R) \quad (2. 65)$$

$$\psi_O = \frac{1}{\sqrt{2}}(\psi_L - \psi_R) \quad (2. 66)$$

The dynamics of this isolated two-level system is indeed a rather trivial one. The real complication occurs when the environmental interaction is introduced. In almost all cases, the coupling to the environment is taken as $\sigma_z \Omega$ type, where Ω is an environmental operator. This kind of coupling commutes with the eigenenergy part of the Hamiltonian, but it doesn't commute with the coupling (tunneling) between the states. As a result it will not effect the diagonal elements of the density matrix, also called as the population of states, but rather effect the non-diagonal elements. Another way to explain the effect of this interaction would be to say that it causes the dephasing of the system, but doesn't have a relaxation effect. There are still non-neglectable interactions possible with the environmental like σ_x or σ_y type couplings. Depending on the type the interaction may cause relaxation, dephasing, or both. However, as much as the spin-boson model is concerned the interaction will be taken as σ_z type.

As the environmental coupling is assumed to be weak it is also possible to assume the environment to be consisted of harmonic oscillators and the coupling with the system to be with the oscillator coordinate or momenta.² As the coupling is taken to be with the environmental coordinate, we reach to the well-known spin-boson Hamiltonian

$$H_{SB} = -\frac{1}{2}\hbar\Delta\sigma_x + \frac{1}{2}\varepsilon\sigma_z + \sum_k \left(\frac{1}{2}m_k\omega_k x_k^2 + p_k^2/2m_k \right) + \frac{1}{2}\sigma_z \sum_k C_k x_k \quad (2. 67)$$

where Δ is a bare tunneling matrix element, x_k , p_k , ω_k , and m_k are respectively coordinate, momentum, frequency, and mass of the k^{th} oscillator in the environment. The parameter C_k defines the coupling strength of the system with the k^{th} oscillator. The Hamiltonian has a sum over the environmental degree of freedom k , and the dependence of the coupling on this coupling strength C_k

may be defined with a function which is called the spectral function, the spectral strength of the environment with respect to the frequency of the environment, and usually denoted with $J(\omega)$. By this definition, the dynamics of the system are governed by the parameters Δ , ε and the spectral function $J(\omega)$. The spectral function is generally accepted to be a smooth function of environmental frequency ω . Under these circumstances, the spin-boson model and the Hamiltonian (2.67) is extensively used in the literature, whether the system in consideration is a genuine two-level system or a multi-level system truncated into two levels.

2.3.2 Central spin model

The central spin system^{6,26} is similar to the spin-boson model in most aspects. The system is again truncated to two levels. However, in this model, the environment is different, so that the system is not coupled to a set of bosonic harmonic oscillators, but instead coupled to a spin bath. So in this case, the environment consists of two-level systems. The Hamiltonian for this system may be given as

$$H_{CS} = \left\{ \Delta \tau_z \cos \left[\Phi - \sum_k \vec{V}_k \cdot \vec{\sigma}_k \right] + h.c. \right\} \quad (2.68)$$

$$+ \tau_z \sum_{k=1}^N \omega_k^{\parallel} \vec{l}_k \cdot \vec{\sigma}_k + \sum_{k=1}^N \omega_k^{\perp} \vec{m}_k \cdot \vec{\sigma}_k + \sum_{k=1}^N \sum_{k'=1}^N V_{kk'}^{\alpha\beta} \sigma_k^{\alpha} \sigma_{k'}^{\beta}$$

where τ is the central spin, and the σ_k operators define the spin bath degrees of freedom. There are also some restrictions and assumptions made to achieve this form of the central-spin Hamiltonian. For instance, the phase of the central spin is restricted to a $\cos(\Phi)$ form while the terms Δ and Φ incorporate spin bath renormalization effects. There are also assumptions such as that the diagonal couplings $\omega_k^{\parallel}, \omega_k^{\perp} \ll \Omega_0$, where Ω_0 is the ultraviolet cutoff frequency for the spin bath, and that the inter-spin coupling $V_{kk'} \ll \omega_k^{\parallel}, \omega_k^{\perp}$. However the ratio of $V_{kk'}/\Delta$ remains arbitrary. In the weak coupling limit, this model can also be reduced to spin-boson model.

This model is usually used to solve systems like nanomagnets or SQUIDs coupled to nuclear and paramagnetic spins. Though this model turns out to be a useful and simple model, still it assumes a two-level system on top of an environmental bath consisting of two-level spin systems.

2.3.3 Bloch-Redfield model

The Bloch-Redfield formalism is rooted in the Bloch equations that were derived by Bloch in 1946⁷ and further development of the Bloch equations by Redfield.⁸ Bloch equations were first used in the nuclear magnetic resonance problems where an N-level atom is in interaction with a magnetic field, and the main feature of these generalized Bloch equations were to describe the relaxation process with two real time scales, T_1 and T_2 . T_1 describes the time scale for the relaxation, and T_2 describes the time scale for the dephasing processes.

Later it was discovered that these generalized Bloch equations were also applicable to optical problems related to maser or laser,²⁹ and optical Bloch equations were generated. Though the generalized Bloch equations were derived for N-level atoms, the optical Bloch equations were applied to spin systems, i.e. 2-level systems. In order to obtain these optical Bloch equations, first a fictitious quantity, a pseudo-spin vector \mathbf{v} is defined with the components

$$\begin{aligned} v_x &= \text{Tr}[\rho_S(t)\sigma_x] = \rho(t)_{12} + \rho(t)_{21} \\ v_y &= \text{Tr}[\rho_S(t)\sigma_y] = i[\rho(t)_{12} - \rho(t)_{21}] \\ v_z &= \text{Tr}[\rho_S(t)\sigma_z] = \rho(t)_{11} - \rho(t)_{22} \end{aligned} \quad (2. 69)$$

where $\rho_S(t)$ defines the reduced density matrix for the system. Then the optical Bloch equations are given as

$$\begin{aligned} \frac{dv_x}{dt} &= [\boldsymbol{\omega} \times \mathbf{v}]_x - \frac{v_x}{T_2} \\ \frac{dv_y}{dt} &= [\boldsymbol{\omega} \times \mathbf{v}]_y - \frac{v_y}{T_2} \end{aligned} \quad (2. 70)$$

$$\frac{dv_z}{dt} = [\boldsymbol{\omega} \times \mathbf{v}]_z - \frac{v_z}{T_1}$$

with the $\boldsymbol{\omega}$ vector having components

$$\begin{aligned}\omega_x &= \frac{V_{12} + V_{21}}{\hbar} \\ \omega_y &= \frac{V_{12} - V_{21}}{\hbar} \\ \omega_z &= -\frac{E_1 + E_2}{\hbar}\end{aligned}\tag{2. 71}$$

where the terms $V_{ij} = \langle i|v|j\rangle$ are the interaction matrix elements defining the interaction between the atom and the electromagnetic field. Here, as mentioned before, T_1 defines the relaxation of the diagonal elements, whereas T_2 defines the dephasing of the non-diagonal elements of the reduced density matrix.

Starting from the Bloch equations, the Bloch-Redfield formalism is constructed where the reduced density matrix in the eigenbasis of the unperturbed Hamiltonian has an equation of motion

$$\frac{d}{dt}\rho_{nm} = -i\omega_{nm}\rho_{nm} - \sum_{kl} R_{nmkl}\rho_{kl}\tag{2. 72}$$

where the Bloch-Redfield tensor is defined as

$$R_{nmkl} = \delta_{lm} \sum_r \Gamma_{nrrk}^{(+)} + \delta_{nk} \sum_r \Gamma_{lrrm}^{(-)} - \Gamma_{lmnk}^{(-)} - \Gamma_{lmnk}^{(+)}\tag{2. 73}$$

and the rates Γ are found by the Fermi's Golden Rule¹⁷ are

$$\Gamma_{lmnk}^{(+)} = \frac{1}{\hbar^2} \int_0^\infty dt e^{-i\omega_{nk}t} \langle H_{I,lm}(t) H_{I,nk}(0) \rangle_B\tag{2. 74}$$

$$\Gamma_{lmnk}^{(-)} = \frac{1}{\hbar^2} \int_0^\infty dt e^{-i\omega_{nk}t} \langle H_{I,lm}(0) H_{I,nk}(t) \rangle_B\tag{2. 75}$$

where $H_{I,lm}(t)$ are the matrix elements of the interaction Hamiltonian in the interaction picture, and defined in the eigenbasis of the uncoupled system Hamiltonian. The averages are taken over the bath degrees of freedom.

The Bloch-Redfield formalism makes use of the Fermi Golden Rule equations, and also has the Born-Oppenheimer approximation fused in it. Although it leads to analytically solvable results for 2LS,^{10,20} the drawbacks of this formalism have been explored in the context of spin magnetic resonance and relaxation.¹¹⁻¹³

2.3.4 Lindblad formalism

The Lindblad formalism^{17,14} is also one of the widely used techniques for the solution of the master equation. The popularity of the Lindblad formalism stems from its simplicity. This formalism has the Markov approximation integrated in it. In its simplest form, the Lindblad equation is known as

$$\frac{d}{dt}\rho_s(t) = \mathcal{L}\rho_s(t) \quad (2. 76)$$

where the \mathcal{L} defines a Liouville super-operator, and $\rho_s(t)$ is the system density matrix. For a finite dimensional Hilbert space of the environment, where the dimension is given as N , the corresponding Liouville space is a complex space of dimension N^2 and N^2 orthonormal basis operators are described to span the basis, as $F_i, i = 1, \dots, N^2$. For convenience one of these operators is taken as identity, and the rest of the operators are used to define a new set of operators as

$$F_i = \sum_{k=1}^{N^2-1} u_{ki} A_k \quad (2. 77)$$

where the solution for the u matrix and evaluation of the final step as in Fig. 2. 78 is described extensively in.¹⁷ The final form of the Lindblad equation Eq. 2. 76 is found to be

$$\mathcal{L}\rho_s = -i[H, \rho_s] + \sum_{k=1}^{N^2-1} \gamma_k \left(A_k \rho_s A_k^\dagger - \frac{1}{2} A_k^\dagger A_k \rho_s - \frac{1}{2} \rho_s A_k^\dagger A_k \right) \quad (2. 78)$$

where the first part defines the unitary part of the dynamics generated by the Hamiltonian, and the second part is defined as the *dissipator*. Operators A_k and

A_k^\dagger as described in Eq. 2. 77 are often named as the Lindblad operators.

The Lindblad formalism, as seen in Eq. 2. 78 is pretty simple though there are some drawbacks. First, Markovian dynamics are assumed from the beginning. Furthermore, finite dimension for the environmental Hilbert space is used. We basically discard all approximations except the BOA. We have a cautious treatment of this single approximation used with a proof convincing the reader of the validity of this approximation in the range of our interest.

As I have introduced the basic models, approximations and formalisms in this chapter, in the next chapter, I will be investigating the physical systems of interest for our analysis of decoherence phenomenon, and present a solution for the adopted system, rf-SQUID.

Chapter 3

Superconducting systems and the Josephson effect

Concerning the quantum computation there are several physical systems that are considered to be applicable to obtain qubits. NMR systems,³⁰⁻³² SQUIDs,^{33,34} spin or charge based solid state systems are among the most frequently used systems, although there are many other possibilities. Yet perhaps, both in theoretical and experimental studies the most popular systems, are the SQUID systems. In this chapter the theoretical basics of the SQUID systems will be covered, and some SQUID designs will be discussed.

3.1 Josephson effect

Josephson effect^{35,36} is one of the most important discoveries in the world of superconductivity. It plays an important role in many technological improvements. It is also the phenomenon behind the devices called the SQUIDs which will be discussed in the next section.

The Josephson effect is named after the B.D. Josephson, who first proposed that a zero voltage supercurrent

$$I_s = I_c \sin(\Delta\varphi) \tag{3. 1}$$

should flow through a weak link.³⁵ The weak link is defined as the junction obtained by two superconducting electrodes separated by a thin insulating barrier. Here, the term I_c is the critical current, the maximum supercurrent that the junction can let pass through, and $\Delta\varphi$ is the phase difference in the Ginzburg-Landau wave-function of the two electrodes. Josephson's predictions further included the evolution of this phase difference as a potential difference V is applied through the junction as

$$\frac{d(\Delta\varphi)}{dt} = \frac{2eV}{\hbar} \quad (3. 2)$$

where the $2e$ defines the charge of a Cooper pair. This prediction results in an alternating current with amplitude I_c and frequency $\nu = 2eV/\hbar$. These predictions, called as the dc-Josephson effect and ac-Josephson effect are verified by numerous experiments.

Although Josephson proposed the weak link to be obtained by superconductor-insulator-superconductor junction (S-I-S), it turned out to be valid for other possible junctions, such as superconductor-metal-superconductor junction (S-N-S) where the metal near the junction turns out to be a weak superconductor due to proximity effect, or superconductor-constriction-superconductor junction (S-c-S) where two superconductor electrodes are separated via a short, narrow constriction.

3.1.1 The RCSJ model

Although the predictions of Josephson about the superconductor electrode junctions are solid, further investigations are needed to understand the response of the Josephson junctions to finite voltage applications. In order to deepen the understanding a simple model named RCSJ³⁷ (resistively and capacitively shunted junction) is used. In this model the junction will be treated as an ideal Josephson junction, which is shunted by a resistance and a capacitance as seen in Fig. 3. 1.

Here, the resistance is defined by the dissipation in the finite voltage regime, and capacitance is defined between the superconducting electrodes. As a finite

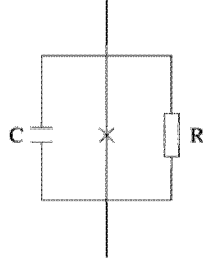


Figure 3. 1: The effective circuit used in the RCSJ model.

bias current is applied to the junction, in order to find the phase γ associated with that, it is appropriate to write a current relation, so that the current from the tree channels in the model will sum up to bias current as

$$I = I_{c0} \sin(\gamma) + \frac{V}{R} + C \frac{dV}{dt} \quad (3. 3)$$

where I_{c0} denotes the original critical current for the ideal junction, which may be greater than I_c for this model. For further simplification, let us define the plasma frequency ω_p as

$$\omega_p = \left(\frac{2eI_{c0}}{\hbar C} \right)^{1/2} \quad (3. 4)$$

and a dimensionless time variable τ as

$$\tau = \omega_p t. \quad (3. 5)$$

When we eliminate the variable V from Eq. 3. 3, we obtain

$$\frac{d^2\gamma}{d\tau^2} + \frac{1}{Q} \frac{d\gamma}{d\tau} + \sin(\gamma) = \frac{I}{I_{c0}} \quad (3. 6)$$

where the term Q defines the quality factor and given as

$$Q = \omega_p RC. \quad (3. 7)$$

The quality factor defined here is identical to $\beta_c^{1/2}$, where β_c is the damping parameter introduced by Stewart and McCumber.^{38,39}

Often, a model named as the tilted-washboard model is also used to describe the system defined as the RCSJ model, as they are analogous to each-other. In

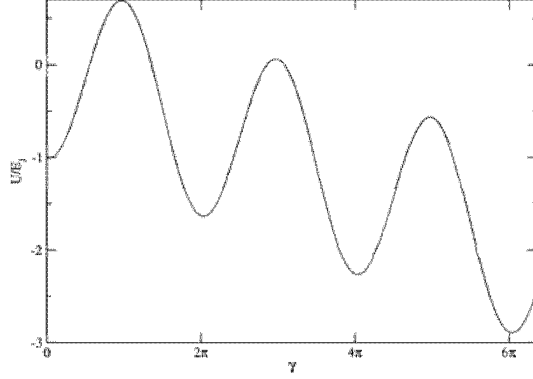


Figure 3. 2: The tilted-washboard potential for $I/I_{c0} = 0.1$.

the tilted-washboard model, a particle of mass $(\hbar/2e)^2 C$ is moving in a potential

$$U(\gamma) = -E_J \cos(\gamma) - \left(\frac{\hbar I}{2e}\right) \gamma \quad (3. 8)$$

in the γ axis, with a dissipative drag force of

$$F_d = \left(\frac{\hbar}{2e}\right)^2 \frac{1}{R} \frac{d\gamma}{dt}. \quad (3. 9)$$

Here E_J is the energy scale used, named as the Josephson coupling energy, and defined as $E_J = (\hbar/2e)I_{c0}$. The tilted-washboard potential as can be seen in Fig. 3. 2 consists of local minima going down with the axis γ for $I < I_{c0}$. However for $I > I_{c0}$ there are no minima or stable equilibrium points.

As C is chosen small, so that the quality factor Q satisfies the relation $Q \ll 1$, we have an overdamped junction, and the Eq. 3. 6 can be reduced to

$$\frac{d\gamma}{dt} = \frac{2eI_{c0}R}{\hbar} \left(\frac{I}{I_{c0}} - \sin(\gamma)\right). \quad (3. 10)$$

Due to this equation, if I is greater than I_{c0} , $d\gamma/dt$ always stays positive, but varies with sine function with frequency γ . In order to obtain the average voltage we need to take the time average of this equation over one period T , which takes γ to scan the interval $0 \rightarrow 2\pi$. Using the Josephson frequency relation $2eV/\hbar = 2\pi/T$ we find the relation for average voltage as

$$V = R(I^2 - I_{c0}^2)^{1/2}. \quad (3. 11)$$

It can be seen that the voltage V is zero for $I < I_{c0}$, and $V = IR$ for $I \gg I_{c0}$.

However for $Q > 1$ the junction is underdamped, and we observe a hysteretic I-V characteristic. As I is increased from zero the potential stays zero, until it jumps up to a finite value at $I = I_{c0}$, and then it raises continuously with I . However as I is decreased below I_{c0} , V does not drop to zero at $I = I_{c0}$, but rather drops to zero near $I \approx 4I_{c0}/\pi Q$.

3.1.2 Josephson effect in the presence of magnetic flux

In order to understand the SQUID devices and their principles, it is important to work out the behavior of Josephson junctions in the presence of a magnetic field. Although the magnetic field may effect the superconductor electrodes, for the sake of simplicity we may just study the effect on the gauge invariant phase difference, and ignore the effect on the electrodes. The gauge invariant phase difference is given as

$$\gamma = \Delta\varphi - \frac{2\pi}{\Phi_0} \int \mathbf{A} \cdot d\mathbf{s} \quad (3.12)$$

where the superconductor flux quanta is denoted with Φ_0 and \mathbf{A} is the relevant vector potential. The integration here is calculated from one electrode to the other. The supercurrent through an ideal Josephson junction, in terms of this gauge invariant phase γ is given as

$$I_s = I_c \sin(\gamma) \quad (3.13)$$

Let us consider a double junction configuration as in Fig. 3.3. It is convenient to analyze the system with respect to the magnetic flux through the system as it is a gauge invariant quantity, so that we would avoid the sensitivity of vector potential due to arbitrary gauge choice. As we choose a specific closed contour and evaluate the integral, the result gives us the flux Φ through the system as $\mathbf{B} = \nabla \times \mathbf{A}$, and the line integral of \mathbf{A} on a closed contour gives the enclosed flux as a result. Let us choose the contour just inside the electrodes, assuming that the thickness of the electrodes are greater than the skin depth λ , so that the supercurrent velocity \mathbf{v}_s is zero along the contour. Then using the relation

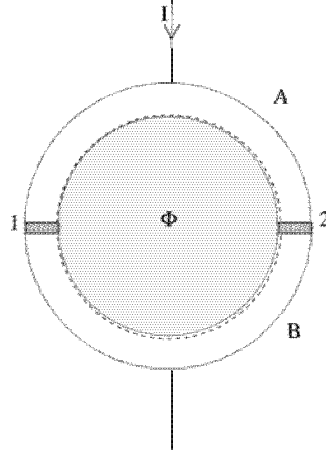


Figure 3. 3: A circular ring with two Josephson junctions. The dotted lines indicate the contour for the integration.

$m^* \mathbf{v}_s = \hbar(\nabla\varphi - 2\pi \mathbf{A}/\Phi_0)$ that can be obtained by the Ginzburg-Landau theory,³⁷ we obtain the vector potential as $\mathbf{A} = (\Phi_0/2\pi)\nabla\varphi$. Using this form of the vector potential we obtain the flux equation as

$$\Phi = \oint \mathbf{A} \cdot ds = \frac{\Phi_0}{2\pi} \int_{electrodes} \nabla\varphi \cdot ds + \int_{weak-links} \mathbf{A} \cdot ds \quad (3. 14)$$

It is obvious that the sum of the phase differences across the weak links φ_1, φ_2 and the integral $\int_{electrodes} \nabla\varphi \cdot ds$ should be zero or an integer multiple of 2π since the phase must be a single-valued quantity. Using this fact as we take the integrals over the weak-links in the same direction through the contour, we obtain the sum of gauge invariant phase differences $\varphi_{1,2}$ to be $2\pi\Phi/\Phi_0$. But in order to obtain the total supercurrent through the weak-links we should evaluate the integrals over the weak links, both from electrode A to electrode B. In that case, the difference of the gauge invariant phase differences turns out to be

$$\gamma_1 - \gamma_2 = \frac{2\pi\Phi}{\Phi_0} (\text{mod}(2\pi)). \quad (3. 15)$$

According to this equation, if the supercurrent through both junctions are maximum due to Eq. 3. 13, both phase differences $\gamma_{1,2}$ should be $\pi/2$, and this is only possible if the flux through the ring is an integral multiple of the

flux quanta Φ_0 . For the special case, $I_{c1} = I_{c2} = I_c$, the maximum supercurrent passing through the parallel junctions satisfy the condition

$$I_m = 2I_c \left| \cos\left(\frac{\pi\Phi}{\Phi_0}\right) \right|. \quad (3.16)$$

The sensitivity of these rings having Josephson junctions on them to the magnetic flux, makes them useful tools for several applications such as magnetometers, gradiometers, voltmeters, amplifiers, etc. This is also the basic idea behind the SQUID devices.

3.2 SQUID devices

SQUID devices are based on the interaction of a superconducting loop, including junction(s), with a magnetic field. The basics of this interaction have been explained briefly in the previous section, yet there are two different basic types of SQUIDs that are being studied both theoretically and experimentally. The dc-SQUIDs (direct current SQUIDs) which has two parallel junctions, and rf-SQUIDs (radio frequency SQUIDs) that have only one junction. Although dc-SQUID was first to be developed, and has higher sensitivity, since rf-SQUID was commercially available before the dc-SQUID, it remains popular among scientists.

Yet the popularity of SQUID systems is due to another fact. It has been discussed by several researchers, both theoretically and experimentally, that macroscopic quantum coherence (MQC) is observable in SQUID systems^{3,15,40} is indeed a very unique phenomenon, where the quantum behavior can be observed macroscopically. MQC also show itself in laser and superfluidity. Leggett and Garg¹⁵ discuss that two assumptions are made by most physicists at macroscopic level that

- a) Macroscopic systems with two or more macroscopically distinct states available will at all times will be in one of these states.
- b) In principle, it is possible to perform a noninvasive measurement on macroscopic systems so that the system will experience small perturbation on its subsequent dynamics.

Though they claim that the extrapolation of quantum mechanics at the macroscopic level contradicts these assumptions. Consider electronic wavefunctions in a superconductor. As indistinguishable electrons with identical wavefunctions come together, with the same phase, the phase state which can be observable macroscopically can show quantum mechanical behavior, such as tunneling, or superposition. For example a superposition of current in a superconductor ring so that the current flows in both directions, or tunneling of a flux state through a potential barrier are examples of such behavior. Recently, there are many experimental schemes proposed and applied to observe these superposition states and macroscopic quantum tunneling phenomena.⁴²⁻⁴⁴ As SQUIDs are characterized by the flux and charge states, they exhibit perfect medium to observe the MQC phenomenon.

3.2.1 dc-SQUID

A basic treatment of the dc-SQUID^{37,45} which has two parallel junctions around a loop, has been made in the previous section. However, as real life applications have finite voltage values, we will make use of the RCSJ model. Also, to avoid further complications related with the hysteresis in the I-V characteristic, the devices are usually operated at a slightly overdamped regime. Therefore, we can make use of the I-V relation in Eq. 3. 11 and obtain

$$V = \left(\frac{R}{2}\right) \left\{ I^2 - \left[2I_c \cos\left(\frac{\pi\Phi}{\Phi_0}\right) \right]^2 \right\}^{1/2} \quad (3. 17)$$

where I_{c0} is obtained from Eq. 3. 16, and $R/2$ comes from the two parallel resistively shunted junctions. It is assumed here that the two junctions have the same critical current and resistance values, for simplicity. Using the double angle relation with the cosine term in Eq. 3. 17, we see that the potential is periodic with flux Φ with frequency Φ_0 , the flux quanta. This shows that a dc-SQUID can be used as a flux-to-voltage transducer in complex devices.

However, the external bias flux is not considered here. The total current through the dc-SQUID is the sum of currents passing through junctions 1 and 2

in Fig. 3. 3, and given as

$$I = I_c [\sin(\gamma_1) + \sin(\gamma_2)] \quad (3. 18)$$

and the circulating supercurrent through the superconducting ring is given by the difference of the currents mentioned above, as

$$I_s = \left(\frac{I_c}{2}\right) [\sin(\gamma_2) - \sin(\gamma_1)] \quad (3. 19)$$

yet, both these equations are constrained by Eq. 3. 15. The term Φ in Eq. 3. 15 is the total flux, i.e. the sum of the externally supplied bias flux Φ_x and the screened flux Φ_s which is given by $\Phi_s = LI_s$ where L is the inductance of the loop. If the total current through the SQUID I and the total flux Φ is known, one can calculate the screened flux Φ_s and the external flux Φ_x .

3.2.2 rf-SQUID

The rf-SQUID^{37,45} is different from the dc-SQUID in that, it only contains one junction, instead of the two parallel junctions. As the SQUID loop is shorted by a single superconducting electrode, observation on this SQUID is made at radio frequency, and hence the name rf-SQUID is used. In the rf-SQUID, the basis states are the flux states, so the flux threading the ring (or equivalently, the current circulating the ring) is observed. This observation is made by inductively coupling an rf current to the SQUID loop. This rf circuit is usually, as seen in Fig. 3. 4, consists of a coil that inductively couples to the rf-SQUID, and driven by a constant current I_1 . The voltage V_T is detected in the circuit to observe the flux from the loop.

As we further study the phase across the weak link, we may obtain a relation similar to the relation of a dc-SQUID obtained in section 3.1.2, Eq. 3. 15, but a single junction variant, as

$$\gamma = \frac{2\pi\Phi}{\Phi_0} [\text{mod}(2\pi)]. \quad (3. 20)$$

This relation emphasizes that the current circulating in the SQUID loop is

$$I_s = I_c \sin\left(\frac{2\pi\Phi}{\Phi_0}\right) \quad (3. 21)$$

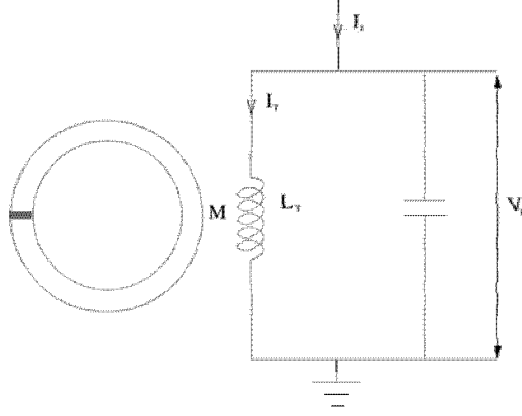


Figure 3. 4: A rf-SQUID coupled to a rf circuit with mutual inductance coupling M .

and the external flux Φ_x through the loop is given as

$$\Phi_x = \Phi + LI_c \sin\left(\frac{2\pi\Phi}{\Phi_0}\right) \quad (3. 22)$$

where Φ is the screened flux.

3.2.3 SQUID-EM field model

There are several SQUID designs, making use of the basic properties of dc-SQUIDS and rf-SQUIDS, and aiming to simulate a qubit system, i.e. a two-level system. However, for the sake of simplicity, a simple model is adopted, where a rf-SQUID ring is coupled to an electromagnetic field inductively, in the presence of an external bias flux as pictured in Fig. 3. 5.⁴⁶

The Hamiltonian for such a system is written as

$$H = H_s + H_e + H_I \quad (3. 23)$$

where the SQUID Hamiltonian is written as⁴⁷

$$H_s = \frac{Q_s^2}{2C_s} + \frac{(\Phi_s - \Phi_x)^2}{2L_s} - \hbar\nu \cos\left(\frac{2\pi\Phi_s}{\Phi_0}\right). \quad (3. 24)$$

Here, the variables Φ_s , the flux threading the ring, and Q_s , the total charge across the weak link are conjugate variables, and satisfy the commutation relation

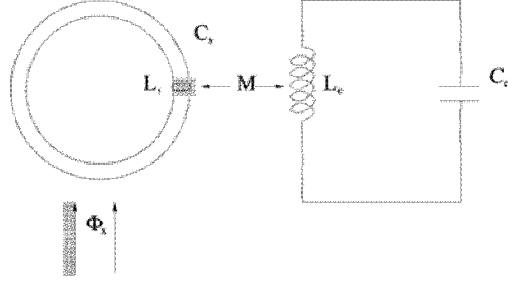


Figure 3. 5: A rf-SQUID coupled to an electromagnetic field with mutual inductance coupling M . There is also an external flux Φ_x affecting the SQUID ring.

$[\Phi_s, Q_s] = i\hbar$. Φ_0 defines the the external bias flux, and $\hbar\nu/2$ defines the matrix element for the pair tunneling across the weak link. The electromagnetic field having the Hamiltonian H_e may be modelled using a circuit having capacitance C_e and inductance L_e , so that the Hamiltonian H_e turns out to be

$$H_e = \frac{Q_e^2}{2C_e} + \frac{\Phi_e^2}{2L_e} \quad (3. 25)$$

where, as before, the variables Φ_e and Q_e define the magnetic flux and the electric charge associated with the cavity, respectively. Finally, the interaction Hamiltonian H_I between the circuit and the SQUID loop is given by

$$H_I = \frac{M}{L_s}(\Phi_s - \Phi_x)\Phi_e \quad (3. 26)$$

where M is the inductive coupling constant as mentioned before.

Next, by making a unitary translation with the operator $\mathcal{U} = \exp(-i\Phi_x Q_s/\hbar)$, the flux of the SQUID ring in the H_s and H_I is translated by Φ_x so that the SQUID Hamiltonian becomes

$$H'_s = \mathcal{U}^\dagger H_s \mathcal{U} = \frac{Q_s^2}{2C_s} + \frac{\Phi_s^2}{2L_s} - \hbar\nu \cos\left(\frac{2\pi(\Phi_s + \Phi_x)}{\Phi_0}\right) \quad (3. 27)$$

and the interaction Hamiltonian becomes

$$H'_I = \mathcal{U}^\dagger H_I \mathcal{U} = \frac{M}{L_s}\Phi_s\Phi_e. \quad (3. 28)$$

Next, we define the dimensionless operators making use of the fact that the charge and flux are conjugate variables,

$$\begin{aligned}
 x_e &= \sqrt{\frac{C_e \omega_e}{\hbar}} \Phi_e & (3. 29) \\
 p_e &= \sqrt{\frac{1}{\hbar \omega_e C_e}} Q_e \\
 x_s &= \sqrt{\frac{C_s \omega_s}{\hbar}} \Phi_s \\
 p_s &= \sqrt{\frac{1}{\hbar \omega_s C_s}} Q_s
 \end{aligned}$$

where the frequencies ω_s and ω_e are defined as $1/\sqrt{C_s L_s}$ and $1/\sqrt{C_e L_e}$ respectively. Making use of the operators at Eq.3. 30, we can define the raising and lowering operators as

$$\begin{aligned}
 a_e &= \frac{1}{\sqrt{2}}(x_e + ip_e) & (3. 30) \\
 a_e^\dagger &= \frac{1}{\sqrt{2}}(x_e - ip_e) \\
 a_s &= \frac{1}{\sqrt{2}}(x_s + ip_s) \\
 a_s^\dagger &= \frac{1}{\sqrt{2}}(x_s - ip_s)
 \end{aligned}$$

Using these operators, the total translated Hamiltonian becomes

$$\begin{aligned}
 H' &= \hbar \omega_s \left(a_s^\dagger a_s + \frac{1}{2} \right) + \hbar \omega_e \left(a_e^\dagger a_e + \frac{1}{2} \right) & (3. 31) \\
 &- \hbar \nu \cos \left(\frac{2\pi}{\Phi_0} \sqrt{\frac{\hbar}{C_s \omega_s}} x_s + 2\pi \varphi_x \right) \\
 &- \frac{M}{L_s} \sqrt{\frac{\hbar^2}{4C_s C_e \omega_s \omega_e}} (a_s^\dagger + a_s)(a_e^\dagger + a_e)
 \end{aligned}$$

where the dimensionless phase φ_x is defined as Φ_x/Φ_0 . Using this form, the system Hamiltonian may be solved for the eigenvalues and the eigenstates, so

that they may be used as a basis for the master equation approach, with a numerical approach, though a truncation will be needed.

In order to solve the system Hamiltonian, one should take the harmonic oscillator states as the basis. By doing so, the diagonal elements of the Hamiltonian matrix will have elements $H_{nn} = \hbar\omega_s(n + 1/2)$. The second contribution to the matrix would come from the term with cosine, and have non-diagonal elements due to the x_s term. As we define the parameters $\hbar\nu$ as β and $\frac{2\pi}{\Phi_0}\sqrt{\frac{\hbar}{C_s\omega_s}}$ as γ' , knowing that the dimensionless operator x_s is defined as $(a_s^\dagger + a_s)/\sqrt{2}$, the non-diagonal terms of the matrix will arise from the term

$$-\beta \cos\left(\frac{\gamma'(a_s^\dagger + a_s)}{\sqrt{2}} + 2\pi\varphi_x\right). \quad (3.32)$$

As we further use the trigonometric sum rule $\cos(A + B) = \cos(A)\cos(B) - \sin(A)\sin(B)$, we may further simplify the term to

$$-\beta \left\{ \cos\left(\frac{\gamma'(a_s^\dagger + a_s)}{\sqrt{2}}\right) \cos(2\pi\varphi_x) - \sin\left(\frac{\gamma'(a_s^\dagger + a_s)}{\sqrt{2}}\right) \sin(2\pi\varphi_x) \right\}. \quad (3.33)$$

In the next step of evaluating the terms, we can express the cos and sin terms with the system operators as

$$\cos\left(\frac{\gamma'(a_s^\dagger + a_s)}{\sqrt{2}}\right) = \text{Re} \left[\exp\left(i\frac{\gamma'(a_s^\dagger + a_s)}{\sqrt{2}}\right) \right] \quad (3.34)$$

$$\sin\left(\frac{\gamma'(a_s^\dagger + a_s)}{\sqrt{2}}\right) = \text{Im} \left[\exp\left(i\frac{\gamma'(a_s^\dagger + a_s)}{\sqrt{2}}\right) \right]. \quad (3.35)$$

Further, as we make use of the Baker-Hausdorff Lemma, that states

$$\exp(A)\exp(B) = \exp(A + B)\exp\left(\frac{[A, B]}{2}\right) \quad (3.36)$$

if the operators A and B commute with the commutator $[A, B]$, which in our case, holds, since $[a_s^\dagger, a_s] = -1$ and a constant commutes with any operator. In order to find the non-diagonal terms, one needs to evaluate the term

$$\exp(-\gamma^2/2)\langle n | \exp(i\gamma a_s^\dagger) \exp(i\gamma a_s) | m \rangle \quad (3.37)$$

and multiply the real and imaginary parts of this expression by $\cos(2\pi\varphi_x)$ and $\sin(2\pi\varphi)$ respectively. Here, $\gamma = \gamma/\sqrt{2}$, $\langle n|$ and $|m\rangle$ are the harmonic oscillator eigenstates. The term in Eq. 3. 37 further expands as

$$\exp(-\gamma^2/2) \sum_{l=0}^N \frac{(i\gamma)^l}{l!} \langle n|(a_s^\dagger)^l \sum_{k=0}^N \frac{(i\gamma)^k}{k!} (a_s)^k |m\rangle \quad (3. 38)$$

where N is the truncation limit of the system. This equation further turns into

$$\exp(-\gamma^2/2) \sum_{l=0}^m \frac{(i\gamma)^l}{l!} \langle n-l| \sqrt{\frac{n!}{(n-l)!}} \sum_{k=0}^m \frac{(i\gamma)^k}{k!} \sqrt{\frac{m!}{(m-k)!}} |m-k\rangle \quad (3. 39)$$

and the inner product in this term reduces to the delta function $\delta_{n-l,m-k}$ and cancels out one of the summations, due to the orthogonality of the eigenstates.

Obtaining the full system Hamiltonian, both diagonal and non-diagonal parts, and diagonalizing it numerically with the help of a numerical Lapack subroutine, we may inspect the role of the two main parameters γ and β in the eigenvalues and eigenfunctions. There is also a third parameter, φ_x , which depends on the external flux. The role of this parameter is to define the symmetry of the system potential. As we consider the total potential of the system, including the harmonic oscillator potential and the cosine term, it is in the form

$$V(x_s) = \frac{\alpha x_s^2}{2} - \beta \cos(\gamma x_s + 2\pi\varphi_x). \quad (3. 40)$$

Here, as the parameter φ_x is 0.5, meaning the external flux is half the flux quanta, the cosine term remains even, as well as the harmonic potential. This results in a symmetric double-well potential. However, for different values of φ_x in the range from 0 to 1, the cosine term is no longer even, and the resulting potential is asymmetric. For the symmetric case, as we inspect the derivative of the potential, to find the minima of the potential, we see that for two minima, which result in double-well potential, β should remain small compared to $5\alpha\pi/2$, where α is on the order of the harmonic frequency. The higher levels just see a harmonic potential weakly modulated by a cosine term. The β parameter defines the barrier between the double-wells, and the γ parameter defines the width of these wells.

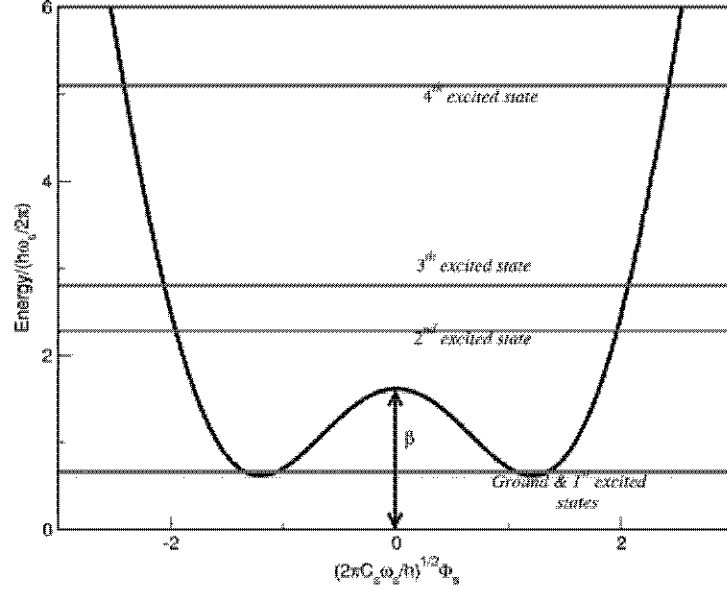


Figure 3. 6: The potential and low lying energy eigenvalues, for a specific single degenerate case. Here the parameters are $\beta \simeq 1.616$ and $\gamma \simeq 1.753$. The axes are normalized and dimensionless.

For the symmetric potential, which exhibits interesting results, it is possible to manipulate the parameters β and γ so that the eigenenergies of the system may be configured freely. An interesting case would be to choose the parameters so that the lowest lying two levels, i.e. ground state energy and first excited state energy, are degenerate. As a degeneracy parameter η for a two level system is defined as

$$\eta_{sd}^{(2)} = \frac{E_0 + E_1}{E_1 - E_0} \quad (3. 41)$$

and for a multileveled system as

$$\eta_{sd}^{(N)} = \frac{E_2 - E_1}{E_1 - E_0} \quad (3. 42)$$

it is possible to obtain $\eta_{sd}^{(2)}$ and $\eta_{sd}^{(N)}$ on the order of 10^7 . Such a set of parameters and the relevant energy levels are displayed on Fig. 3. 6. Also interesting features arise when the system is configured so that the lowest two levels, and the next two levels above them are degenerate in each-other. We name such a case as double-degeneracy. Here, definition of another degeneracy parameter is needed

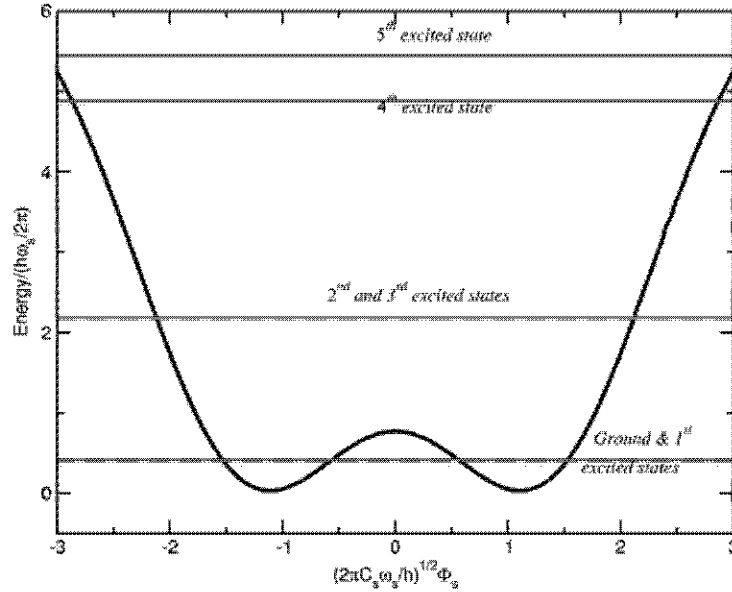


Figure 3. 7: The potential and low lying energy eigenvalues, for a specific double degenerate case. Here the parameters are $\beta \simeq 0.772$ and $\gamma \simeq 2.187$. The axes are normalized and dimensionless.

as

$$\eta_{dd}^{(N)} = \frac{E_4 - E_3}{E_3 - E_2}. \quad (3. 43)$$

It is also possible to obtain the degeneracy parameters $\eta_{sd}^{(2)}$ and $\eta_{dd}^{(N)}$ on the order of 10^6 for different set of $\beta - \gamma$ parameters. Again, a sample case with eigenvalues is displayed in Fig. 3. 7.

In the next chapter, the evolution of these system states will be considered and calculated in the presence of the non-classical electromagnetic field, as modeled in Eq. 3. 32.

Chapter 4

Noise and decoherence of the system

In this chapter, we will go one step further from the last chapter, by inserting the system-environment interaction into the system defined in the previous chapter. So this will be the final step in reaching the decoherence solution that we have sought.

In the next section, we will solve the SQUID-EM field model, introduced and described in the previous chapter, using the methodology described in the second chapter. During this solution, the important parameters of this system and the environment, i.e. the spectral properties will be revealed. Next we will investigate the effect of the environmental spectrum on decoherence, introduce the spectral models, and try to identify the effect of each spectral parameter, both in short and long time limits. As there are several parameters concerning the environmental spectrum, this will be a somewhat tedious work, and the analysis will be mainly qualitative. Though after the reader gets acquainted with the spectral effects, the quantitative analysis will take place in the next chapter. The system parameters will also be discussed in the next chapter, along with the discussion of the 2LA.

4.1 Decoherence in SQUID-EM field model

The solution of the model that is introduced in section 3.2.3 will be very similar to the one that is gone through in section 2.2.5. However we will try to avoid the approximations as far as we can. Namely, we will not be using Rotating wave approximation or the Markov approximation. However, in order to obtain a solvable master equation form, we will be using the Born-Oppenheimer approximation. As BOA is safe in the short time scales where the back reaction of the system on the environment is negligible. The short times are defined as to be shorter than the environmental equilibration time. A detailed discussion on the safety of BOA will be held in the next chapter.

Remembering the most simple master equation in the interaction picture that is given in Eq. 2. 53, we will need the interaction part of the Hamiltonian in Eq (3.31) in the interaction picture. There is also another term used in the interaction Hamiltonian conventionally, for compensation of the frequency renormalization effects on the system induced by the H_{int} used. Our formulation does not include this compensating term, and the reasons are discussed in Appendix A. For the simplicity in analytical progress, we express the coordinate-coordinate coupling between environment and system in Eq. 3.31 as⁴⁸

$$H_{int} = \frac{\alpha}{2} \sum_{r,s=0}^{N-1} (\varphi)_{sr} |\zeta, s\rangle \langle \zeta, r| \varphi_e \quad (4. 1)$$

where α defines the coupling strength and the symbol ζ symbolizes the relevant parameters defining the system, such as the height of the potential barrier between the wells, the bias that tilts the wells, Josephson energy or harmonic frequency. Here, the outer product of the system states $|r\rangle$ and $|s\rangle$ defines the transition from state $|r\rangle$ to state $|s\rangle$ where r might be an energetically lower or higher state than s . The system coordinate φ_s , which is an x-like coordinate, also permits transitions to both higher and lower states at the same time. There is also the noise induced dipole matrix elements $(\varphi)_{sr}$ that are described as

$$(\varphi)_{sr} = \langle \zeta, s | \varphi | \zeta, r \rangle. \quad (4. 2)$$

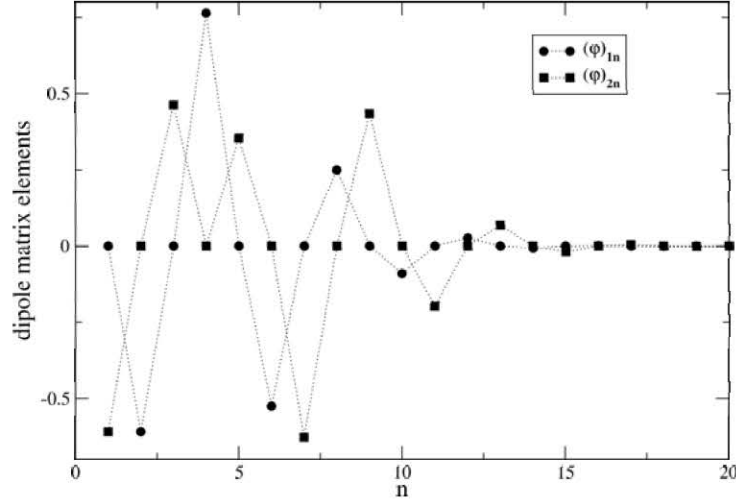


Figure 4. 1: The dipole matrix elements defining the transitions from ground and first excited state for a specific single degenerate case. Here the parameters are $\beta \simeq 1.616$ and $\gamma \simeq 1.753$. Here, the potential wells are symmetric with $\varphi_x = 0.5$

These noise induced dipole matrix elements are one of the key variables in the decoherence mechanism. They describe the weight of the transitions from one system state to another. As we take the symmetric configuration of the double well potential, the dipole matrix elements $(\varphi)_{sr}$ turns out to be zero where $r + s = \text{even}$, i.e. both of the states have even or odd parity, due to the parity rules. There are finite dipole matrix elements between the even and odd states. (Fig. 4. 1) However, as the potential is tilted with an external phase φ_x and asymmetric double-well is formed, the system states will have mixed parities, and as a result, the dipole matrix elements will have finite values for all possible transitions. (Fig. 4. 2). Eventually for any case, as the states become energetically highly separated, these dipole matrix elements tend to drop to zero. These facts become important when considering a multi-level system, and will be revisited in the next chapter.

In the next step we will be dealing with the environmental part of the interaction Hamiltonian. The environment may be considered as harmonic oscillator modes with different energies. Considering the master equation expanded to second order as given in Eq. 2. 55, the next step is modified as

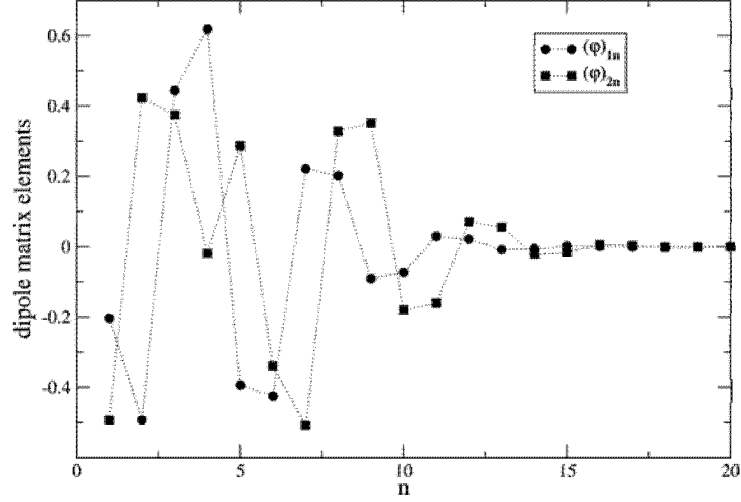


Figure 4. 2: The dipole matrix elements defining the transitions from ground and first excited state for a specific single degenerate case. Here the parameters are $\beta \simeq 1.616$ and $\gamma \simeq 1.753$. Here, the potential wells are asymmetric with $\varphi_x = 0.6$

follows:

$$\dot{\rho}(t) = - \int_0^t Tr_e \left[\left(\frac{\alpha}{2} \sum_{r,s=0}^{N-1} (\varphi)_{sr}(t) |\zeta, s(t)\rangle \langle \zeta, r(t)| \varphi_e(t) \right) \right. \\ \left. \left[\frac{\alpha}{2} \sum_{p,q=0}^{N-1} (\varphi)_{pq}(t') |\zeta, p(t')\rangle \langle \zeta, q(t')| \varphi_e(t'), \rho_e(0) \otimes \rho(t') \right] \right] dt'. \quad (4. 3)$$

Here, the density matrix for the system is expressed as $\rho(t)$ and the environmental density matrix is expressed as $\rho_e(t)$. Whenever the total density matrix will be used, we will be using the notation $\rho_T(t) = \rho(t) \otimes \rho_e(t)$ or rather $\rho_T(t) = \rho(t) \otimes \rho_e(0)$. As we express the environmental coordinate φ_e as

$$\varphi_e = \sum_k \eta_k (b_k^\dagger + b_k) \quad (4. 4)$$

where the operators b_k are the environmental raising and lowering operators, and the factor η_k describes the coupling strength of the relevant environmental mode k . Inserting this form into the Eq. 4. 4, and ignoring the parameter set ζ for clarity, we obtain

$$\dot{\rho}(t) = \frac{-\alpha^2}{2} \int_0^t \sum_{k,k'} \sum_{p,q,r,s=0}^{N-1} \eta_k \eta_{k'}(\varphi)_{sr}(t)(\varphi)_{pq}(t') \times \quad (4.5)$$

$$\text{Tr}_e \left[|s(t)\rangle\langle r(t)| (b_k^\dagger(t) + b_k(t)), \left[|p(t')\rangle\langle q(t')| (b_{k'}^\dagger(t') + b_{k'}(t')), \rho_e(0) \otimes \rho(t') \right] \right] dt'$$

which expands as

$$\dot{\rho}(t) = \frac{-\alpha^2}{2} \int_0^t \sum_{k,k'} \sum_{p,q,r,s=0}^{N-1} \eta_k \eta_{k'}(\varphi)_{sr}(t)(\varphi)_{pq}(t') \times \quad (4.6)$$

$$\left[|s(t)\rangle\langle r(t)|p(t')\rangle\langle q(t')|\rho(t')\text{Tr}_e \left((b_k^\dagger(t) + b_k(t))(b_{k'}^\dagger(t') + b_{k'}(t'))\rho_e(0) \right) \right.$$

$$- |s(t)\rangle\langle r(t)|\rho(t')|p(t')\rangle\langle q(t')|\text{Tr}_e \left((b_k^\dagger(t) + b_k(t))\rho_e(0)(b_{k'}^\dagger(t') + b_{k'}(t')) \right)$$

$$- |p(t')\rangle\langle q(t')|\rho(t')|s(t)\rangle\langle r(t)|\text{Tr}_e \left((b_{k'}^\dagger(t') + b_{k'}(t'))\rho_e(0)(b_k^\dagger(t) + b_k(t)) \right)$$

$$\left. + \rho(t')|p(t')\rangle\langle q(t')|s(t)\rangle\langle r(t)|\text{Tr}_e \left(\rho_e(0)(b_{k'}^\dagger(t') + b_{k'}(t'))(b_k^\dagger(t) + b_k(t)) \right) \right]$$

The trace operations over the environmental spectrum will turn out to be the averages of the relevant operator products over the initial environmental collective state, as we are taking the environment to be stationary in time. As we are taking the expectation over a fixed state, we safely neglect the expectations of two annihilation or two creation operators. Furthermore, the two environmental mode indices k and k' should be identical to obtain a non-zero contribution. The inner products of the system states also reduce to Kronecker-delta functions as we take out their time dependence out. In order to clarify the master equation further, we can check the time derivative of the individual matrix elements and obtain their relation to the other matrix elements as

$$\dot{\rho}_{kl}(t) = \frac{-\alpha^2}{2} \int_0^t \sum_k \sum_{p,q,r,s=0}^{N-1} \eta_k^2(\varphi)_{sr}(t)(\varphi)_{pq}(t') \times \quad (4.7)$$

$$\left[\delta_{k,s} \delta_{r,p} \rho_{q,l}(t') \left(\langle b_k^\dagger(t) b_k(t') \rangle + \langle b_k(t) b_k^\dagger(t') \rangle \right) \right]$$

$$\begin{aligned}
& - \delta_{k,s}\rho_{r,p}(t')\delta_{q,l} \left(\langle b_k^\dagger(t')b_k(t) \rangle + \langle b_k(t)b_k^\dagger(t') \rangle \right) \\
& - \delta_{k,p}\rho_{q,s}(t')\delta_{r,l} \left(\langle b_k^\dagger(t)b_k(t') \rangle + \langle b_k(t')b_k^\dagger(t) \rangle \right) \\
& + \rho_{k,p}(t')\delta_{q,s}\delta_{r,l} \left(\langle b_k^\dagger(t')b_k(t) \rangle + \langle b_k(t)b_k^\dagger(t') \rangle \right)
\end{aligned}$$

where the dipole matrix elements include the time dependence of the states as

$$(\varphi)_{sr}(t) = (\varphi)_{sr} \exp(-i(E_s - E_r)t) \quad (4. 8)$$

$$(\varphi)_{pq}(t') = (\varphi)_{pq} \exp(-i(E_p - E_q)t'). \quad (4. 9)$$

We can also simplify the environmental part of the master equation further by using an environmental spectral model to define the coupling strength of the environmental modes to the system. Although the environmental modes are represented as discrete modes, for the sake of reality, we will treat the environment to be a continuous bath, so the sum over the environmental mode index k will turn into an integral over the environmental mode frequency ω .

Throughout our calculations, we will be using different environmental models. Firstly we will use a realistic model as

$$\sum_k \eta_k^2 \Rightarrow I(\omega) = \omega^{1+\nu} \exp(-\omega^2/4\Lambda^2) \coth \frac{\omega}{2T}. \quad (4. 10)$$

This type of spectrum is used widely in the decoherence calculations,⁴ where the first power term characterizes the low frequency regime of the spectrum, and the second exponential part characterizes the high frequency regime. The parameter ν defines the spectral character, so that for $\nu = 0$ we have an ohmic spectrum, for $\nu < 0$ we have a sub-ohmic and for $\nu > 0$ we have a super-ohmic spectrum. These names are used conventionally to describe how the spectrum is dependent on the frequency. A Gaussian cut-off frequency Λ is used to limit the high frequency regime realistically. The coth term comes as a thermal enhancement, due to the $2n_\omega + 1$ factor comes from the expectation values of the environmental operators as we treat the environment as a bosonic bath. In order to understand the behavior

of this spectral function better, one can examine Fig. 4. 3. The parameter Λ in a way defines the width of the spectrum. As for the amplitude of the spectrum, all parameters Λ, ν, T are effective. T amplifies the amplitude independently, whereas for higher Λ as the cut-off is effective at higher frequencies, so for ohmic and super-ohmic parts, the spectrum amplitude has more room to increase.

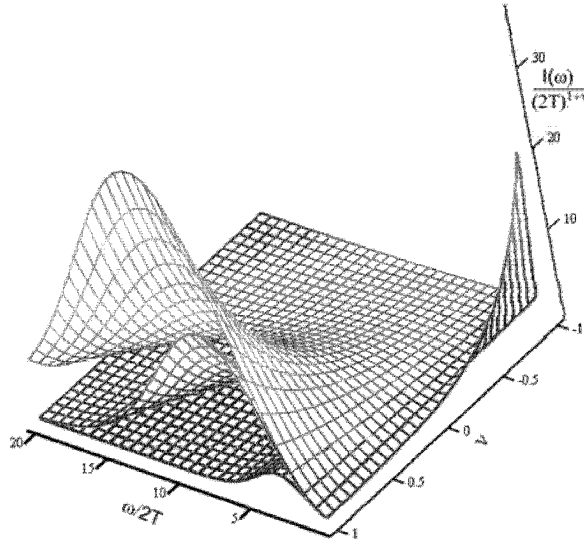


Figure 4. 3: The variation of the spectral function $I(\omega)$ versus ω and ν for $-1 \leq \nu \leq 1$ and parametrized as $\Lambda/T = 10, 50, 100$ from the innermost to the outermost surfaces respectively.

Another widely used spectral model in our calculations is a Lorentzian spectral model. Although the power-law spectral model is quite realistic and has plenty of parameters to manipulate, it is not flexible enough. As we try to investigate the effects of different parts of the spectrum, while isolating and nullifying the rest, a power-law spectrum is not very suitable. As a result we also used a toy spectrum model as

$$I(\omega) = \frac{A}{\pi} \frac{\epsilon^2}{(\omega - \omega_0)^2 + \epsilon^2} \quad (4. 11)$$

where the parameter A defines the total area under the spectrum, ω_0 defines the center of the spectrum and ϵ defines the width of the spectrum. As a result we

can manipulate the width, height, and location of the spectrum independently with this spectral function (Fig.4. 4).

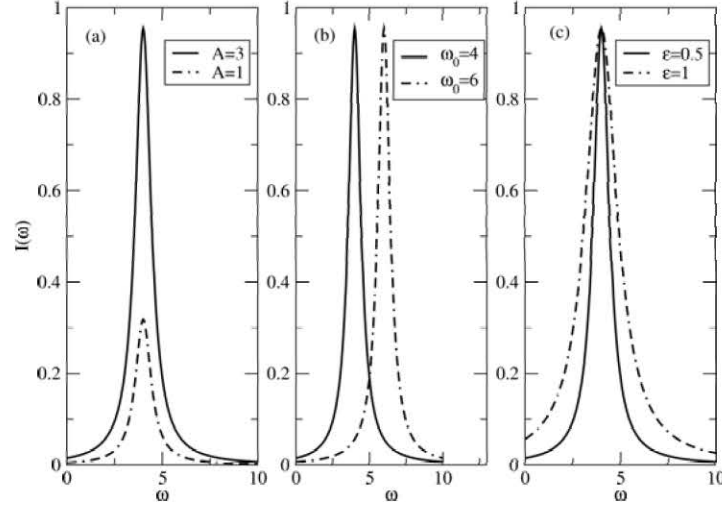


Figure 4. 4: The variation of the spectral function $I(\omega)$ versus ω for Lorentzian spectrum. In (a), $\epsilon = 0.5$ and $\omega_0 = 4$ are fixed parameters whereas A changes. In (b), $\epsilon = 0.5$ and $A = 3$ are fixed parameters and ω_0 changes. In (c), $\omega_0 = 4$ and $A = 3$ are fixed parameters and ϵ changes.

This Lorentzian spectrum is quite useful in observing the non-resonant effects of the environment as we can locate the spectrum at a resonant frequency or non-resonant frequency quite precisely. The results will be discussed in the following sections.

In order to calculate the time dependence of specific reduced density matrix elements, we will continue from Eq. 4. 8. Due to the two Kronecker-delta functions for each term, the summation over four indices drop to two indices and the sum over the environmental mod index k turns into an integral over environmental frequency ω in order to obtain a more realistic continuous model. The remaining master equation for the reduced density matrix may be shown most simply as

$$\dot{\rho}_{kl}(t) = - \int_0^t dt' \sum_{rs} K_{rs}^{kl}(t, t') \rho_{rs}(t') \quad (4. 12)$$

where the kernel $K_{rs}^{kl}(t, t')$ is similar to the Bloch-Redfield tensor as given in Eq. 2.72, though as it includes both time indices, it is free of the Markov approximation. The open form of this kernel is written as

$$\begin{aligned} K_{rs}^{kl}(t, t') &= \{ \mathcal{F}(t-t') [(\varphi(t)\varphi(t'))_{kr} \delta_{s,l} - (\varphi(t'))_{kr} (\varphi(t))_{sm}] \\ &+ \mathcal{F}^*(t-t') [(\varphi(t')\varphi(t))_{sl} \delta_{r,k} - (\varphi(t))_{kr} (\varphi(t'))_{sm}] \}. \end{aligned} \quad (4.13)$$

Here, the function $\mathcal{F}(t-t')$ is the complex noise correlation function, and defined as⁵⁰

$$\begin{aligned} \mathcal{F}(t-t') &= Tr_e [\varphi_e(t)\varphi_e(t')\rho_e(0)] = \langle \varphi_e(t)\varphi_e(t') \rangle \\ &= \int_0^\infty d\omega I(\omega) \coth(\omega/2T) \exp(-i\omega(t-t')) \end{aligned} \quad (4.14)$$

with the conjugation

$$\mathcal{F}(t-t') = \mathcal{F}^*(t'-t). \quad (4.15)$$

Note that the noise correlation function has two time indices, which indicates it's non-Markovian nature. The non-Markovian reservoirs have also been a point of interest recently,⁵¹⁻⁵³ and as it gives more realistic results, we avoid the Markov approximation in our calculations. The terms $\varphi(t)$ are defined as

$$\varphi(t) = \sum_{k,l=0}^{N-1} (\varphi)_{kl} \exp(-i(E_k - E_l)t) |k\rangle\langle l| \quad (4.16)$$

where N is the truncation limit and $(\varphi)_{kl}$ are the dipole matrix elements as defined in Eq. 4.2.

The calculation of the time evolution of the reduced density matrix is trivial from this point. We perform a numerical nonadaptive Euler algorithm⁴⁸ where we use an infinitesimal time increment dt . The elements of the reduced density matrix are calculated one by one with the help of simple equation

$$\rho_{kl}(t) = \rho_{kl}(0) + \int_0^t \dot{\rho}_{kl}(t) = \rho_{kl}(0) - \int_0^t dt' \sum_{r,s}^{(s)} K_{rs}^{kl}(t, t') \rho_{rs}(t') \quad (4.17)$$

During the evolution calculation, time is increased discretely from zero by dt steps. More clearly, first $\rho_{kl}^{(s)}(dt)$ is calculated using the kernel $K_{rs}^{kl}(dt, 0)$ and the reduced density matrix $\rho_{rs}^{(s)}(0)$. In the next step, $\rho_{kl}^{(s)}(2dt)$ is calculated using the kernel values $K_{rs}^{kl}(2dt, dt)$ and $K_{rs}^{kl}(dt, 0)$ and their multiplications with the reduced density matrices $\rho_{kl}^{(s)}(dt)$ and $\rho_{kl}^{(s)}(0)$ respectively. The calculation continues like this, up to a finite time value $t = n \cdot dt$ where n is on the order of 10^4 . However this numerical calculation becomes costly in terms of time, as the dimension of the reduced density matrix, i.e. the truncation limit of the system is increased and the calculation is carried on up to longer times. The complexity increases with N^4 since the number of elements of which the time evolution to be calculated increases with N^2 and for each element, we need to calculate a sum with two indices running up to N . For instance the calculation of a 4 leveled system takes 16 times longer time than the calculation of a 2 leveled system. The complexity also increases with n^2 , i.e. the time required to calculate the evolution up to $t = 100/\omega_s$ takes 100 times more time to calculate the evolution up to $t = 10/\omega_s$, where ω_s is the harmonic frequency of the system, used to obtain normalized, dimensionless time parameter.

Next, we will be calculating the RDM evolution for various parameters involving the spectrum and system, and examine the effects of these parameters.

4.2 Spectral dependencies

In this section we will be examining the effects of spectral parameters on the decoherence mechanism of system. There are several parameters of a typical spectrum. We have been using two spectrum models throughout the calculations, so we will be inspecting the parameters of these spectral models. After going through the spectral parameters, we will focus on the system parameters in the

next chapter. Throughout this section, the system will be taken as a two level system, i.e. the truncation limit will be set to 2. Also the system will be set to a degenerate configuration, so the two levels will have almost the same energy. Finally, the initial state that the system is prepared will be a superposition state $|\psi(0)\rangle = a|0\rangle + b|1\rangle$ where $a^2 + b^2 = 1$. For convenience we choose $a = \sqrt{0.9}$ and $b = \sqrt{0.1}e^{i\pi/2}$.

4.2.1 Temperature

Temperature is common to all spectral models in thermal equilibrium, so we will be inspecting temperature first. As we are dealing with a bosonic environmental bath, we use the bosonic occupation factors at finite temperatures, and due to the $2n_\omega(T) + 1$ factor obtained in Eq. 4. 8, we have an effective hyperbolic cotangent function with argument $\omega/2T$, where the constants \hbar and k_B are taken as 1. The hyperbolic cotangent function goes to infinity as $\omega/2T$ approaches zero, and goes to 1 as $\omega/2T$ approaches infinity. So effectively, temperature brings an enhancement to the spectral form, and this enhancement is much more dominant at low frequencies than at high frequencies.

While justifying the 2LS approximation, low temperature constraint is highly relied upon, so that if the thermal energy is low enough, i.e. lower than the separation of the qubit subspace and higher levels, it is said that the system cannot have transitions to higher levels. We will be observing the effect of temperature for both spectral models, power-law type, and Lorentzian type. As we are also questioning the validity of the 2LS as well as some other approximations mentioned in Chapter 2, our further calculations will only have zero temperature. Therefore we will be working with ideal conditions for 2LS, and can check the validity of the approximation in the next chapter, more confidently.

First we will be inspecting the effects of temperature in the presence of a power-law spectrum. As we are using a 2LS, there are two main mechanisms that we can inspect, relaxation and dephasing. In the relaxation graphs, only $\rho_{11}(t)$ is plotted, as the reduced density matrix has a trace of 1, $\rho_{22}(t)$ is simply

$1 - \rho_{11}(t)$. As for the dephasing mechanism, $|\rho_{12}(t)|$ is plotted. As this value goes to zero, the reduced system loses its phase information. As we can see from Fig. 4. 5, which shows the relaxation pattern for different temperature values, as the temperature increases, the relaxation gains an oscillatory behavior on the overall, the higher the temperature, the higher the oscillation frequency. However as we closely observe the short time range, apart from the envelope of the oscillations which shows an exponential behavior, there is a Gaussian-like behavior range, and as the temperature increases, the relaxation becomes faster. For all temperature values, the diagonal elements of the density matrix goes to 0.5, the maximum entropy-minimum information limit. These data are obtained for a sub-ohmic spectrum ($\nu = -1$) for which the low frequency range of the spectrum is most dominant.

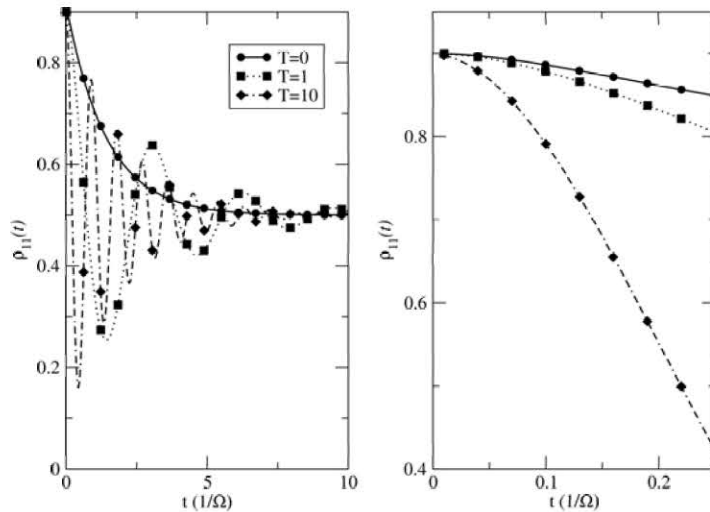


Figure 4. 5: The relaxation curves for a degenerate two level system, that is in interaction with a power-law type spectrum with $\Lambda = 10$ and $\nu = -1$ for various temperatures. On the left, we have a broader time range where time is normalized with an energy scale Ω , and on the right we observe closely the short time range.

As for the dephasing mechanism, we obtained Fig. 4. 6 for the same parameter set. As we are checking for a modulus, there seems to be a reflection-like behavior for higher temperatures from the axis $|\rho_{12}(t)| = 0$. The effect of temperature on

dephasing mechanism is very similar to the effect on relaxation mechanism. For both cases the temperature induces oscillatory behavior which has increasing frequency with increasing temperature. Moreover, the general behavior is also very similar, an exponential-like envelope function for oscillatory curves (the function itself is exponential-like, when there is no oscillation at $T = 0$), and Gaussian-like drop-off at short time ranges.

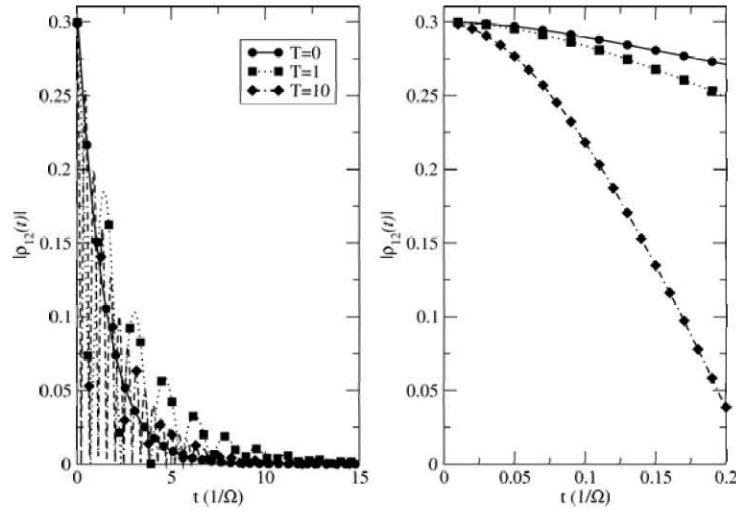


Figure 4. 6: The dephasing curves for a degenerate two level system, that is in interaction with a power-law type spectrum with $\Lambda = 10$ and $\nu = -1$ for various temperatures. On the left, we have a broader time range where time is normalized with harmonic frequency, and on the right we observe closely the short time range.

As we check the effect of finite temperatures for ohmic power-law spectra, we observe a similar behavior as shown for in Fig. 4. 7. The increasing temperature speeds up the decoherence processes both for relaxation and dephasing. However the oscillatory behavior observed in the sub-ohmic case is non-existent in the ohmic case.

Next, we check the simpler Lorentzian spectrum, just to be safe about the role of the temperature. The system is again set to be a degenerate two level system, and the Lorentzian spectrum parameters are chosen as $A = 3$, $\epsilon = 3$ and $\omega_0 = 5$. The relaxation pattern as shown in Fig. 4. 8 is very similar to the one

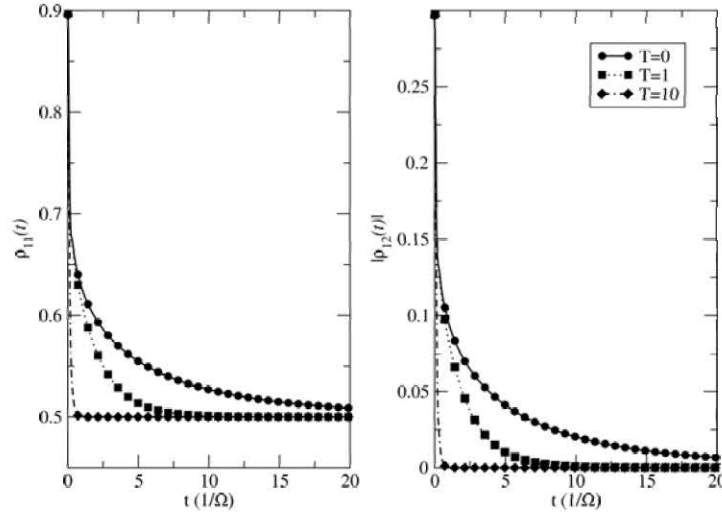


Figure 4. 7: The relaxation and dephasing curves for a degenerate two level system, that is in interaction with a power-law type spectrum with $\Lambda = 10$ and $\nu = 0$ for various temperatures.

in sub-ohmic power-law as well as the relaxation pattern as shown in Fig. 4. 9.

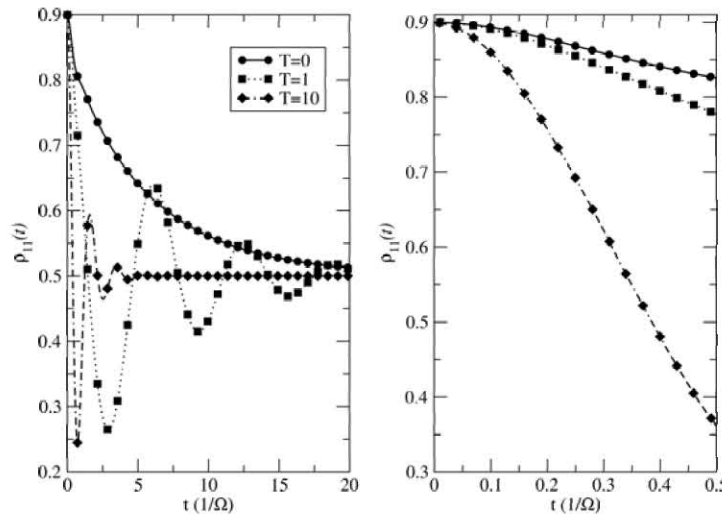


Figure 4. 8: The relaxation curves for a degenerate two level system, that is in interaction with a Lorentzian type spectrum with $A = 3$, $\epsilon = 3$ and $\omega_0 = 5$ for various temperatures. On the left side is the overall behavior where short time range is magnified on the right hand side.

As seen from the above figures, temperature indeed increases both relaxation

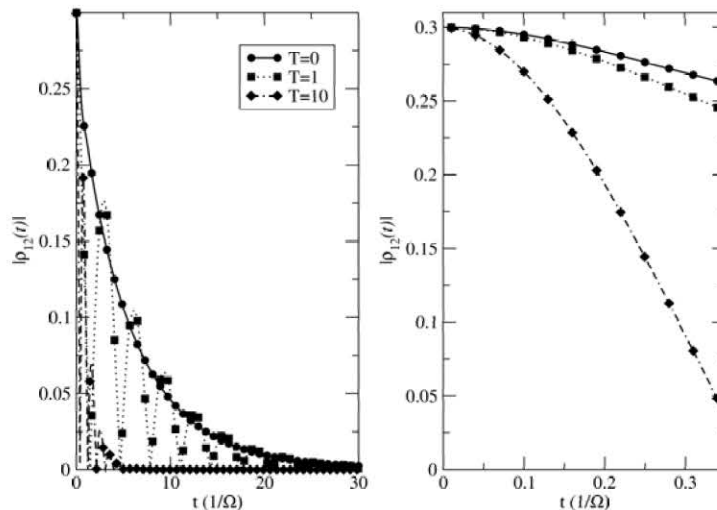


Figure 4. 9: The dephasing curves for a degenerate two level system, that is in interaction with a Lorentzian type spectrum with $A = 3$, $\epsilon = 3$ and $\omega_0 = 5$ for various temperatures. On the left side is the overall behavior where short time range is magnified on the right hand side.

and dephasing rates. The effect of temperature is not quantitatively investigated, but only qualitatively demonstrated. But it is observable that the relaxation and dephasing rates are finite for the 2LS even at $T = 0$. The finite relaxation rates also depend on the non-diagonal coupling between the system and the environment, i.e. the non-diagonal dipole matrix. There are also other approaches that are taking a diagonal coupling in order to observe just dephasing, without relaxation.⁵⁴ But recently there are other claims using realistic models on decoherence effects in mesoscopic systems^{55,56} as well as some experimental confirmations on the saturations of the RD rates at low temperatures.⁵⁷ Also theoretical studies have been made for zero temperature decoherence mechanisms.⁵⁸⁻⁶¹ In order to investigate the zero temperature decoherence and make a critique of 2LA, we will be using zero temperature calculations from now on, which is accepted as the ideal temperature for the two-level system approximation.

4.2.2 Ohmic dependencies

We will now check the effect of the character of the spectrum on relaxation and dephasing mechanisms. The system used, again, will be a degenerate two level system and the temperature will be taken zero. The cut-off frequency is taken as $\Lambda = 1$. As it is shown in Fig. 4. 10 for all characteristic ν values, we have oscillations over the time domain. The symbols in the figures are chosen so that the envelope function may be visualized easily. As we check the short times, we see that sub-ohmic spectrum is more slow in relaxation than the ohmic or super-ohmic spectra. However, the envelopes of the oscillations on the long time range, show a different behavior, so that the sub-ohmic envelope decays fastest, whereas the super-ohmic envelope decays slowest. As we return our attention to Eq. 4. 10 and Fig. 4. 3, we see that for sub-ohmic spectrum function with $\nu = -1$ the low frequency part of the spectrum is much more effective than the low frequency part in ohmic or super-ohmic spectra. On the other hand, for the super-ohmic spectrum with $\nu = 1$, the high frequency part of the spectrum is more pronounced than the others. Our system is a degenerate system (not exactly degenerate but the energy difference is on the order of 10^{-4}), so the resonant frequency to induce a transition between the two states is very close to zero. So on the long range, sub-ohmic spectrum is more effective, where resonant frequency is more pronounced, however, on the short range, super-ohmic spectrum (which has a greater total area) tends to relax the system faster. This behavior will be investigated more quantitatively in the next chapter.

As we check the relaxation pattern for the same parameter set as seen in Fig. 4. 11 we observe the same behavior as in the relaxation case qualitatively. The quantitative analysis will be presented in the next chapter.

4.2.3 Cut-off frequency

Next we will be checking the second parameter of the power-law spectrum, the Gaussian cut-off frequency Λ . Increasing Λ has two major effects on the spectrum. First, it increases the range of spectrum, as cut-off takes effect at

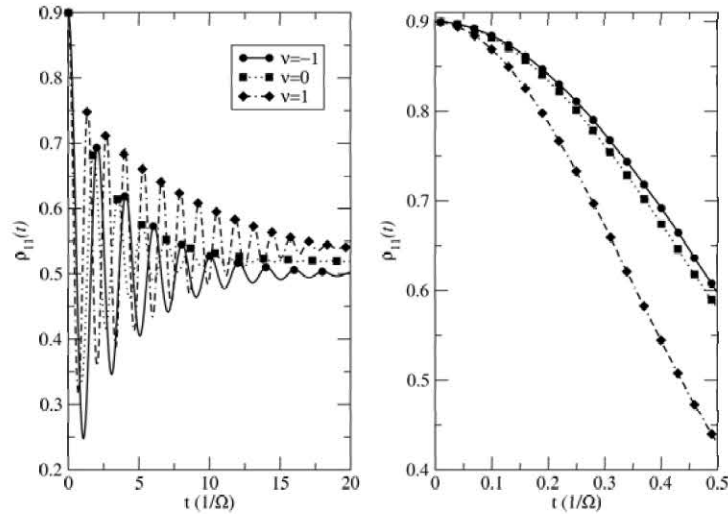


Figure 4. 10: The relaxation curves for a degenerate two level system, that is in interaction with a power-law type spectrum with $\Lambda = 1$, $T = 0$ for various ν values. On the left side is the overall behavior where short time range is magnified on the right hand side.

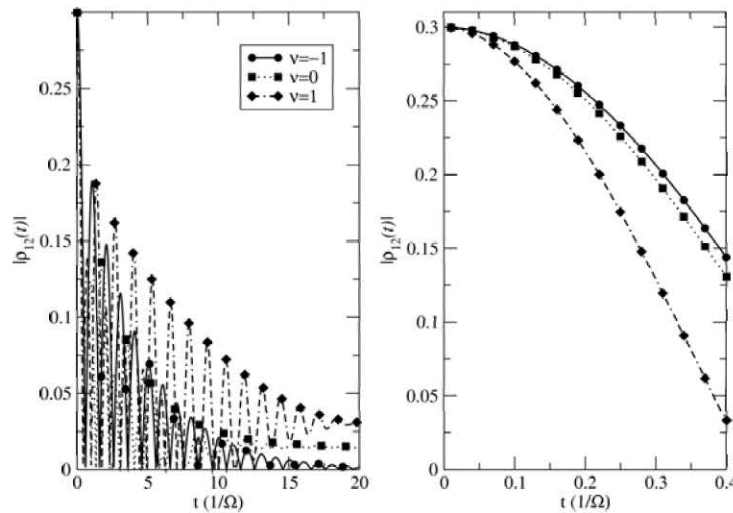


Figure 4. 11: The dephasing curves for a degenerate two level system, that is in interaction with a power-law type spectrum with $\Lambda = 1$, $T = -$ for various ν values. On the left side is the overall behavior where short time range is magnified on the right hand side.

higher frequencies, i.e. the spectral width is increases. Second, as the range is

increased, the spectrum finds more room to increase with the effect of power term without being majorly suppressed by the Gaussian cut-off. So increasing Λ increases both width and amplitude of the spectrum, regardless of the spectral characteristic, ν . As we check the relaxation curves in Fig. 4. 12, we see that for smaller Λ values, relaxation rates are smaller both in the short and long time ranges. Again the symbols on the left side are spaced so that the envelope of the oscillations may be observed easily.

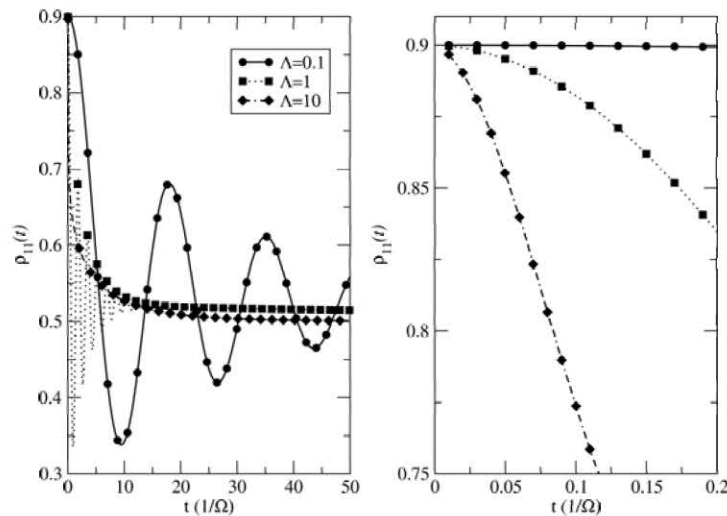


Figure 4. 12: The relaxation curves for a degenerate two level system, that is in interaction with a power-law type spectrum with $\nu = 0$, $T = 0$ for various Λ values. On the left side is the overall behavior where short time range is magnified on the right hand side.

As in the previous cases, dephasing shows no different behavior than the relaxation qualitatively, as shown in Fig. 4. 13.

4.2.4 Spectral center

We have checked the basic parameters of the realistic power-law spectrum. However power-law spectrum is not the best candidate to inspect the spectral parameters independently as increasing the cut-off frequency Λ both increases the width and the amplitude of the spectrum, or changing the characteristic ν

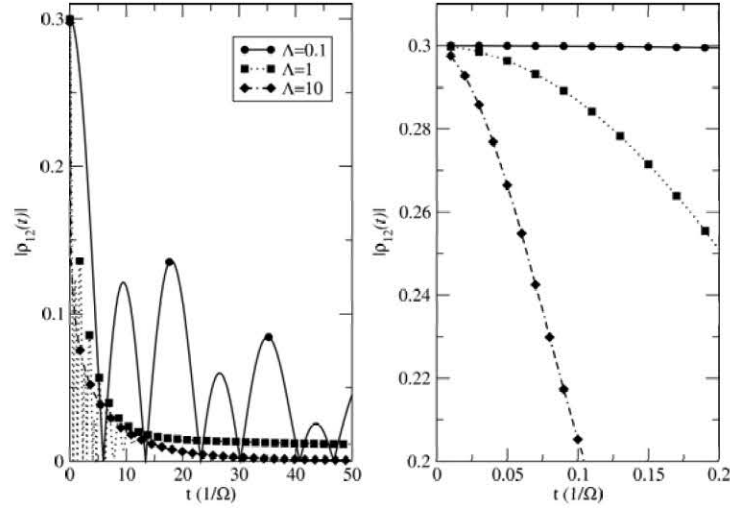


Figure 4. 13: The dephasing curves for a degenerate two level system, that is in interaction with a power-law type spectrum with $\nu = 0$, $T = 0$ for various Λ values. On the left side is the overall behavior where short time range is magnified on the right hand side.

value changes the low frequency and low frequency regimes independently. So we will be using a Lorentzian spectrum to check the effect of width, spectral location (also noted as spectral center ω_0) and spectral amplitude independently.

First we will be checking the effect of spectral center, i.e. ω_0 . We will be using the other two parameters fixed as $A = 3$ and $\epsilon = 3$. Changing the spectral center does not change the total area under the spectrum, as the height or the width of the spectrum remains unchanged. As we check in the long time range to the relaxation as shown in Fig. 4. 14, as the spectrum gets further away from the resonant frequency which is located very close to zero, i.e. as ω_0 is increased, the relaxation rates decrease in the long range. However as we check the short time behavior, we observe a different behavior from the rest of the parameters. For a short but noticeable time, the rates of the Gaussian-like relaxation are same, independent of the spectral location. So this also shows that there is a parallelism between the unchanged spectral area and unchanged Gaussian regime rates. This parallelism will also be discussed comprehensively in the next chapter.

Checking for the relaxation curves as presented in Fig. 4. 15 we observe the

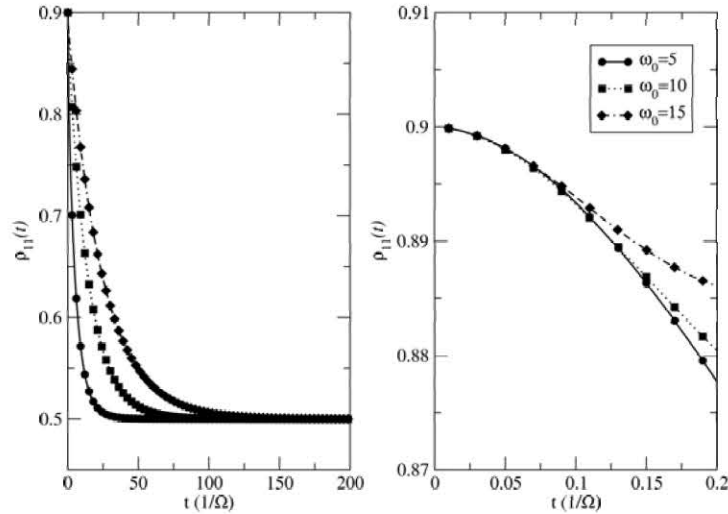


Figure 4. 14: The relaxation curves for a degenerate two level system, that is in interaction with a Lorentzian type spectrum with $A = 3$ and $\epsilon = 3$ for various ω_0 values. On the left side is the overall behavior where short time range is magnified on the right hand side.

same behavior, i.e. same rates at short times for all spectral locations, however, smaller rates for increasing center frequency.

4.2.5 Spectral width

Next we examine the effect of spectral width over the relaxation and dephasing. As we check the Lorentzian function we see that the width is directly proportional to the spectral area. As the amplitude is fixed, and the spectral location is irrelevant, increasing the spectral width does nothing except increasing the spectral area. As we see the relaxation in Fig. 4. 16 and dephasing in Fig. 4. 17 we see that for greater spectral width, the relaxation and dephasing rates at both short time and long time regimes are greater. This also gives us the hint about the role of total spectral area over the decoherence mechanisms.

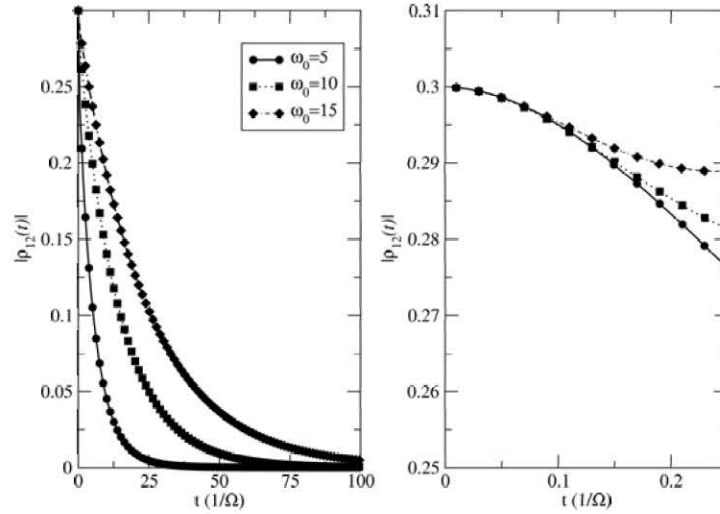


Figure 4. 15: The dephasing curves for a degenerate two level system, that is in interaction with a Lorentzian type spectrum with $A = 3$ and $\epsilon = 3$ for various $\omega_0 = 5$ values. On the left side is the overall behavior where short time range is magnified on the right hand side.

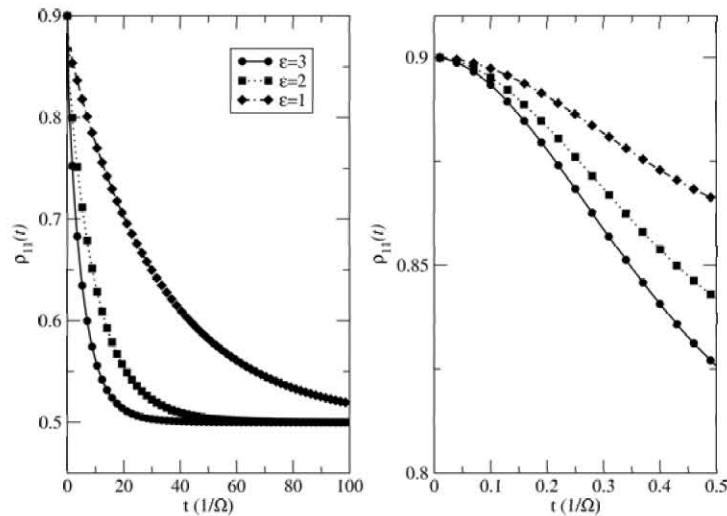


Figure 4. 16: The relaxation curves for a degenerate two level system, that is in interaction with a Lorentzian type spectrum with $A = 3$ and $\omega_0 = 5$ for various ϵ values. On the left side is the overall behavior where short time range is magnified on the right hand side.

4.2.6 Spectral amplitude

Spectral amplitude is indeed the most trivial parameter of the three. As the amplitude comes in front of the Lorentzian form as a factor, it can be taken out

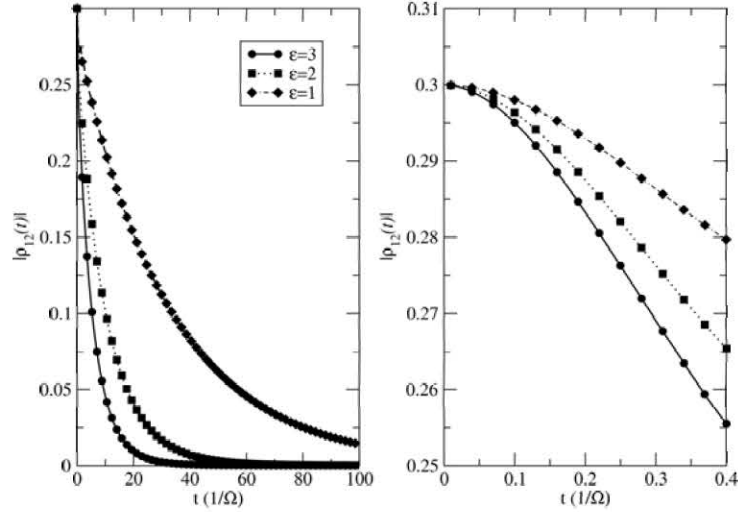


Figure 4. 17: The dephasing curves for a degenerate two level system, that is in interaction with a Lorentzian type spectrum with $A = 3$ and $\omega_0 = 5$ for various ϵ values. On the left side is the overall behavior where short time range is magnified on the right hand side.

of the integral in Eq. 4. 15, so that it can as well be assumed to be a factor of the coupling constant between the system and environment. Trivially, as the coupling constant increases, the decoherence becomes more prominent, over all the time range. As we see the effect of amplitude on relaxation in Fig. 4. 18 and on dephasing in Fig. 4. 19, we see that unsurprisingly, for higher A values, the relaxation and dephasing rates becomes higher.

As we have plenty of spectral parameters for both realistic and model spectrum functions, it is a bit tedious to investigate the effect of each parameter independent of the other parameters. In this chapter, we have inserted the environment into the SQUID-EM field model introduced and solved in the previous chapter, solved the master equation down to coupled integro-differential equations and observed the effects of the environmental parameters on the system qualitatively. In the next chapter, we will also check the role of system parameters and observe the advantages and disadvantages of different system configurations. Also there will be more quantitative analysis and the well-known 2LS approximation will be questioned in detail.

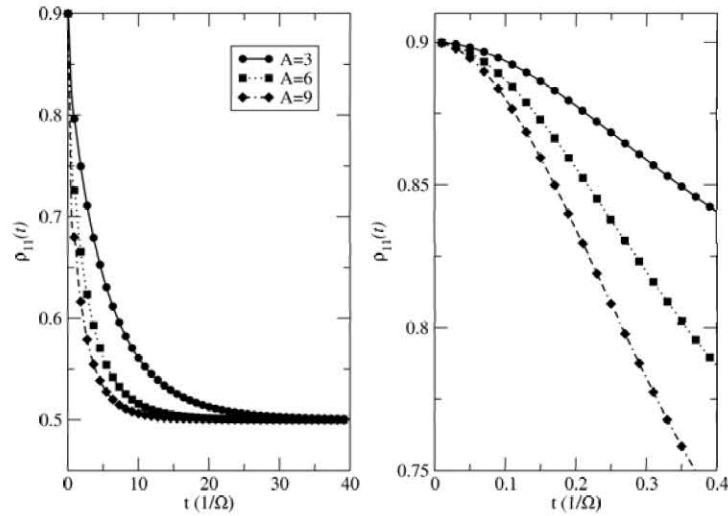


Figure 4. 18: The relaxation curves for a degenerate two level system, that is in interaction with a Lorentzian type spectrum with $\epsilon = 3$ and $\omega_0 = 5$ for various spectral amplitudes. On the left side is the overall behavior where short time range is magnified on the right hand side.

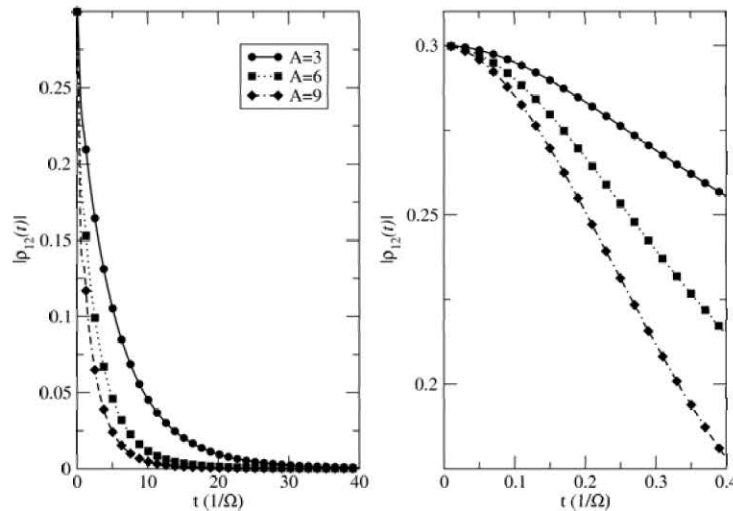


Figure 4. 19: The dephasing curves for a degenerate two level system, that is in interaction with a Lorentzian type spectrum with $\epsilon = 3$ and $\omega_0 = 5$ for various spectral amplitudes. On the left side is the overall behavior where short time range is magnified on the right hand side.

Chapter 5

Effects of Noise Parameters in Decoherence

While environment plays the most effective role in the decoherence mechanisms, the system parameters also effect the overall process. As we have explained in the previous chapter, the crucial variables of the system that enter the decoherence calculations are the system's energy eigenvalues, the dipole coupling matrix elements, and the truncation limit that defines the number of levels of the system explicitly.

The truncation limit is completely arbitrary, as we can choose any limit for a system, except for some manifestly N level systems such as spin systems, or some organic molecule that has certain discrete rotational symmetries. Although our focus is now on SQUID systems, which are systems with infinitely many states, so we are inserting a truncation limit. However, our truncation limit will be regarding the finite coupling range of the system levels as illustrated in Figs. 4. 1 and 4. 2.

We also presented a solution for a SQUID system in chapter 3, where we mentioned that by the appropriate choice of the potential parameters γ and β , we may obtain some special energy level configuration. We can even obtain a singly degenerate (where the ground state energy and the first excited state energy are same), or a doubly degenerate (where both ground and first excited,

and second-third excited states are degenerate separately) configurations. Of course the configurations are obtained by numerical search routines, and the degeneracies are not absolute though the degeneracy parameters as defined in Eqs. 3. 41, 3. 42 and 3. 43 can be as high as 10^6 . Although we haven't searched for every possible configuration, we believe that we have quite a lot of flexibility on preparing a SQUID system in MQC regime, in terms of energy eigenvalues.

The final crucial parameters are the environmentally induced dipole matrix elements as given in Eq. 4. 2. The matrix elements may have parity conservation if the potential is symmetric, so that the eigenstates show even and odd parities alternatingly, or the matrix may have no zero element in case of asymmetric potential as shown in Figs. 4. 1 and 4. 2. We also observed in these figures that, for a real SQUID system, the dipole matrix elements tend to decay to zero as the two indices are different from each other by an order of 10, i.e. as $n - m > 10$, $\varphi_{nm} = \varphi_{mn}$ tend to approach zero. This means that the direct coupling from ground state to $\sim 15^{th}$ excited state or above is negligible.

In the light of this information, we can as well define a toy system model, where we can freely manipulate the energy configurations or dipole coupling matrix elements.⁶² Of course we are not in pursuit of some marginally configured systems, but as we know the general behavior of the dipole matrix elements and that we can obtain eigenvalue configurations quite flexibly, it is simpler to use a toy system model. Throughout this chapter we will be using such a toy model, unless otherwise stated, for which the energy levels may be degenerate or simply non-degenerate. As for the dipole coupling matrix elements, we will be using a model such as

$$\varphi_{nr} = \begin{cases} \kappa e^{-|n-r|/R} & \text{if } n + r = \text{odd} \\ 0 & \text{if } n + r = \text{even} \end{cases} \quad (5. 1)$$

where R is the range of dipole couplings and κ defines the coupling strength. For compatibility with the SQUID system, we will be taking this range as $R = 10$. Note that this type of dipole coupling is for the symmetric potential wells, where parity selection rules are valid. For an asymmetric potential configuration, the condition will be necessary no more, and all the matrix elements will be finite

within the range.

There will be two main issues that we will probe, in this chapter. First, we will be comparing the decoherence rates of multileveled systems and 2LS, under the ideal 2LS conditions, and also investigate the leakage phenomenon, the third mechanism of decoherence. Second, we will be observing the effect of non-resonant transitions, which are often overlooked as compared to the resonant transitions. By combining the result of these two sections, we will be questioning the 2LS approximation, which is widely used since it has been proposed.⁶³

5.1 Decoherence rates at short and long times

The density matrix usually starts with a Gaussian-like time variation, as shown in detail in the previous chapter, unless the system-noise kernel is abruptly changing at short times, i.e. $t \rightarrow t'$. It should be remarked that those processes in the solution of Eq. 4. 12 with a finite first derivative surviving in the limit $t \rightarrow 0$ are necessarily Markovian with delta-function like correlations, i.e. $\mathcal{F}(t - t') \propto \delta(t - t')$. On the other hand, most physical noise sources display non-Markovian correlations at short times and the usual practice is to represent them by a power-Gaussian^{48,50} or power-exponential.^{2,3,24,13,26,28,27} The zero derivative of the density matrix elements at $t = 0$ is trivial, as from Eq. 4. 12, we have

$$\dot{\rho}_{kl}(0) = - \int_0^0 dt' \sum_{rs} K_{rs}^{kl}(0, t') \rho_{rs}(t') = 0. \quad (5. 2)$$

Therefore the leading term in the short time limit is the second time derivative given by

$$\frac{d^2}{dt^2} \rho_{kl}(t = 0) = - \sum_{rs} K_{rs}^{kl}(0, 0) \rho_{rs}(t = 0) \quad (5. 3)$$

provided at least one of the terms in the summation on the right-hand side is non-zero. It can also be checked by direct calculation that only the even derivatives of the reduced density matrix are non-zero at $t = 0$. Note that the Eq. 5. 3 is correct only at $t = 0$ and should not be interpreted as a differential equation at

vanishingly short times. The decohering density matrix therefore starts with a time evolution which is Gaussian-like as

$$\rho_{kl}(t) \simeq \sum_{rs} \left[\delta_{kr} \delta_{ls} - \frac{t^2}{2} K_{rs}^{kl}(0, 0) \right] \rho_{rs}(0). \quad (5. 4)$$

where the Gaussian decoherence rates $(\tau_{RDL}^{(G)})^{-1} = \Lambda_{RDL}^{(G)}$ enter as a sum over the square roots of the positive eigenvalues of a characteristic operator $\mathbf{K}(0, 0)$ representing the system-noise kernel. In appendix B, the positive definiteness of $\mathbf{K}(0, 0)$ and its relation to $K_{rs}^{kl}(0, 0)$ are demonstrated.

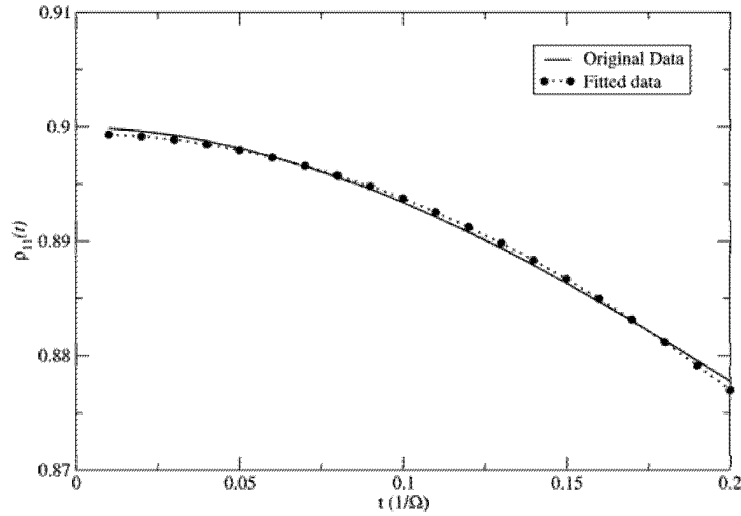


Figure 5. 1: The Gaussian decay fit to the RDM element $\rho_{11}(t)$ at short times, under the influence of a Lorentzian spectrum with spectral parameters $A = 3$, $\epsilon = 3$ and $\omega_0 = 5$. The system is taken as a degenerate 2LS.

As we fit a Gaussian-like decay to the short time ranges in the diagonal RDM element $\rho_{11}(t)$, so that

$$\rho_{11}(t) = 0.9 \exp(-t/\tau_R^{(G)})^2 \quad (5. 5)$$

where the term $\tau_R^{(G)}$ defines the Gaussian relaxation time at short time limit, and the factor 0.9 comes due to the initial state preparation, we obtain a good fit as shown in Fig. 5. 1. Only a candidate diagonal element is demonstrated, though the fit can be applied to all RDM curves, diagonal or non-diagonal, i.e. relaxation or dephasing, for any spectral parameter set. The relevant Gaussian decay rates

are obtained from these fits at short times. Though it should be noted that for the dephasing curves for our initial state choice of $|\psi(0)\rangle = \sqrt{0.9}|0\rangle + \sqrt{0.1}e^{i\pi/2}|1\rangle$, the factor before the fitting function should be 0.3 as it is the initial value of the non-diagonal element ρ_{12} .

As we have also showed in the previous chapter, for non-Markovian systems the exponential behavior can be reached after a significant decoherence has already taken place at short and intermediate times. Here we should also remark that, although a Lorentzian type noise spectrum has Markovian correlations in sufficiently long observational times, there are also physical spectra without a Markovian limit. For instance, the widely used Rubin model which represents a bosonic environment with Einstein phonons has power law dependence of the noise correlations at long times.⁴ This indicated that the long time decoherence, in contrast to the short time decoherence, depends on the type of physical process generating the spectrum.

Taking the same data as shown in Fig. 5. 1 and focusing on the long time range of it, we can fit the data to an exponential function as

$$\rho_{11}(t) = \xi \exp(-t/\tau_R^{(E)}) + 0.5 \quad (5. 6)$$

where $\tau_R^{(E)}$ defines the exponential relaxation time at the long time limit, and a factor of 0.5 is added as the exponential decay does not approach to 0, but rather to 0.5 as the informationless limit. The fitting to the data, as shown in Fig. 5. 2 is perfect. Just like the Gaussian decoherence fitting, exponential decoherence fitting may also be applied to non-diagonal elements in order to obtain dephasing times, though in that case, the final additive factor 0.5 would be absent as the dephasing curves decay to 0.

The decoherence times and rates, i.e. $\tau_{RD}^{(G,E)}$ and $(\tau_{RD}^{(G,E)})^{-1}$ can be obtained using the above methods, and the values obtained from now on, through-out this chapter will be calculated like this.

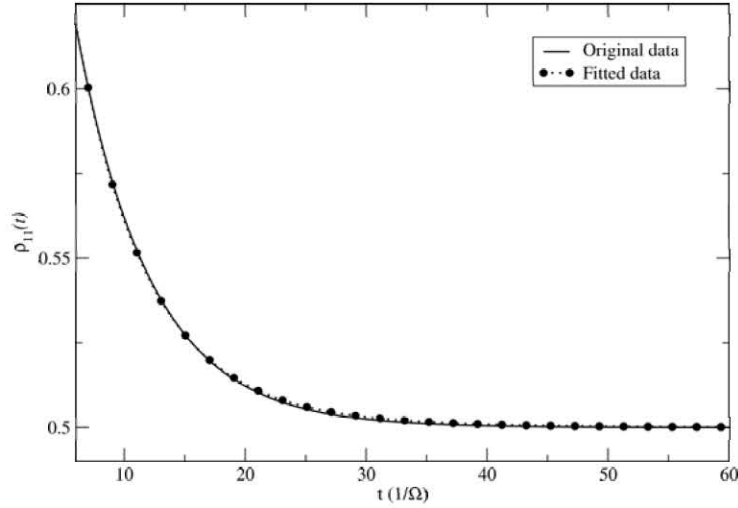


Figure 5. 2: The exponential decay fit to the RDM element $\rho_{11}(t)$ at short times, under the influence of a Lorentzian spectrum with spectral parameters $A = 3$, $\epsilon = 3$ and $\omega_0 = 5$. The system is taken as a degenerate 2LS.

5.2 Multilevel effects

The 2LA is the most commonly used approximation in the literature. However the validity of the approximation is not confirmed in most cases. As we recall the facts, the 2LA has, in its essence, three assumptions:

- (a) that the incoherent transitions caused by the environment in the system are generated by the resonant processes: implicit in the 2LA is the belief that the spectrum must have non-negligible couplings at the *right transition frequencies* at which the system makes transitions to higher levels;
- (b) at zero or sufficiently low temperatures there are no available environmental states to couple with the system. This assumption and the notion of the *right transition frequency* is basically tempting one to neglect all parts of the spectrum $\Delta E \leq \omega$ because of the long standing belief that at sufficiently low temperatures the interacting part of the spectrum is in the low energies $\omega \leq T \ll \Delta E$ of which coupling is believed to be suppressed by the low temperature;

(c) negligible leakage of the qubit subspace occupations to higher levels.

These three fundamental assumptions will be discussed in detail. First we will attempt to challenge the assumption (b). As we have mentioned earlier, in order to satisfy the low temperature condition for any system configuration, we will use zero temperature calculations. As assumed above, the relaxation and dephasing rates should not be effected by the number of levels, as there won't be any available environmental modes to assist the transition to higher levels.

In order to check this assumption, we increase the truncation limit N and calculate the relaxation and dephasing rates as a function of the total number of levels in the system. We focus our interest in the short time Gaussian rates, as they are more crucial than the long time exponential rates. The system experiences significant decoherence till the exponential decay governs the decoherence rates. We use the toy system model defined in this chapter with coupling strength $\kappa = 0.1$ and coupling range $R = 10$ with a singly degenerate configuration, where the lowest two levels are degenerate and higher levels have equally spaced energy values with $\Delta E_{n,n+1} = 1$ in terms of a fixed energy scale, like the one used for the SQUID model, i.e. the harmonic energy scale. The resulting relaxation and dephasing rates of the RDM element ρ_{11} as shown in Fig. 5. 3 show an increasing behavior. Also, as expected, the rates reach to a saturation as the number of levels go over 10. There is also a significant step-like behavior in the relaxation curve. This is also expected, as with the parity selection rules, the dipole matrix elements forbid transitions from odd levels to odd levels and from even levels to even levels. So adding a third level to the system does not increase the relaxation rate, since transition from ground state to this state is forbidden. A similar step-like behavior would be seen, if the relaxation rates of RDM element ρ_{22} were to be calculated, but the steps would not be between even-odd states but between odd-even states.

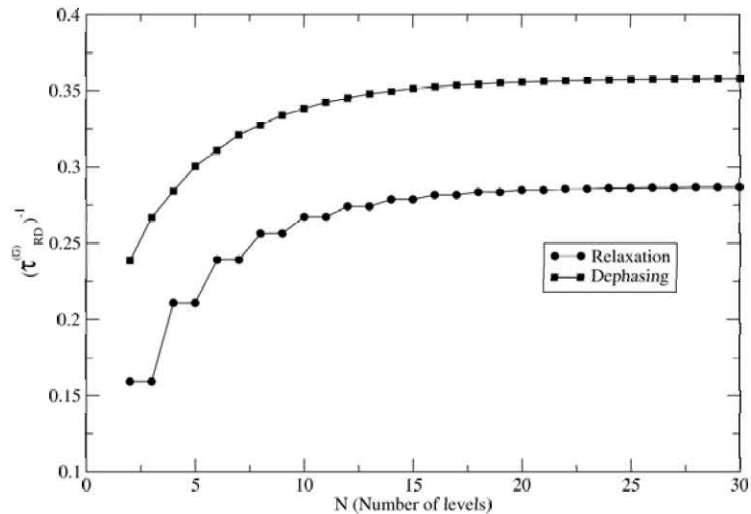


Figure 5. 3: The relaxation and dephasing rates for a degenerate two level system, that is in interaction with a Lorentzian type spectrum with $\epsilon = 0.1$, $\omega_0 = 1$ and $A = 1$. The coupling range is $R = 10$ and the coupling strength is $\kappa = 0.1$. The system is a singly degenerate system.

5.2.1 Leakage

As mentioned before, leakage is defined as the occupation of the states other than the qubit subspace, i.e. the ground state and the first excited state, as defined in Eq. 2. 21. It is often assumed to be zero as part of the 2LA, though this assumption has not been seriously questioned until recently. Counter-arguments against neglecting the leakage effects in the long time dynamics can be found for instance in the recent publications.^{19,64,65}

In order to examine the importance of leakage, we need to have a multilevel system by default. So as in the previous section, we calculate the leakage for different truncation limits, and the results are shown in Fig. 5. 4. As expected, the short time behavior of the leakage also shows Gaussian-like behavior and in the long time, the behavior turns into an exponential. Though the Gaussian and exponential forms are inverted.

As we calculate the Gaussian leakage rates $\tau_L^{(G)}$ for different truncation limits, we obtain Fig. 5. 5. Note that the calculated rates are on the order of the relaxation and dephasing rates as presented in Fig. 5. 3. This comparison shows

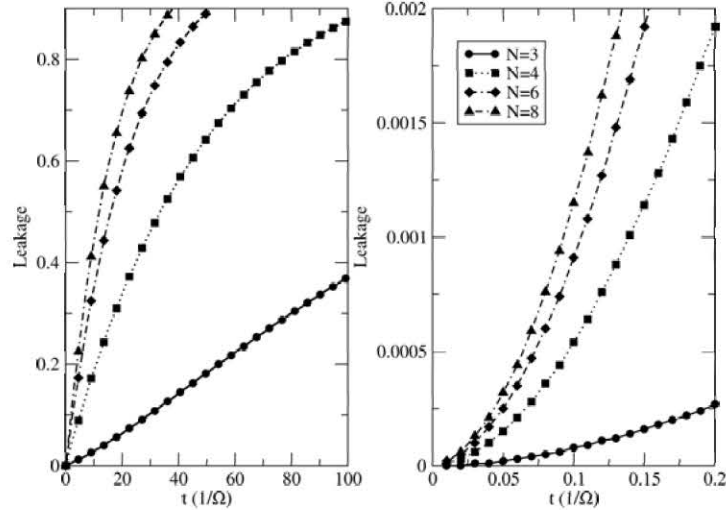


Figure 5. 4: The Leakage curves for multileveled systems in interaction with a Lorentzian spectrum with $A = 3$, $\omega_0 = 5$ and $\epsilon = 3$. The system has coupling range $R = 10$ and coupling strength $\kappa = 0.2$. On the left side we see the long time range whereas the short time range is focused on the right hand side.

us that, even at $T = 0$, the leakage is not a negligible phenomenon, and may effect the overall decoherence significantly. The effects of leakage will also be considered in the next chapter.

5.3 Nonresonant effects

Throughout the transition calculations in the literature and textbooks, the non-resonant transitions are often ignored. Due to a crucial difference between the resonant and non-resonant transitions, which is the energy conservation, it is usually more convenient to consider only the resonant transitions. In the non-resonant transitions, as the energy of the transition experienced by the system does not match the energy of the environmental process necessarily, these transitions occur in very short time scales, due to the uncertainty principle. The higher the energy difference, the shorter is the time to observe the transition. The rotating wave approximation discussed in Chapter 2 is used mainly to avoid the non-resonant terms. However, the effect of these non-resonant transitions are

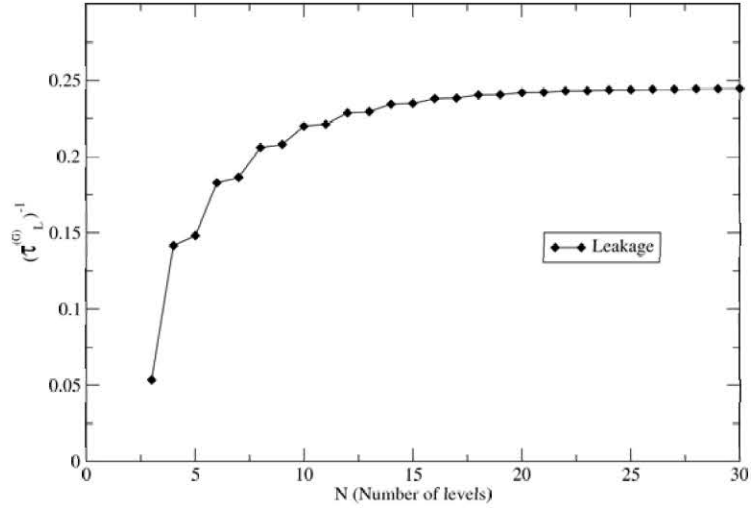


Figure 5. 5: The leakage rates for a degenerate two level system, that is in interaction with a Lorentzian type spectrum with $\epsilon = 0.1$, $\omega_0 = 1$ and $A = 1$. The coupling range is $R = 10$ and the coupling strength is $\kappa = 0.1$. The system is a singly degenerate system.

not discussed extensively.

The final assumption to be discussed for the 2LA is the resonant transitions assumption. In order to check for the validity of this assumption, we make use of the Lorentzian spectrum as it can be prepared at any width and at any frequency location. We prepare a spectrum with a very narrow width, $\epsilon = 0.1$ and by moving this localized spectrum around the resonant and non-resonant frequencies, we check the relaxation, dephasing and leakage rates. The short-time Gaussian rates and the long-time exponential rates will be investigated respectively.

5.3.1 Short-time behavior

As we have examined the effects of the environmental parameters on the decoherence mechanism qualitatively in the previous chapter we have shown that for various spectral locations, the short time relaxation and dephasing rates does not differ. As we calculate the Gaussian rates for various number of levels at different spectral locations, we verify this observation as demonstrated in Fig. 5.

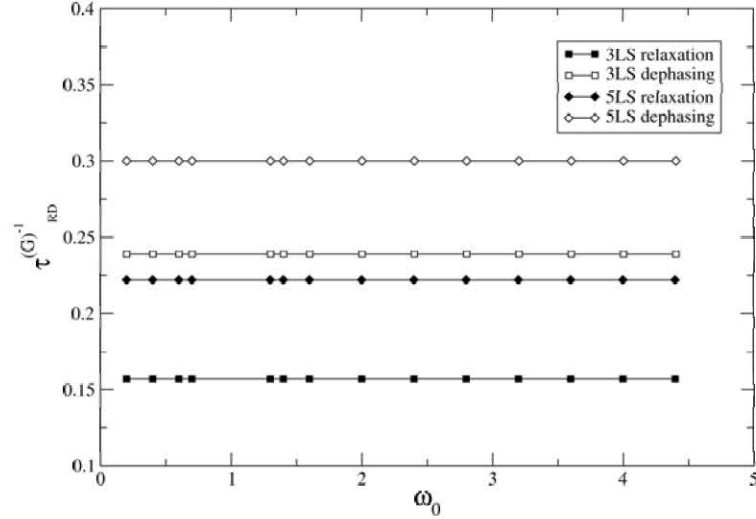


Figure 5. 6: The relaxation and dephasing rates for a multi-level system, that is in interaction with a Lorentzian type spectrum with $\epsilon = 0.1$ and $A = 1$ for various spectral locations. The system is prepared with coupling range $R = 10$ and coupling strength $\kappa = 0.1$. Energy levels are equally spaced with $\Delta E = 1$.

6. These results show that the spectral location, i.e. the resonant or non-resonant frequencies at the spectrum, have no effect on the Gaussian decoherence rates.

Next, we check the effect of the spectral area on the Gaussian rates. We have previously observed that increasing the ϵ or A increased the Gaussian rates, while increasing the total spectral area. In the Lorentzian spectral function given in Eq. 4. 11, the total area is found as $A\epsilon$. We have checked the Gaussian relaxation, dephasing and leakage rates for multi-level systems and the results are presented in Fig. 5. 7. As we can see, rates increase with increasing spectral area, though not linearly.

As we check the Eq. 5. 4, the kernel in the right hand side, K_{rs}^{kl} is proportional to the squared dipole coupling constants and $\mathcal{F}(0)$. Also due to the Eq. 4. 15, $\mathcal{F}(0)$ is proportional to the spectral area under the spectral function. Hence the short time decoherence rates are expected to have contributions not only from the resonant terms but from the entire spectrum as a whole. We thus expect for all the Gaussian rates for RDM, $(\tau_{RDL}^{(G)})^{-1} \propto (\text{spectral area})^{1/2}$. The Gaussian decoherence rates corresponding to the relaxation, dephasing and

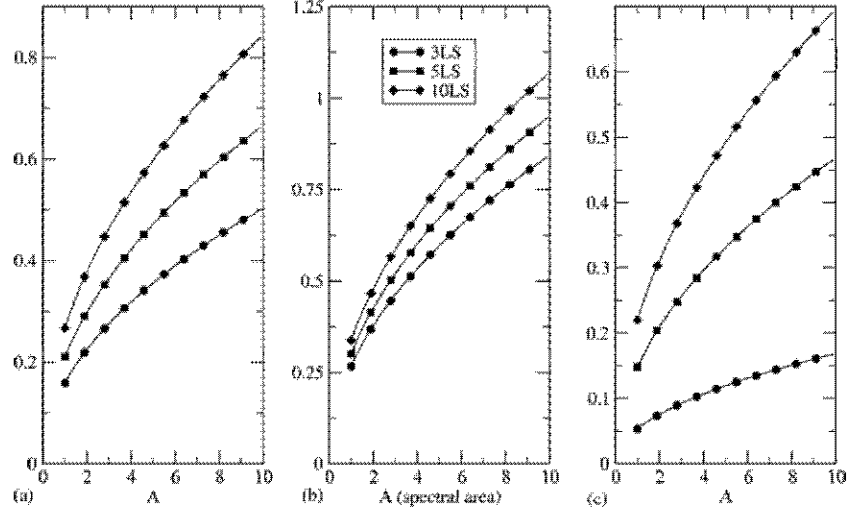


Figure 5. 7: The Gaussian (a)relaxation, (b)dephasing and (c)leakage rates for multi-level systems, that is in interaction with a Lorentzian type spectrum with $\epsilon = 0.1$ and $\omega_0 = 2.4$ for various spectral amplitudes. The system has equal energy level spacings $\Delta E = 1$, coupling range $R = 10$ and coupling strength $\kappa = 0.1$.

leakage contributions differ only in their dependence on the sum over the allowed dipole couplings φ_{rs} . As we plot the rates as in Fig. 5. 7, but this time in a log-log axes configuration, we obtain Fig. 5. 8. Note that the log-log plots are linear, and the slope confirms the dependence of the rates over the area as $\sqrt{\text{spectral area}}$.

The same relation also applies to the power-law spectrum. Although the spectrum characteristic (sub-ohmic, ohmic or super-ohmic) seem to change the decoherence pattern, as we focus on the short time scales we see that the Gaussian rates are not effected by the ν parameter. As we change the total area under the spectrum by varying the cut-off frequency Λ , and plot the decoherence rates as a function of total spectral area we obtain Fig. 5. 9. Note that all the plots have the same slope on the log-log axes scales, and the ν parameter merely changes the location of data points for the same Λ on the line.

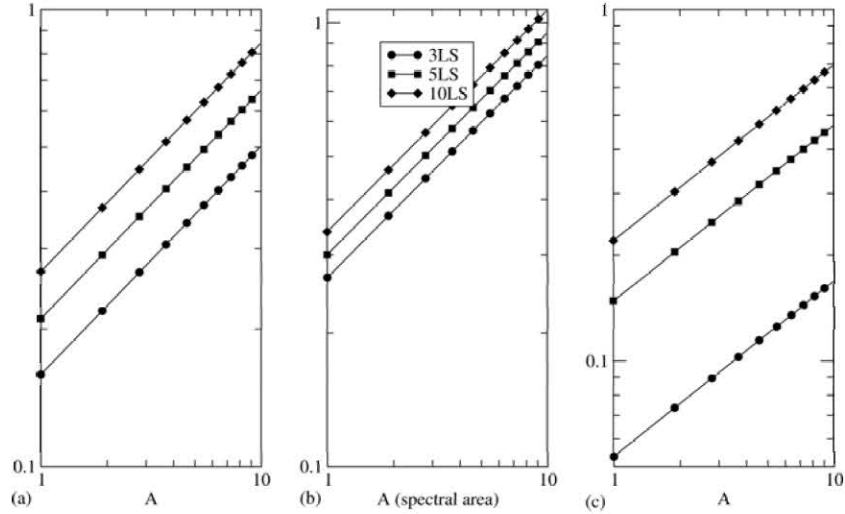


Figure 5. 8: The Gaussian (a)relaxation, (b)dephasing and (c)leakage rates for multi-level systems, that is in interaction with a Lorentzian type spectrum with $\epsilon = 0.1$ and $\omega_0 = 2.4$ for various spectral amplitudes. The system has equal energy level spacings $\Delta E = 1$, coupling range $R = 10$ and coupling strength $\kappa = 0.1$. The axes have logarithmic scales this time.

5.3.2 Long-time behavior

After verifying the dependence of Gaussian rates on the square root of spectral area, we now check the same dependence on exponential rates. We have also observed in the previous chapter that, though spectral location does not effect the Gaussian rates, it indeed effects the exponential rates. Changing the spectral center, for various number of levels, we obtained the relaxation, dephasing and leakage (RDL) rates of RDM element $\rho_{11}(t)$ as shown in Fig. 5. 10. We have experienced some numerical instabilities while ω_0 approaches to the resonant frequencies. It was possible to overcome the instabilities by decreasing the time increment dt , though in that case, the computational times would increase by an order of 10^2 . For the 2LS, we have only $\omega_0 = 1$ as the resonant frequency, though for 3LS we have $\omega_0 = 2$ as well and for 5LS, $\omega_0 = 3$ and $\omega_0 = 4$ are also added. Though, again, due to parity selection rules, for the 3LS, transition from ground state to second excited state is forbidden, hence we have no instability at $\omega_0 = 2$ at any plot. Likewise, the transition from ground state to fourth excited state is

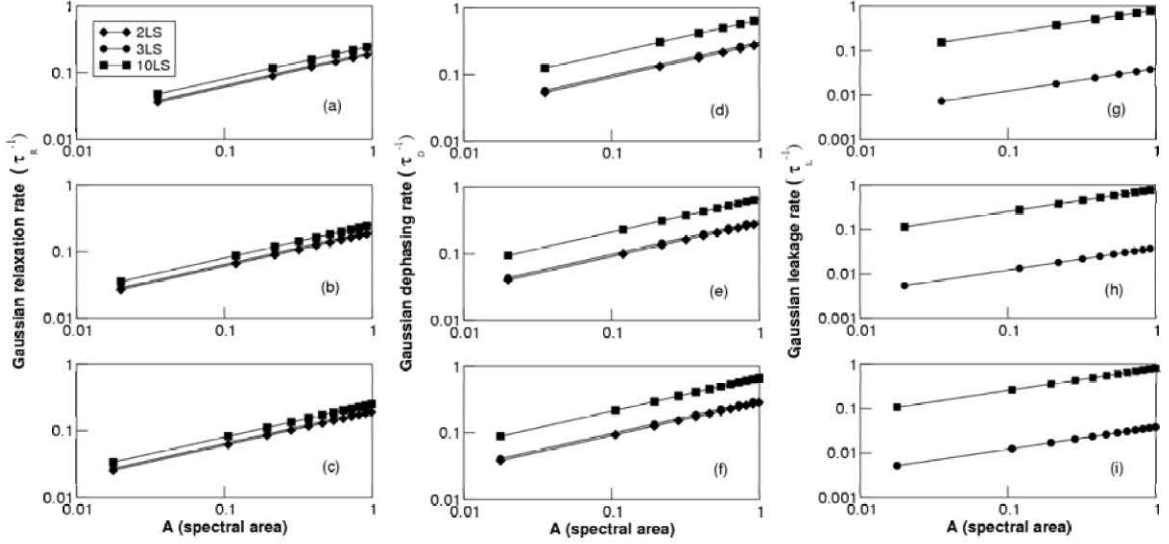


Figure 5. 9: The Gaussian relaxation (first column), dephasing (second column) and leakage (third column) rates for multi-level systems, that is in interaction with a realistic power-law spectrum of different characteristics, sub-ohmic (first row), ohmic (second row) and super-ohmic (third row) for various cut-off frequencies A . Note that the axes have logarithmic scales.

also forbidden. As a result $\omega_0 = 4$ point does not suffer from the instabilities for the 5LS.

We have observed that the resonant frequencies do not cause any difference at short time ranges, whereas at the long time range, they increase the decoherence rates significantly. This is indeed natural as the non-resonant transitions die out in the long times, and the resonant transition probabilities approach to 1 at $t \rightarrow \infty$. However, we have demonstrated that the Gaussian rates are more crucial in determining the decoherence times, since till the exponential rates dominate in the long times, great deal of decoherence is experienced by the system in short and intermediate times. As a result, non-resonant transitions cannot be neglected that easily as in the 2LA.

In the previous sections, we have discussed the validity of the assumptions that the 2LA is built upon. First we have demonstrated that zero temperature is not sufficient to suppress the effect of higher levels over the qubit subspace. Then we also showed that leakage cannot be neglected, even at zero temperature, since

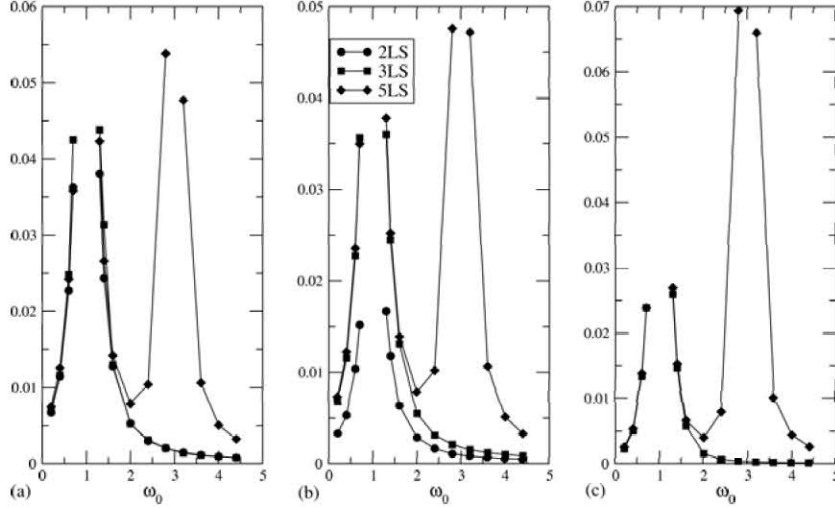


Figure 5. 10: The exponential (a)relaxation, (b)dephasing and (c)leakage rates for multi-level systems, that is in interaction with a Lorentzian type spectrum with $\epsilon = 0.1$ and $A = 1$ for various spectral locations. The system has equal energy level spacings $\Delta E = 1$, coupling range $R = 10$ and coupling strength $\kappa = 0.1$.

transitions from qubit subspace to higher levels cannot be suppressed completely even at zero temperature. And finally, we have shown that non-resonant transitions are the main source of decoherence at short times. Throughout the calculations, we avoided the Markov and rotating wave approximations (RWA), and solely used the Born-Oppenheimer approximation. Now we will also question the validity of the BOA in the next section, where the rates $(\tau_{RDL}^{(G,E)})^{-1}$ will be expressed as $\Lambda_{RDL}^{(G,E)}$ for convenience.

5.4 Limitations of the Born-Oppenheimer approximation

The essence of the Born-Oppenheimer approximation is in neglecting the back influence of the quantum system on the environment. At sufficiently short observation times, in contrast with the typical environmental equilibration time, this approximation holds well and our results within those observational times

are reliable. The crucial question is whether the BOA holds at intermediate as well as exponential regimes.

For a rigorous check of the BOA one has to solve the equations without this approximation. This can be done by using other techniques for instance, the Nakajima-Zwanzig Projection Operator Method or the Time Convolutionless Projection Operator (TCL) formalism.¹⁷ Another alternative are the analytic real time renormalization group calculations.⁶⁶ However, these analytic calculations can only be applied, by any practical means, to the two-leveled systems.

There is, nevertheless, an intuitively very simple method for estimating the range of the BOA. For a multileveled system with a large number of resonant frequencies, the smallest resonance energy sets the onset of the exponential behavior. In our case, this energy scale is $\Lambda_c \simeq \Delta E = 1$ and for times $1 = 1/\Lambda_c \ll t$ exponential behavior should be manifest. The BOA continues to hold in the exponential regime if the Born-Oppenheimer time (a typical reaction time scale of the environment which is on the order of the inverse width of the spectrum $1/\epsilon$) is much larger than the transition time $1/\Lambda_c$ to the exponential behavior.

An estimate for the critical region can be made by looking at the crossover between the short and the long time behavior. Assume that after some crossover time t_c , the Gaussian amplitudes are in the same order of magnitude as the exponential ones. This amounts to

$$e^{-(\Lambda_c^{-1} + t_c)\Lambda^{(E)}} \simeq e^{-(\Lambda^{(G)})^2 t_c^2} \quad (5. 7)$$

Solving this equation for the exponents, one obtains for t_c

$$t_c = \frac{\Lambda^{(E)}}{2\Lambda^{(G)^2} \left[1 + \sqrt{1 + 4\Lambda^{(G)^2 / (\Lambda^{(E)} \Lambda_c)} \right]} \quad (5. 8)$$

as an estimate for the crossover time between the intermediate and the exponential regions. Crudely, for $t \ll t_c$ Gaussian and for $t_c \ll t$ exponential behavior are manifest. However, for the BOA to be accurately valid in the exponential regime an additional constraint has to be satisfied: the Born equilibration time $1/\epsilon$ has to be much longer than the crossover time t_c thus

$$t_c \ll \frac{1}{\epsilon}. \quad (5.9)$$

By defining a test parameter $\mu = t_c \epsilon$ and using Eq. 5.9 we find that the Born approximation holds well in the exponential regime if $\mu \ll 1$ and it is unreliable for $1 \ll \mu$. Within the ranges of parameters investigated in this thesis, we calculated the μ parameter by the corresponding RDL rates. The results are tabulated in the Table 5.1 for 2LS, 3LS and 5LS.

The μ parameter is influenced both by the short and the long time scales. As it can be seen from the table, there are certain regions where the BOA is threatened. For instance, close to resonant frequencies μ increases towards unity and for the opposite case of off-resonant ones, $\mu \ll 1$. The basic relation is that, the contribution of the long time resonant coupling is to increase the exponential rates which increases μ . In this regime the possibility arises that the environmental back reaction takes place before the onset of exponential behavior. On the other hand, and independently from the decohering system, the contribution of the off-resonant parts of the spectrum is to increase the Gaussian rates. This in turn decreases the parameter μ by the relations 5.8 and 5.9.

We also examined the BOA as a function of the number of levels. Considering the behavior of μ with respect to N , $\Lambda^{(G)}$ as well as $\Lambda^{(E)}$ are both monotonically increasing functions of N for $N \leq R$. Therefore, using Eq. 5.8 the overall dependence is $t_c \simeq 1/N$. Since ϵ is independent of N , $\mu \simeq N$ which explains why the BOA improves in MLS with larger number of levels. This behavior is illustrated in Fig. 5.11 for $N \leq 5$ and can be studied for larger N values provided sufficient computing power.

In the next chapter, we will be examining the realistic outcome of the driving fields, that are the main manipulation tools to execute the quantum computation algorithms, in the presence of the environmental bath.

ω_0	2LS		3LS			5LS		
	μ_R	μ_D	μ_R	μ_D	μ_L	μ_R	μ_D	μ_L
0.2	0.027	0.006	0.028	0.010	0.080	0.015	0.008	0.012
0.4	0.046	0.009	0.047	0.016	0.177	0.025	0.014	0.024
0.6	0.092	0.018	0.100	0.032	0.470	0.049	0.026	0.063
0.7	0.147	0.027	0.172	0.050	0.837	0.072	0.039	0.109
1.3	0.154	0.029	0.177	0.051	0.909	0.086	0.042	0.123
1.4	0.099	0.021	0.127	0.034	0.514	0.054	0.028	0.070
1.6	0.052	0.011	0.052	0.018	0.203	0.029	0.015	0.030
2.0	0.021	0.005	0.021	0.008	0.055	0.016	0.009	0.018
2.4	0.012	0.003	0.013	0.004	0.023	0.021	0.011	0.036
2.8	0.008	0.003	0.008	0.003	0.013	0.109	0.053	0.316
3.2	0.006	0.002	0.006	0.002	0.008	0.097	0.052	0.301
3.6	0.005	0.001	0.004	0.002	0.006	0.022	0.012	0.046
4.0	0.004	0.001	0.004	0.001	0.005	0.010	0.006	0.020
4.4	0.003	0.001	0.003	0.001	0.004	0.007	0.004	0.012

Table 5.1: The μ parameter of the RDL processes for 2LS, 3LS and 5LS against varying ω_0 . The other spectral parameters are $\epsilon = 0.1$ and $A = 1$.

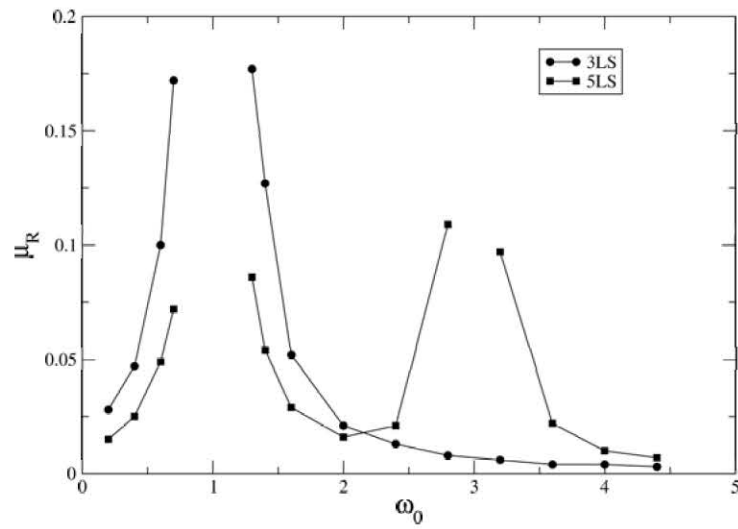


Figure 5. 11: μ_R for 3LS and 5LS as a function of spectrum center ω_0 . The figure is an illustration of the data in the Table 5.1.

Chapter 6

Driving fields in the realistic system-environment model

Quantum computation makes use of the quantum algorithms, and quantum algorithms rely on the manipulation of the quantum systems of interest by external means. Quantum computation, very basically, consists of a series of external manipulations on a quantum system, and a final read-out. These manipulations are named as gate operations, referring the logical gate operations, and an algorithm may consist of gate operations on the order of 10^3 . So, the ultimate goal nowadays is to obtain a system, for which the destructive effects of decoherence are not felt before the read-out. As we focus our interest on the widely used SQUID systems, since we know that SQUID systems interact with external fields, it is most natural to perform the gate operations via an external field. In this section, we will try to demonstrate the results of applying an external field to a multileveled system, in the presence of environmental noise. So we will have a chance to observe the effects of higher levels and environment on the gate operations more realistically.

First we will focus on the most simple manipulation, an external field at a resonant frequency which will result in Rabi oscillations. We will present the case of ideal Rabi oscillations, and then investigate the effects of higher levels and the presence of the environment. The modifications on the Rabi oscillations

should give an idea about the outcome of some experiments.^{67,70} Later, we will simulate the operation of a small and simple gate series, and comment on the success of the outcome.

6.1 Rabi oscillations

Rabi oscillations are mainly defined for two-level systems. When an external field is applied to the system, the populations in the system tend to oscillate. The oscillations' frequency depends on the amplitude of the Rabi field applied, not on the intensity of the field. As the applied field's frequency is resonant with the 2LS, i.e. $\omega_R = \Delta E$, it is possible to observe the population inversion as shown in Fig. 6. 1. Though, for a non-resonant Rabi frequency, full population inversion is not observable, as also shown in Fig. 6. 1. Rabi oscillations are named after the Nobel prize winner physicist Isidor Isaac Rabi (1898-1988). Recently, in the experimental studies concerning the quantum computation, Rabi oscillations are commonly measured, as they are the simplest way to make system modifications.

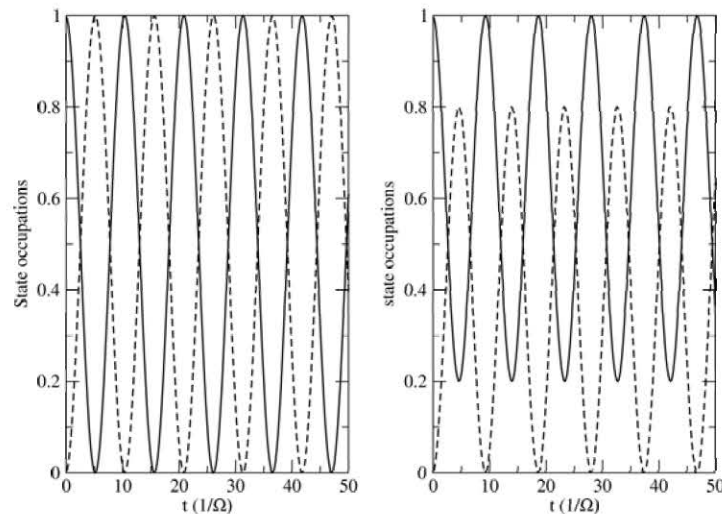


Figure 6. 1: Rabi oscillations in a 2LS. On the left hand side, we have full population inversion as the Rabi field is resonant with ΔE , whereas on the right hand side, as $\omega_R \neq \Delta E$, we cannot observe a full population inversion.

The interaction of the system with the Rabi field may be written as

$$H_R = p(t)g_{12} \{ |1\rangle\langle 2|a^\dagger + |2\rangle\langle 1|a \} \quad (6.1)$$

where the system is taken as a 2LS and RWA is used. Here g_{12} defines the real coupling strength between the two levels due to Rabi field. The operators a and a^\dagger are the operators for the Rabi field. The time dependent function $p(t)$ defines the shape of the Rabi pulse in time, as the pulse may have any specific shape, though using a step function as a pulse shape would be much easier.

The Rabi oscillations and full population inversions can be observed in 2LS, though as stated before, many physical systems are indeed multileveled and truncated to two levels explicitly. So, firstly we wish to observe the changes in Rabi oscillations on a multileveled system first, on the next subsection. Later, we will also introduce the environment.

6.1.1 The effect of higher levels

Rabi oscillations are observable in 2LS, though as the number of levels in the system is higher, we cannot observe perfect oscillations. As we have demonstrated and explained in the previous chapter, although the field that the system interacts does not include a resonant transition frequency, the system may experience non-resonant transitions in the short time limit. In order to observe this non-resonant effect, we prepare a system with four levels, where the energy level spacings are $\Delta E_{12} = 1$, $\Delta E_{23} = 1.5$, and $\Delta E_{34} = 2$ in terms of an arbitrary energy scale Ω . The dipole couplings in the system are also chosen so that the couplings between the higher levels are weaker than the one in the qubit subspace, i.e. $\varphi_{12} = 0.3$, $\varphi_{23} = 0.2$ and $\varphi_{34} = 0.1$. We apply a Rabi field with the resonant frequency $\omega_R = 1$ to this system. One could expect that the Rabi field may just generate transitions in the qubit subspace, so that the occupation of the higher levels may remain zero throughout the entire time range. Though, as it may be seen in Fig. 6. 2, the Rabi field also initiates non-resonant transitions to higher levels, and as a result, the occupations of the higher levels may increase up to ~ 0.4 . Naturally, full population inversion is not observable.

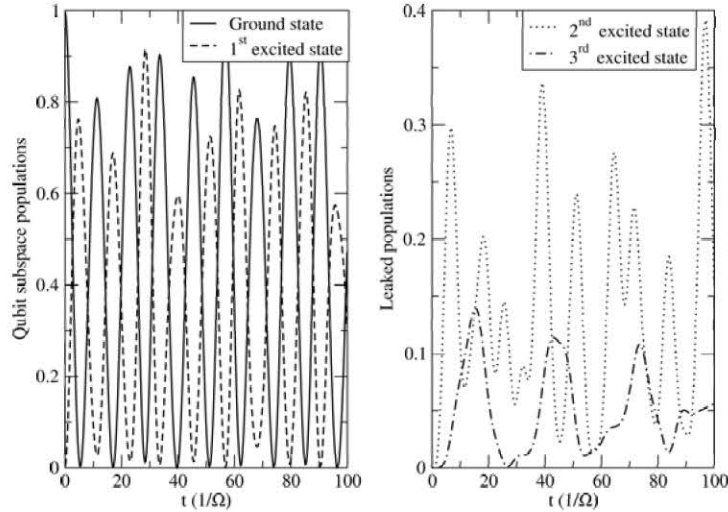


Figure 6. 2: Rabi oscillations in a 2LS. On the left hand side, we have full population inversion as the Rabi field is resonant with ΔE , whereas on the right hand side, as $\omega_R \neq \Delta E$, we cannot observe a full population inversion.

The effect of multilevels can even be more crucial, depending on the system configuration. As we set the system's energy level spacings to be equal so that $\Delta E_{n,n+1} = 1$ and apply the resonant Rabi field, the outcome may even be worse. As it can be seen in Fig. 6. 3 the occupations of the higher levels may go up to ~ 0.8 this time, and the oscillations in the qubit subspace becomes more disordered. Of course it is not very probable to have a system with the exactly same level spacings, though, in order to demonstrate the importance of the higher levels, it was a proper example.

There is also a recent experimental result⁶⁷ obtained on a dc-SQUID, where a strong deviation from the strict linear law between the Rabi frequency and the field strength is observed. This deviation is explained by the increasing number of multilevels participating in the dynamics by the increasing field strength at fixed microwave frequency.

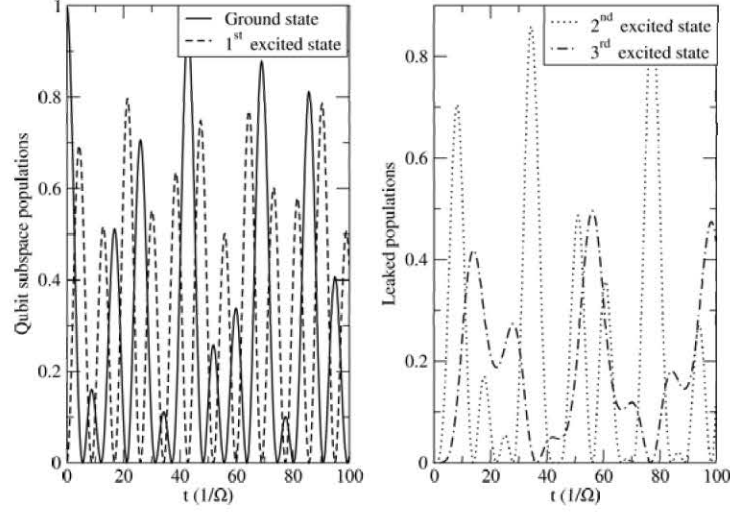


Figure 6. 3: Rabi oscillations in a 2LS. On the left hand side, we have full population inversion as the Rabi field is resonant with ΔE , whereas on the right hand side, as $\omega_R \neq \Delta E$, we cannot observe a full population inversion.

6.1.2 The effect of the environment

In order to observe the effect of environment on the Rabi oscillations, we need to include the systems interaction Hamiltonians with both the Rabi field and the environmental bath. Then the total interaction Hamiltonian would be

$$H_{int} = H_R + H_E = \sum_{n,r=1}^N \varphi_{nr}(t) |n\rangle \langle r| (p(t)a(t) + h.c.) + \sum_{n,r=1,k}^N \varphi_{nr}(t) \eta_k |n\rangle \langle r| (b(t) + h.c.) \quad (6. 2)$$

where the function $p(t)$ defines the pulse shape of the Rabi field, a is the Rabi field operator and b is the environmental bath operator. Throughout this chapter, we will use a pulse shape like a step function, like

$$p(t) = \begin{cases} 1 & \text{if } t \leq t_p \\ 0 & \text{if } t > t_p \end{cases} \quad (6. 3)$$

where t_p is the pulse time. As we put this Hamiltonian in Eq. 2. 55, we obtain the master equation to solve. However, for the environmental part, we have discussed that the first order commutation would yield zero, due to the expectation of

single annihilation and creation operators before. So that we would iterate the commutation once more and obtain finite results in the second order. Though, for the Rabi part of the interaction, we have finite outcomes at the first commutation, so there is no need to iterate to second order. As we are supplying the Rabi field at high intensity, with a source like a laser beam, the expectation of a single creation or annihilation operator is generally assumed unity. As the Rabi field and environmental bath commute with each other, we can treat them separately. Finally we obtain the master equation as

$$\frac{d}{dt}\rho_{nm}(t) = i\langle n|[H_R(t), \rho(t)]|m\rangle - \int_0^t dt' \sum_{r,s} K_{rs}^{nm}(t, t')\rho_{rs}(t') \quad (6.4)$$

for the reduced density matrix.

Solving Eq. 6.4 similarly as in Chapter 4, we obtain the Rabi oscillations in presence of environment as in Fig. 6.4. In our calculations, we used a Lorentzian spectrum with $\omega_0 = 5$, $\epsilon = 3$ and $A = 3$. The system parameters are same as in the previous section. However, in order to observe the changes for different Rabi and environmental coupling strengths, we defined two coupling strengths, α_R for the Rabi coupling and α_E for the environmental coupling. In our calculations, α_R seems about 7-20 times greater than α_E , though as the environmental processes are calculated at second order, the real ratio of coupling strengths is on the order of 10^2 . As the intentionally applied Rabi pulse should be much more stronger than the environment, which is tried to be avoided, this type of ratio in the couplings is expected. In the final section of this chapter, even higher ratios, which seems to be closer to the ideal case, will be used.

6.1.3 Expected outcome of realistic Rabi oscillations

Finally, as the effects of the multi-level and the environmental interaction are combined, we obtain the outcome of the Rabi field applied to a realistic system. We have presented the oscillations in Fig. 6.5 for different environmental coupling strengths. Note that, significant leakage to higher levels takes place

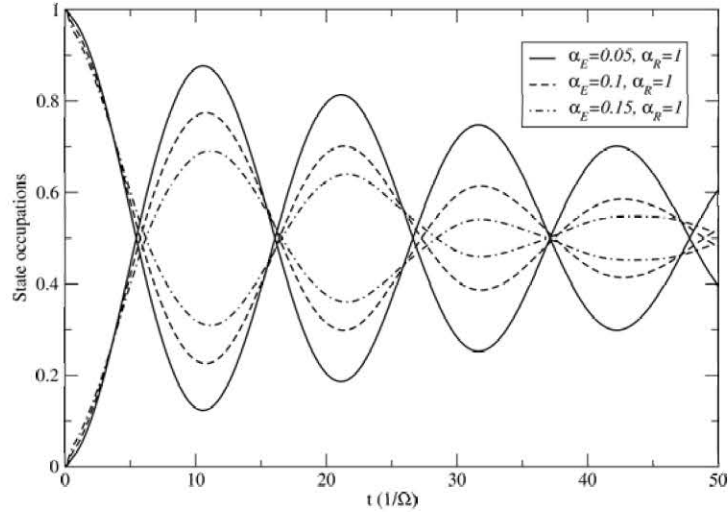


Figure 6. 4: Rabi oscillations in a 2LS in interaction with an environmental bath, as the environmental coupling strength is varied.

in addition to the damped oscillations due to the environmental effects. The environmental and system parameters are same as in the previous section.

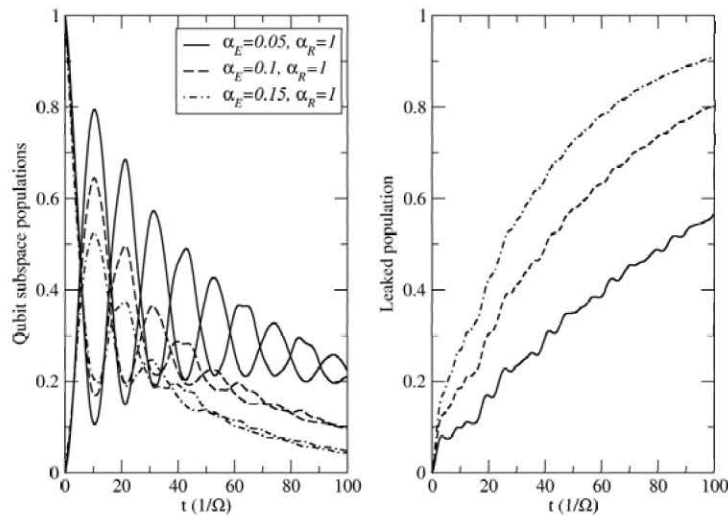


Figure 6. 5: Rabi oscillations in a 4LS in interaction with an environmental bath, for various environmental coupling strengths. On the left hand side, we see the populations of the qubit subspace, whereas on the right hand side, we see the leakage to higher levels.

We have demonstrated the possible results, as a Rabi field is applied to a

multi-level system that is interacting with an environmental field. These results may shed some light upon recent experimental results. For instance there is the experiment by Zrenner *et al*⁶⁸ where single self-assembled excitonic q-dots are used to create excitons by a strong Rabi field, which are then tunneled out and transformed into a photocurrent. The anomaly appears in the damping of the Rabi induced oscillations in the pulse averaged photocurrent as the area under the Rabi pulse is increased. This effect within the fixed time of the short 1 ps pulse (dephasing and relaxation times are reported to be approximately 500 ps) could not be observed in a purely 2LS as it would violate the fundamental principle of unitarity. The pulse width is shorter than the decoherence time by three orders of magnitude and it is clear that the observed damping does not originate from decoherence. The short timescale of the effect indicates the influence of higher excitonic states. In a simple approach it has been shown that the damping of the oscillations as the intensity of the short pulse is increased is due to off-resonant leakage into biexcitonic levels.^{69,70} Considering this argument, we have solved the system-Rabi coupling, while neglecting environmental effects for a three-leveled system and calculated the average occupation of third level, i.e. $\langle \rho_{33}(t) \rangle_{pulse} = 1/t_p \int_0^{t_p} dt \rho_{33}(t)$, as a function of the pulse area. The frequency of the Rabi pulse is taken as resonant between the first two levels, for three different third-level energies. It can be seen from Fig.6. 6 that the average occupation is largely independent from the third-level energies. Another point is that the peak position occurs at $t_p \leq 1/\alpha_R$. Using the dipole matrix model Eq.5. 1, this implies $t_p \leq \varphi_{12} T_R / (2\pi)$, where T_R is the Rabi oscillation period; therefore $t_p \simeq 0.1 T_R$, concluding that the third level is already occupied maximally before the completion of a single Rabi period. This short time effect is counterintuitive from the traditional way of thinking in terms of the long time resonant transitions. It must be remarked that this is an exact result. It appears that a multileveled system decides to act like so at very short times in comparison with typical resonant timescales. Thus, Fig.6. 6, in confirmation of the earlier theoretical calculations,^{69,70} manifests the effect of the strong influence of the non-resonant processes on leakage.

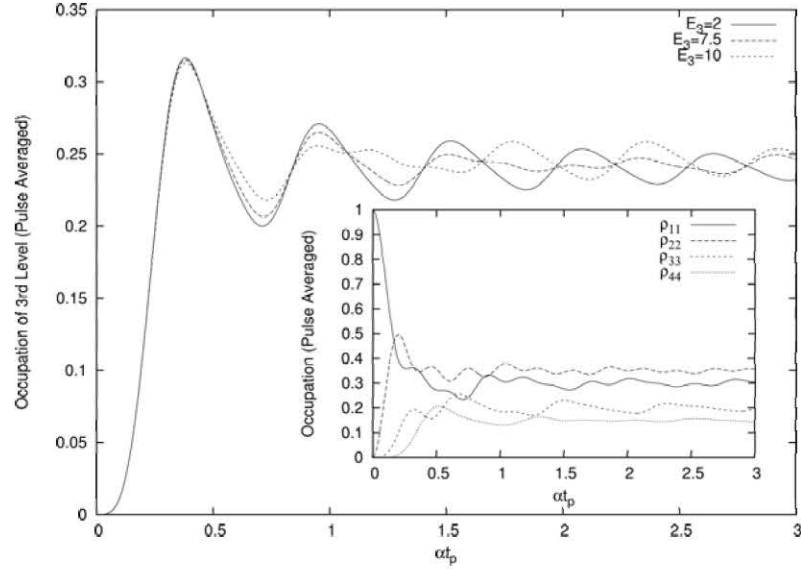


Figure 6. 6: The time average over the Rabi pulse of the third-level occupancy is shown as a function of pulse area, for different third level energies, where $E_1 = 1$, $E_2 = 2$. The Rabi frequency is set as resonant with the first two levels. The inset shows the state occupations for the equally spaced system levels, resonant with the Rabi frequency.

6.2 NOT gate simulation

As a final step to check the effect of the multilevels and the environment, we will demonstrate a quantum logic gate operation on a single qubit. NOT gate is a very simple gate, which changes the input, i.e. if the input is 1, the output would be 0, if the input is 0, the output would be 1. Adapting the NOT gate to the quantum mechanical system, for the qubit subspace, if the excited state is occupied, i.e. $\rho_{22} = 1$, the NOT gate would switch the state to occupy the ground state. i.e. $\rho_{11} = 1$, or vice versa. As we have explained the effects of the Rabi field and Rabi oscillations previously, it is clear that we can use Rabi field to perform NOT operation on our system.

The key point of the demonstration would be that, after how many gate operations, we will still be able to read-out the expected result. The testing scheme will be like applying a NOT gate, wait for some time, and applying another NOT gate, and so on. In order to perform numerous NOT gates in

our feasible computation limit ($t=200$), we further increase the Rabi strength to $\alpha_R = 5$. We calibrated the time to switch on and off the Rabi field, due to a 2LS without environment, i.e. the ideal situation. Let us call this time as t_{NOT} . With our parameters, we measured $t_{NOT} = 2.1$ normalized with the arbitrary energy scale Ω as the energy levels. First, we will prepare the system as the ground state is fully occupied, i.e. $\rho_{11} = 1$ and $\rho_{22} = \rho_{12} = \rho_{21} = 0$. So we will apply Rabi field for a duration of t_{NOT} , then switch off the field. We will wait for another t_{NOT} , then switch on the field for another t_{NOT} . Ideally, the system would return to its starting configuration at this point. Then we will wait for another t_{NOT} and at the middle of this waiting period, we will measure the occupation of the ground state. The procedure goes on like that, and after each couple of NOT operations, there will be a measurement.

As we applied the explained procedure to the 2LS, with the same parameters as in previous section, that is in interaction with an environment, which has again the same parameters as in previous section, we obtained measurement results as shown in Fig. 6. 7 for different environmental coupling strengths. Note that, after about 20 couples of NOT operations, we are no longer able to deduce any information from the system for $\alpha_E = 0.05$, as the system approaches an equally occupied configuration, i.e. the maximum entropy limit. For an even weaker environmental coupling of $\alpha_E = 0.01$, the system does not reach the maximum entropy situation even after ~ 20 couples of NOT operations. Though an exponential approach to that limit is obvious.

As we further introduce the higher levels of our systems into the calculations, we obtain dramatically worse results as seen in Fig. 6. 8. To put it into simpler words, the NOT gate duration t_{NOT} that is obtained for the 2LS is not valid for 4LS, and as a result, we perform the measurements before, or after the maximum population inversion occurs in the qubit subspace. Of course, as shown before, full population inversion is not achievable in the presence of environment and higher system levels. As a result, the readings of the measurements may approach to the desired value, as the expected and real operation frequencies coincide, though the rest of the measurements are far from the desired values. Note that, as a

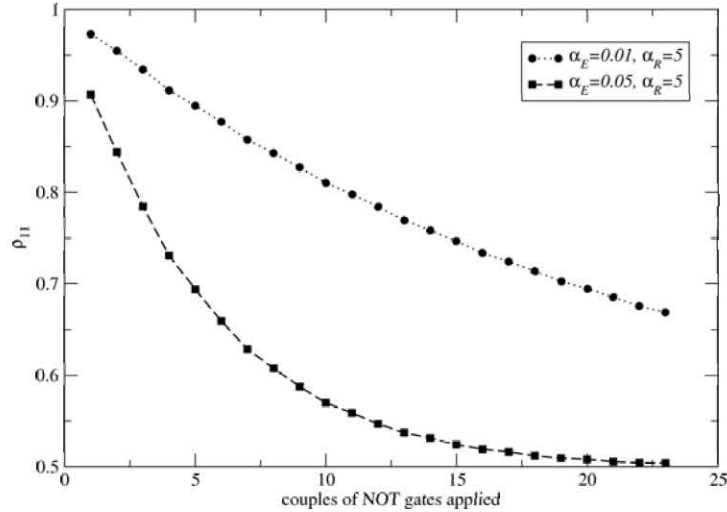


Figure 6. 7: The occupation $\rho_{11}(t)$ versus the number of couples of NOT operations performed, in a 2LS that is in interaction with the environment, for various environmental coupling strengths.

measurement of ρ_{11} is close to 0.5, we say that we cannot obtain any information as measuring 1 or 0 has about the same probability. Though for $\rho_{11} < 0.5$, the measurements give us wrong results, as the probability to obtain 0 as an outcome of a measurement is greater than to obtain 1.

So, as demonstrated above, the environment plays the role that is expected of it. But the higher levels of the system, above the qubit subspace, which is often neglected may have drastic effects on the operations, that are to be applied to the system. Apart from trying to get rid of the environment, one also must precisely adjust the course of operations on the system.

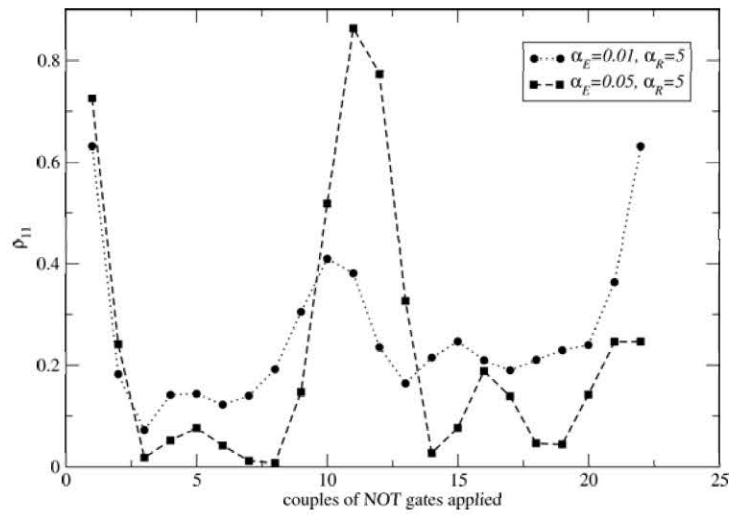


Figure 6. 8: The occupation $\rho_{11}(t)$ versus the number of couples of NOT operations performed, in a 4LS that is in interaction with the environment, for various environmental coupling strengths.

Chapter 7

Conclusions

In this thesis, we studied on the decoherence mechanisms in open quantum systems. There is an increasing number of studies in the literature in the recent years about decoherence, as it has also been a key problem in quantum computation.

Decoherence is mainly described as the destruction of quantum coherence in a system due to an interaction with an environmental bath. The most general method to analyze the decoherence is using the master equation approach, and it has also been used in this thesis. Though, as the exact analytical analysis of the interaction is impossible by any means, there have been numerous approximations and models used. We have briefly introduced the most commonly used approximations and models in Chapter 2. We have also presented introductory information about the SQUID systems, as they are one of the most commonly used physical systems in quantum computation field, and also introduced the solution for a rf-SQUID. Later, the interaction of the system and environment is presented, as coordinate-coordinate coupling introduced by Caldeira and Leggett, and solved for various environmental spectra. The key point in our solution was that, apart from the Born-Oppenheimer approximation, for which the validity region is discussed, we have not used any approximation technics, and obtained our results by numerical means.

Our main goal was to observe the effects of the system and environmental

parameters in the decoherence mechanism. In our calculations, we have perceived that the most commonly used 2LA is not as safe as thought. The decoherence shows different behaviors at short times and long times. We have shown that decoherence at short times, is affected by the entire spectrum, rather than the only resonant parts of the spectrum, therefore it is possible to experience serious decoherence at short times, even if the resonant frequencies in the spectrum are avoided. Numerical and analytical analyse have been done to reveal the direct proportion of the short time decoherence rates with the square root of the total spectral area. We have also shown that, the higher levels in a physical system cannot be avoided totally, as the energy level spacing between the qubit subspace and higher levels is large, even if the environmental temperature is set to zero. Because, the key point in the higher level transitions is the environmentally induced dipole coupling matrix elements, rather than the sole energy level differences. It is also shown that, due to these higher level transitions, leakage cannot be neglected in favor of the 2LA that easily.

Finally, we have also demonstrated the possible outcome of the driving fields applied to a system in interaction with the environmental bath. Apart from the expected result of environmental interaction, which is quite like the effect of damping on an oscillating system, we have probed the effect of higher levels. It has been demonstrated that, as the driving fields are adjusted for the 2LS approximation, it is possible to obtain dramatically erroneous results due to the interference of the higher levels. Even without the wide environmental spectrum, the monochromatic Rabi field may also initiate non-resonant transitions to higher levels.

In conclusion, it has been discussed that, the validity of the 2LA is not that straightforward as thought. The critical parameters for the safety of the system are shown to be different than the ones commonly believed. The basic decoherence mechanisms have been demonstrated.

Appendix A

The analysis of the compensating term

In the calculations of the system-reservoir models, there is usually a compensating part of the interaction Hamiltonian which is included in order to compensate the frequency renormalizations on the system.⁴ This compensating term may contain environmental parameters, though it cannot contain the environmental dynamical variable, which is in our case the environmental phase. We write down the compensating term of the Hamiltonian we use as

$$H_c = \sum_{n,r} \varphi_{nr}^2 |n\rangle\langle r| \int d\omega \eta_\omega^2. \quad (1. 1)$$

The effect of this compensating term is to shift the system basis by a unitary transformation

$$U_t = T \exp(-i \int_0^t dt' H_c(t')) \quad (1. 2)$$

where T is the time ordering operator. With this transformation, the full density matrix $\rho_T(t)$ is transformed like $\rho_T^U(t) = U_t^\dagger \rho_T(t) U_t$. The reduced density matrix is again found by tracing over the environmental degrees of freedom of which the matrix elements in the original system are found. Repeating the same algebra as

in Chapter 4, one finds for the reduced density matrix that

$$\frac{d}{dt}\rho_{nm}^U(t) = - \int_0^t dt' K_{rs}^{nm}(t, t') \rho_{rs}^U(t') \quad (1. 3)$$

where the kernel is now found as

$$\begin{aligned} K_{rs}^{nm}(t, t') &= \{ \mathcal{F}(t-t')(\varphi^U(t)\varphi^U(t'))_{nr}\delta_{s,m} - (\varphi^U(t'))_{nr}(\varphi^U(t))_{sm} \} \\ &+ \mathcal{F}^*(t-t')[(\varphi^U(t')\varphi^U(t))_{sm}\delta_{r,n} - (\varphi^U(t))_{nr}(\varphi^U(t'))_{sm}] \}. \end{aligned} \quad (1. 4)$$

Here, the transformed dipole matrix elements are

$$(\varphi^U(t))_{nr} = (\varphi^U(0))_{nr} e^{-i(E_n - E_r)t}. \quad (1. 5)$$

Therefore, the net effect of the transformation due to compensating term is transforming the original system dipole matrix into

$$\varphi^U(t) = U_t \varphi(t) U_t^\dagger. \quad (1. 6)$$

The new dipole matrix elements due to this transformation are

$$\varphi_{nm}^U(t) = \sum_{r,s} U_{nr}(t) \varphi_{rs}(t) U_{sm}^\dagger(t). \quad (1. 7)$$

At the short times for the perturbative dipole interaction, the first few terms are given as

$$\varphi^U(t) \simeq \varphi(t) - i \int_0^t dt' [H_c(t'), \varphi(t)] - \frac{1}{2!} T \int_0^t dt_1 \int_0^{t_1} dt_2 [H_c(t_1), [H_c(t_2), \varphi(t)]] + \dots \quad (1. 8)$$

It is trivially seen that the renormalization of the initial dipole matrix elements are contributed by the terms with odd number of time integrals in the above expansion. The dipole elements that are not presented in the original system, such as the even transitions $\varphi_{n,n-2m}^U(t)$ are created by the terms with even number of integrals. For three and four level systems, it can be seen that the corrections to all dipole matrix elements start with those terms with at least two time integrals.

In calculation of the short time decoherence rates, the effect of the two small parameters, i.e. time and the dipole couplings are multiplicative. This proves that the compensating term does not create an appreciable renormalization of the system basis in the short time limit. For a system with a small number of levels the smallness of this effect should persist even at longer times.

There are arguments that at long times, the effect of the compensating term is also negligible.¹⁹ It is also possible to sum up the infinite series of the expansion to all orders. The general term in the series is given at the operator level by

$$\varphi^U(t) = \varphi(t) + T \sum_{n=1}^{\infty} \frac{(-iA)^n}{n!} \int_0^t dt_1 \dots \int_0^t dt_n [\varphi^2(t_n), \dots [\varphi^2(t_1), \varphi(t)] \dots] \quad (1. 9)$$

where $H_c(t) = A\varphi^2(t)$ is used explicitly. The last term includes an n-fold commutator and T is the time ordering operator. As the short time part is currently the subject of interest, let $t \rightarrow 0$. Due to the time ordering in the expansion, we have

$$\int_0^t dt_1 \dots \int_0^t dt_n 1 \simeq \frac{t^n}{n!}. \quad (1. 10)$$

Hence for sufficiently short times,

$$\varphi^U(t) = e^{iAt\varphi^2(0)}\varphi(t)e^{iAt\varphi^2(0)} \quad (1. 11)$$

which proves that all corrections to the system dipole transitions occur in powers of the square of the transition matrix elements. It can be seen easily that Eq. 1. 11 becomes an appreciable renormalization only when sufficiently large number of levels are involved in the non-resonant transitions.

To examine the effect of compensation at long times, let $t \rightarrow \infty$ so that

$$\begin{aligned} \varphi^U(t) &\simeq \varphi(t) - i \int_0^\infty dt' [H_c(t'), \varphi(t)] \\ &\quad - \frac{1}{2!} T \int_0^\infty dt_1 \int_0^{t_1} dt_2 [H_c(t_1), [H_c(t_2), \varphi(t)]] + \dots \end{aligned} \quad (1. 12)$$

The first term does not include a time ordering and therefore can be calculated easily as

$$-iA \sum_s [\delta(E_n - E_s)\varphi_{ns}^2(0)\varphi_{sm}(t) - \delta(E_s - E_m)\varphi_{ns}(t)\varphi_{sm}^2]. \quad (1. 13)$$

In the limit $t \rightarrow \infty$, $\varphi_{ns}(t)$ is a sharply peaked function for $n = s$, rapidly oscillating otherwise. As this term is approximated as $\delta_{n,s}$ at $t \rightarrow \infty$, it vanishes. Likewise, the next term includes a time ordering which can also be calculated exactly. In this term, the non-zero contributions are restricted to even more energetic conditions and the second term also vanishes in the limit $t \rightarrow \infty$. Moreover, all the terms have, in common, different matrix elements of $\varphi(t)$. In the $t \rightarrow \infty$ limit, these contributions average out anything slower to zero, making it possible to ignore them.

The overall result is that it is possible to ignore the renormalizing effect of the compensating term in our calculations.

Appendix B

Proof of the reality and positivity of $\Lambda^{(G)}$

Let us define a Hermitian dipole transition operator φ_t such that

$$(\varphi_t)_{jk} = \langle j|\varphi_t|k\rangle = e^{i(E_j-E_k)t}\langle j|\varphi_0|k\rangle. \quad (2. 1)$$

By using the above equation, it is trivially checked that the system-noise kernel can be written at $t = t' = 0$ as a non-negative real operator

$$\mathbf{K}(0, 0) = \mathcal{F}(0)|\varphi_0 \otimes \mathbf{I} - \mathbf{I} \otimes \varphi_0^T|^2 \quad (2. 2)$$

where $\mathcal{F}(0) = A$ is the spectral area, which is real by definition and T denotes transpose. Hence Eq. 2. 2 describes a real non-negative operator in the two-folded Hilbert space $|n\rangle \times |m\rangle$ where $n, m = 1, N$. By using Eq. 2. 2, it can be shown easily that the system-noise kernel in Eq. 1. 5 is equivalently written as

$$K_{rs}^{nm}(0, 0) = \langle n| \times \langle m|\mathbf{K}(0, 0)|r\rangle \times |s\rangle. \quad (2. 3)$$

Defining a vector $|V\rangle$ such that

$$\rho_{nm}(0) = \langle n| \times \langle m|V\rangle \quad (2. 4)$$

we can write Eq. 5. 3 in the implicit operator form as

$$|\ddot{V}\rangle = -\mathbf{K}(0, 0)|V\rangle \quad (2. 5)$$

where the left hand side clearly implies the second derivative of the density matrix at $t = 0$. Since $\mathbf{K}(0, 0)$ is real and non-negative, its eigenvalues are real and non-negative; hence a real Gaussian like short decoherence timescale exists.

Another analytic exact result is that the Gaussian-like short decoherence timescales are proportional to the square root of the spectral area. This follows from the fact that the matrix elements of $\mathbf{K}(0, 0)$ have, in common, a term proportional to $\mathcal{F}(0)$ which is just the spectral area. The solution of Eq. 2.5 then indicates that the short time decoherence rates scale with the square root of the spectral area.

Appendix C

Numerical code

The numerical code that is used is presented here in its most general form. The package lgrind is used to create the output from the code. Note that the code can be used for both toy system model and a SQUID system, after commenting out relevant lines. Basic information is supplied within the code with comments.

```
program density_tls
implicit double precision(a-h,o-y)

c      ndim defines the dimension of the Hilbert space

parameter(ndim=4)

c      ntime defines the time steps to be calculated

parameter(ntime=20000)
complex *16 zrho(0:ntime,ndim,ndim),ztr
double precision fi(ndim,ndim),w(ndim)
external initrho,rhot,flush,rabi
intrinsic dfloat,dcmplx,conj,dasin,dacos,datan
intrinsic dsqrt
```

10


```

scale=1.d0/(1.d1*dt)
c      zenv=1.d-4*scale*ztnf(in-ik)
      zenv=env*ztnf(in-ik)
      do ir=1,nhs
        do is=1,nhs

          a1=w(ia)-w(is)
          a2=w(is)-w(ir)
          a3=w(ir)-w(ib)
          a4=a2+a3
          a5=a1+a2

          zenv1=dcmplx(dcos(a2*t),dsin(-a2*t))*
$          dcmplx(dcos(a1*tp),dsin(-a1*tp))

          zenv2=dcmplx(dcos(a5*t),dsin(-a5*t))*
$          dcmplx(dcos(a4*tp),dsin(-a4*tp))

          zenv3=dcmplx(dcos(a2*t),dsin(-a2*t))*
$          dcmplx(dcos(a3*tp),dsin(-a3*tp))

          zenv4=dcmplx(dcos(a5*tp),dsin(-a5*tp))*
$          dcmplx(dcos(a4*t),dsin(-a4*t))

          zaux1=fi(ia,is)*fi(is,ir)*dt*dt*zrho(ik,ir,ib)*zenv1
          zaux2=fi(is,ib)*fi(ia,ir)*dt*dt*zrho(ik,ir,is)*zenv2
          zaux3=fi(is,ir)*fi(ir,ib)*dt*dt*zrho(ik,ia,is)*zenv3
          zaux4=fi(ia,ir)*fi(is,ib)*dt*dt*zrho(ik,ir,is)*zenv4
          zauxs=((zaux1-zaux2)*zenv)+((zaux3-zaux4)*conjg(zenv))
          zaux5=zaux5-zauxs

```

150

160

170

end

cc

c Subroutine to calculate the effect of the driving Rabi field

cc

subroutine rabi(zrabi,dt,w,zrho,fi,nhs,t0,tpp,alpha,w0,in) 210

implicit double precision (a-h,o-y)

parameter (ndim=4)

parameter (ntime=20000)

complex *16 zrho(0:ntime,ndim,ndim)

complex *16 zaux1,zaux2,zaux3,zrabi(ndim,ndim)

complex*16 zrot1,zrot2,zi

double precision fi(ndim,ndim),w(ndim),gt

intrinsic dcos,dsin,dexp,dcmplx,dfloat

intrinsic dreal,dimag,datan,dsqrt

external flush 220

t=dfloat(in-1)*dt

zi=dcmplx(0.d0,1.d0)

gt=0.d0

cc

c Any pulse shape may be defined here

cc

if ((t.gt.(t0-tpp)).and.(t.lt.(t0+tpp))) **then**

gt=dexp(-10.d0/((tpp*tpp)-((t-tpp)*(t-tpp))))

endif

230

do ia=1,nhs

do ib=1,nhs

zaux3=dcmplx(0.d0,0.d0)

cc

```

real*8 function fac(n)
implicit double precision(a-h,o-y)
intrinsic dfloat,dlog
aux=0.d0
if (n.eq.0) then
    fac=1.d0
    goto 30
else
    do i=1,n
        aux=aux+dlog(dfloat(i))
    enddo
endif
fac=aux
30 return
end

```

270

280

cc

c Subroutine to construct the system Hamiltonian

cc

```

subroutine hamiltonian(A,gammap,beta,xinnt,fi)
implicit double precision(a-h,o-y)
parameter (ndim=30)
double precision A(ndim,ndim),fi(ndim,ndim)
external dsyev,fac
intrinsic dcos,dsin,dexp,dlog,dfloat,conjg

```

290

```

intrinsic dcplx,dimag,datan,dreal,dtan,min
complex *16 zi,zaux,zzz,zix,zalt,zig

```

```

pi=4.d0*datan(1.d0)

```

```

eta=1.d-1

```

300

```

fix=xinnt*1.d-2

```

```

zix=dcplx(dcos(2.d0*pi*fix),dsin(2.d0*pi*fix))

```

```

zi=dcplx(0.d0,1.d0)

```

```

egamma=dexp(-gammap*gammap/2.d0)

```

```

do n=0,ndim-1

```

```

  do m=0,n

```

```

    zzz=dcplx(0.d0,0.d0)

```

```

    j=min(m,n)

```

```

    do k=0,j

```

310

```

      zig=dcplx(0.d0,gammap)

```

```

      zalt=zig**dfloat(m+n-2*k)

```

```

      xfac1=(fac(m-k)+fac(n-k)+fac(k))

```

```

      xfac2=0.5*(fac(m)+fac(n))

```

```

      xfac3=dexp(xfac2-xfac1)

```

```

      zaux=(beta*zalt*xfac3*egamma)

```

```

      zzz=zzz+zaux

```

```

    enddo

```

```

  A(n+1,m+1)=dreal(zzz*zix)

```

320

```

  fi(n+1,m+1)=dimag(zzz*zix)

```

```

  A(m+1,n+1)=A(n+1,m+1)

```

```

  fi(m+1,n+1)=fi(n+1,m+1)

```

```

  enddo

```

```

enddo

```

```
do i=1,ndim
  A(i,i)=A(i,i)+dfloat(i)-0.5d0
enddo
```

330

```
return
end
```

Bibliography

- [1] Nielsen M.A., Chuang I.L., *Quantum computation and quantum information*, Cambridge University Press, Cambridge, 2002.
- [2] Leggett A.J., Chakravarty S., Dorsey A.T., Fisher M.P.A., Garg A., Zwerger W., *Reviews of Modern Physics* **59**, 1, 1987.
- [3] Leggett A.J., *Quantum Mechanics at the macroscopic level*, Les Houches, Session XLVI, Elsevier Science Publishers, 1987.
- [4] Weiss, U. *Quantum Dissipative Systems*, World Scientific, Singapore, 1993.
- [5] Dattagupta S., Puri S., *Dissipative phenomena in condensed matter, some applications*, Springer-Verlag, Berlin, 2004.
- [6] Prokof N.V., Stamp P.C.E., *Rep. Prog. Phys.* **63** 669-726, 2000.
- [7] Bloch F. *Phys. Rev.* **105**, 1206, 1957.
- [8] Redfield A.G., *IBM J.Res.Dev.* **1**, 19, 1957.
- [9] Fano U. *Phys. Rev.* **96**, 869, 1954.
- [10] Smirnov A.Yu., *Phys. Rev. B*, **67**, 155104, 2003.
- [11] Argyres P.N., Kelley P.L., *Phys. Rev.*, **134**, 98, 1964
- [12] Suarez A., Silbey R., Oppenheim I., *J. Chem. Phys.*, **97**, 5101, 1992.
- [13] Grifoni M., Paladino E., Weiss U., *Eur. Phys. J. B*, **10**, 719, 1999.

- [14] Lindblad G., *Commun. Math. Phys.*, **48**, 119, 1976.
- [15] Leggett A.J., Garg A., *Phys. Rev. Lett.* **54**, 857, 1985
- [16] Born M., Oppenheimer R., *Zur Quantentheorie der Molekeln. Ann. Phys. (Leipzig)* **84** (20), 457, 1927.
- [17] Breuer, H.P., Petruccione F., *The theory of open quantum systems*, Oxford University Press, Padstow, 2002.
- [18] Governale M., Grifoni M., Scön G., *Chem. Phys.* **208**, 273, 2001.
- [19] Burkard G., Koch, R.H., DiVincenzo D.P., *Phys. Rev. B*, **69**, 064503, 2004.
- [20] Makhlin Y., Scön G., Shnirman A., *New dimensions in Mesoscopic Physics*, edited by R. Fazio, V.F. Gantmakher, Y. Imry, Kluwer publishing, Dordrecht, 2003.
- [21] Barnett S.M., Radmore P.M., *Methods in theoretical quantum optics*, Oxford Science Publications, Oxford, 1997.
- [22] Carmichael H.J., *Statistical methods in quantum optics 1: Master equations and Fokker-Planck equations*, Springer-Verlag, Berlin, 1999.
- [23] Loss D., DiVincenzo D.P., *Int. J. Mod. Phys. B* **17**, 5489, 2003.
- [24] Vorrath T. Brandes T. Kramer B., *Chemical Physics* **296**, 295, 2004.
- [25] Anastopoulos C., Hu B.L., *Phys. Rev. A*, **62**, 033821, 2000.
- [26] Dube M., Stamp P.C.E., *Chemical Physics, Special issue* **268**, 257, 2001.
- [27] Fedichkin L., Fedorov A., Privman V., *Proc. SPIE* **5105**, 243, 2003.
- [28] Stamp P.C.E., Tupitsyn I.S., *Chemical Physics*, **296**, 281, 2004.
- [29] Feynman R.P., Hellwarth R.W., Vernon F.L., *Journal of Appl. Phys.*, **28**, 49, 1957.

- [30] Vandersypen L.M.K., Chuang I.L., Rev. Mod. Phys. **76**, 1037, 2004.
- [31] Price M.D., Somaroo S.S., Dunlop A.E., Havel T.F. Cory D.G., Phys. Rev. A, **60**, 2777, 1999.
- [32] Jones J.A., Mosca M., Phys. Rev. Lett. **83**, 1050, 1999.
- [33] Zhou Z., Chu S.I., Han S., Phys. Rev. B, **66**, 054527, 2002.
- [34] Amin M.H.S., Smirnov A.Yu., Maassen van den Brink A., Phys. Rev. B, **67**, 100508, 2003.
- [35] Josephson B.D., Phys. Lett., **1**, 251, 1962.
- [36] Josephson B.D., Adv. Phys., **14**, 419, 1965.
- [37] Tinkham M., *Introduction to superconductivity*, McGraw-Hill, Inc., New York, 1996.
- [38] Stewart W.C., Appl. Phys. Lett., **12**, 277, 1968.
- [39] McCumber D.E., J. Appl. Phys., **39**, 3113, 1968.
- [40] Tesche C.D., Phys. Rev. Lett., **64**, 2358, 1990.
- [41] Leggett A.J., Ruggiero B., Silvestrini P., *Quantum computing and quantum bits in Mesoscopic systems*, Kluwer academix/Plenum publishers, New York, 2004.
- [42] Caldeira A.O., Leggett A.J., Phys. Rev. Lett., **46**, 211, 1981.
- [43] Chakravarty S., Kivelson S., Phys. Rev. Lett., **50**, 1811, 1983.
- [44] Caldeira A.O., Leggett A.J., Annals of Physics, **149**, 374, 1983.
- [45] Schmidt V.V., *The Physics of superconductors*, edited by Müller P., Ustinov A.V., Springer-Verlag, Berlin, 1997.

- [46] Everitt M.J., Stiffell P., Clark T.D., Vourdas A., Ralph J.I., Prance II., Prance R.J., Phys. Rev B, **63**, 144530, 2001.
- [47] Spiller T.P., Clark T.D., Prance R.J., Widom A., Prog. Low Temp. Phys., **13**, 219, 1992.
- [48] Hakioglu T., Savran K., Phys. Rev. B, **71**, 115115, 2005.
- [49] Savran K, Hakioglu T., *REALIZING CONTROLLABLE QUANTUM STATES Proceedings of the International Symposium on Mesoscopic Superconductivity and Spintronics In the Light of Quantum Computation*, edited by Hidcaki Takayanagi, Junsaku Nitta, p. 233, World Scientific Publishing, 2005.
- [50] Hu B.L., Paz J.P., Zhang Y., Phys. Rev. D, **45**, 2843, 1992.
- [51] Ahn D., Lee J., Kim M.S., Hwang S.W., Phys. Rev. A, **66**, 012302, 2002.
- [52] Alicki R., Horodecki M., Horodecki P., Horodecki R., Phys. Rev. A, **65**, 062101, 2002.
- [53] Maniscalco S., Intravaia F., Piilo J., Messina A., J. Opt. B: Quantum Semiclass. Opt. **6**, S98, 2004.
- [54] Marquardt F., Bruder C., Phys. Rev. B, **65**, 125315, 2002.
- [55] Golubev D.S., Zaikin A.D., Phys. Rev. Lett. **81**, 1074, 1998.
- [56] Golubev D.S., Zaikin A.D., Phys. Rev. B, **62**, 14061, 2000.
- [57] Mohanty P., Jariwala E.M.Q., Webb R.A., Phys. Rev. Lett. **78**, 3366, 1997.
- [58] Natelson D., Willett R.L., West K.W., Pfeiffer L.N., Phys. Rev. Lett., **86**, 1821, 2001.
- [59] Cedraschi P., Ponomarenko V.V., Büttiker M., Phys. Rev. Lett., **84**, 346, 2000.

- [60] Lin J.J., Giordano N., Phys. Rev. B, **35**, 1071, 1987.
- [61] Pookr D.M., Paquin N., Pepper M., Gundlach A., J. Phys.:Condens. Matter, **1**, 3289, 1989.
- [62] Savran K., Hakioglu T., Mese E., Sevincli II., J. Phys,: Condens. Matter, **18**, 345, 2006.
- [63] Chakravarty S., Leggett A.J., Phys. Rev. Lett., **52**, 5, 1984.
- [64] DiVincenzo D.P., Loss D., Phys. Rev. B, **71**, 035318, 2005.
- [65] Fazio R., Palma G.M., Siewert J., Phys. Rev. Lett., **83**, 5385, 1999.
- [66] Kcil M., Schoeller H., Phys. Rev. B, **63**, 180302, 2001.
- [67] Claudon J., Balestro F., Hecking F.W.J., Buisson O., Phys. Rev Lett., **93**, 187003, 2004.
- [68] Zrenner A., Beham E., Stuffer S., Findeis F., Bichler M, Abstreiter G., Nature, **418**, 612, 2002.
- [69] Villas-Boas J.M., Ulloa S.E., Govorov A.O., Phys. Rev. Lett., **94**, 057404, 2005.
- [70] Villas Boas J.M., Govorov A.O., Ulloa S.E., Phys. Rev. B, **69**, 125342, 2004.